SPIRAL TURBULENCE
IN CIRCULAR COUETTE FLOW

Thesis by

Charles William Van Atta

In Partial Fulfillment of the Requirements

For the Degree of

Doctor of Philosophy

California Institute of Technology

Pasadena, California

1965

Submitted September 25, 1964

ACKNOWLEDGEMENT

The author wishes to express his sincere appreciation to Professor Donald Coles, whose guidance and encouragement were a major factor in making the present investigation possible. The helpfulness of many Caltech people, who supported the investigation with equipment and technical assistance, both at the Campus and at Jet Propulsion Laboratory, is gratefully acknowledged. Thanks are also due to the National Science Foundation, which supported the initial phases of the investigation.

The author is indebted to the California Institute of Technology for tuition grants and other financial assistance, and to the Rand Corporation (1958-59), the Convair Division of General Dynamics Corporation (1959-60), and the Ford Foundation (1960-62) for fellowship support.

ABSTRACT

Under certain conditions, the fluid motion between counter-rotating concentric cylinders is made up of alternate helical stripes of laminar and turbulent flow. The present experiments show that, over a large range of cylinder Reynolds numbers, this helical pattern of turbulence rotates steadily at very nearly the mean angular velocity of the two cylinders. When the speed of the outer cylinder is held fixed and the speed of the inner cylinder increases from rest in the opposite direction, spiral turbulence follows a catastrophic breakdown of the toroidal vortices arising from Taylor instability.

The ultimate objective of the present experiments is to measure the local rate of energy transfer between the turbulence and the mean motion in a typical spiral turbulent flow. The working fluid is air, and the instrumentation consists of hot-wire anemometers together with a variety of devices for operating on the resulting signals. Each cycle of the mixed laminar-turbulent flow (as observed by a probe mounted on one or the other cylinder) is treated as a member of an ensemble of realizations. The energy transfer (in a coordinate system rotating with the mean velocity of the turbulence) can be determined by averaging over a large number of instantaneous velocity samples taken at corresponding points in successive cycles of the turbulence.

After some exploratory measurements, a particular flow was selected for which the laminar-turbulent interfaces were sharply delineated across the entire annular gap and for which the dispersion in interface location was a minimum. This flow is about half laminar and

half turbulent: it is characterized by a nose of turbulence associated with the leading interface and projecting into the laminar region near the outer cylinder, while a corresponding tail near the inner cylinder is associated with the trailing interface. The helical pattern is left-handed and makes an angle of about 62 degrees with the axis of the cylinders.

For the flow in question, analog voltage signals from a calibrated array of four hot wires were first recorded on magnetic tape. Several thousand cycles of turbulence were recorded at each of 17 different radial positions. Sampled values from these signals were then obtained and stored in digital form on magnetic tape, and were finally processed by a large electronic computer to restore the voltage data to the original laboratory units. The total amount of digital information available to describe the turbulence is roughly 180,000,000 bits. The amount of noise introduced into the individual sampled voltages by the recording, playback, digitizing, and processing operations so far carried out is believed to be no more than 3 parts in 10,000.

TABLE OF CONTENTS

TABLE OF CONTENTS (contd)

LIST OF FIGURES

LIST OF FIGURES (contd)

LIST OF SYMBOLS

d	Hot-wire diameter
e	Raw sampled voltage
E	Sampled voltage corrected for channel interaction and time-constant effects
f_i	Frequency of interface pattern as observed from inner cylinder
f_o	Frequency of interface pattern as observed from outer cylinder
i	Hot-wire current
I	Input voltage to recorder from hot-wire or calibration source
k	Thermal conductivity of air
ℓ	Hot-wire length
ℓ_t	Apparent length of turbulent region at r = constant
L	Length of annular working space = distance between end plates
N_u	Hot-wire Nusselt number
P	Time interval between probe crossings of a given interface
q_i'	Velocity-fluctuation components in Cartesian coordinates; i = 1, 2, 3
q_i	Mean velocity components in Cartesian coordinates; i = 1, 2, 3
r	Radial coordinate measured from axis of cylinders
r_i	Radius of inner cylinder
r_o	Radius of outer cylinder
R_e	Hot-wire Reynolds number
R_h	Hot-wire resistance
R_i	Reynolds number of inner cylinder; $R_i = \frac{\omega_i r_i^2}{\nu}$
R_o	Reynolds number of outer cylinder; $R_o = \frac{\omega_o r_o^2}{\nu}$

LIST OF SYMBOLS (contd)

t	Time
T	Temperature
T_h	Hot-wire temperature
u'	Radial velocity fluctuation
U	Radial mean velocity
v'	Tangential velocity fluctuation
V	Tangential mean velocity
w'	Axial velocity fluctuation
W	Axial mean velocity
x_i	Cartesian coordinates; i = 1, 2, 3
z	Axial coordinate
α	Pitch angle of helix
γ	Intermittency factor
δ	$P - \overline{P}$
ϵ	Sampled voltage corrected for channel interaction only
θ	Fluctuating component of interface position
Θ	Angular coordinate
μ	Viscosity of air
ν	Kinematic viscosity of air
ρ	Density of air
σ	Standard deviation of random variable
ϕ	Pitch angle of probe
ψ	Yaw angle of probe
ω_i	Angular velocity of inner cylinder

LIST OF SYMBOLS (contd)

ω_o	Angular velocity of outer cylinder
ω_t	Mean angular velocity of spiral turbulence
$\langle\ \rangle$	Stochastic mean value
' (prime)	Fluctuation about mean
NRZ	The operation or resulting signal obtained using a technique known as "non-return-to-zero" for tape-recording of pulses.

I. INTRODUCTION

Under suitable conditions, a fluid motion consisting of alternate helical stripes of laminar and turbulent flow can be observed between concentric rotating cylinders. This phenomenon was first noted in 1956 by Oguro and by Coles (reference 1) at GALCIT, and was given the name "spiral turbulence". Using a suspension of aluminum particles in silicone oil as a means of flow visualization, Coles obtained the photograph in figure 1. The mottled areas indicate turbulent flow, and the smoother areas indicate laminar flow. The spiral pattern, which may be either right- or left-handed, rotates at approximately the mean angular velocity of the two contra-rotating cylinders without changing its general shape. The present experiments confirm that such regular mixed flows are the rule rather than the exception for transition in circular Couette flow when the cylinders rotate in opposite directions.

One example of spiral turbulent flow was studied by Oguro (unpublished) in the larger rotating-cylinder apparatus at GALCIT, using air as the working fluid. His hot-wire measurements, made with the inner cylinder at rest (cf. Fig. 7), show a stable laminar-turbulent configuration in which the laminar flow is confined to narrow regions near both walls. The pattern rotates with approximately half the angular velocity of the outer cylinder. Oguro's measurements provide some evidence that fluid elements move on the average in nearly circular paths, so that an element near either wall repeatedly traverses the pattern and participates alternately in the laminar and

turbulent motion. If this is generally true, it follows that the interfaces separating regions of laminar and turbulent flow are of two kinds. One kind, involving transition in the usual sense, propagates into laminar regions; the other kind, involving inverse or anti-transition, propagates into turbulent regions.

An important question raised by these observations is: what is the mechanism by which the turbulence disappears at the anti-transition interfaces? The almost equal sharpness observed for the two kinds of interfaces, as illustrated by the typical hot-wire signal in figure 2, indicates that this mechanism may not be entirely viscous or diffusive in nature. The present research is an attempt to study this question by measuring the local rate of energy transfer between the mean flow and the turbulence. In a cartesian coordinate system, rotating with the average angular velocity of the spiral pattern, the rate of transfer of energy at any point may be written in terms of mean and fluctuating velocities as

$$-\rho \sum_{i,j} \langle q_i' q_j' \rangle \frac{\partial \langle q_i \rangle}{\partial x_j}$$

Depending on whether the sum is positive or negative, this expression represents a net transfer of energy from the mean flow to the turbulence or from the turbulence to the mean flow.

The absence of any basic symmetry in the flow makes it essential to measure every term in the expression for the rate of energy transfer. All three velocity components have to be measured simultaneously. The heart of the experiment is the determination of these

velocity components, using instantaneous voltage samples from a calibrated array of hot-wire anemometers.

Finally, because the spiral pattern rotates with an average angular velocity different from that of either cylinder, it is impractical to measure the energy transfer in the usual way, in terms of time averages at a fixed point in a statistically stationary flow. However, since the flow pattern is repeatedly traversed by a probe fixed to either cylinder, an alternative method suggests itself. This is to take successive cycles, or alternations of laminar and turbulent flow, as members of an ensemble of realizations of the experiment. The ensemble average over instantaneous measurements made at corresponding points in successive cycles should be equivalent in many respects to a time average at a fixed point in the rotating pattern.

The experiment just outlined is an ambitious one, inasmuch as it requires the breaking of new ground in the application of large electronic data-handling and computing equipment to the problem of turbulence. The research has been carried out in several stages:

(1) Definition of the problem; choice of an optimal flow configuration; development of instrumentation (1960-62). This work is reported in part III of this thesis.

(2) Recording of data in analog form on magnetic tape; calibration of instrumentation (late 1962). This work, which was carried out in collaboration with Professor Donald Coles, will be described in a separate report. Certain essential details of recording technique are mentioned in part IV.

(3) Conversion of analog data to digital form; preliminary study of mean flow structure (1963-64). This work is reported in part V.

(4) Recovery of velocity data; statistical analysis (1964 to present). This work, also being carried out with Professor Coles, is not yet complete. The obstacles remaining to be overcome arise in the probe calibration and are concerned with accuracy rather than technique (see Appendix I). The work is far enough advanced so that there is every reason to believe that the experiment has been successful.

In addition to basic measurements concerning the dependence of the overall interface velocity (Fig. 7) and the intermittency factor on Reynolds number, a number of other interesting fluid mechanical properties of spiral turbulence have been uncovered from the completed phases of the research.

Stable right- and left-handed helical flow configurations were found to occur with equal probability when the flow was established from rest. It was therefore necessary to determine and continuously monitor the hand in order to be certain that the same flow was always being studied. For the tape recorded data, obtained in the left-handed version of the flow, the interface pattern had a helix angle of about 28 degrees (measured with respect to a plane perpendicular to the axis of the cylinders). The helix was found to be wrapped once around the annulus in the total length of the apparatus.

Another intriguing result concerns the mean shape of the interfaces (see figures 21 and 22). A nose of turbulence associated with the leading interface projects into the laminar region near the outer cylinder, while a corresponding tail is associated with the trailing interface near the inner cylinder. The mean interface pattern looks nearly the same when viewed from either of the two moving walls. In contrast to this property of symmetry in the mean, the dispersion in the position of the leading interface was found to be considerably less than the dispersion for the trailing interface (Fig. 23). This result was the first indication of any difference in the character of the two interfaces. The probability densities for interface location and apparent length of the turbulent region were found to be closely Gaussian. Finally, it was inferred from data like that in figure 26 that fluctuations in interface position were rapid compared with the characteristic time scales of the flow, i.e. $2\pi/\omega_o$, $2\pi/\omega_i$, and $2\pi/\omega_t$.

II. EXPERIMENTAL ARRANGEMENT

2.1 Rotating-Cylinder Apparatus

The experiments were performed in the large GALCIT rotating-cylinder apparatus, shown in figure 3, using air as the working fluid. The two concentric aluminum cylinders can be driven independently at continuously variable speeds up to several hundred revolutions per minute. The nominal inner and outer diameters of the two-inch annular working space are 32 and 36 inches respectively, the actual measured values being 32.003 and 35.996 inches. The axial length of the working space can be varied in the range from 34 to 55 inches by means of adjustable endplates which prevent outside disturbances from propagating into the annulus. To allow optical determination of probe positions, the endplates are made of transparent acrylic plastic. The endplates rotate with the outer cylinder, imposing at the ends a boundary condition of solid body rotation with the angular velocity of the outer cylinder. At the inner cylinder, there is a discontinuity in velocity equal to $(\omega_o - \omega_i)r_i$. Thin rings of teflon tubing provide a sliding seal between the surface of the outer cylinder and the endplates.

Hot-wire probes are mounted on aluminum pads, machined to fit snugly into 0.625-inch diameter holes in the wall of each cylinder. The face of each pad exposed to the flow is machined to conform to the curvature of the cylinder.

Each cylinder can be equipped with either of two slip ring assemblies to allow hot-wire and other signals to commute between

laboratory and rotating frames. The two assemblies, having eighteen and eight channels respectively, employ gold plated wipers and rings to minimize contact resistance and provide a low noise level. At the relatively low cylinder speeds employed for most of the experiments, the slip rings produce no significant increase in the noise level of the hot-wire signals.

The circular polar coordinate system used to describe the experiments is defined in figure 4. The z axis is taken along the axis of the cylinders, with positive angles and angular velocities defined by a right-hand convention. The angular velocity of the outer cylinder, which always rotated in the same direction, is arbitrarily taken as negative. The Reynolds numbers for the outer and inner cylinders, R_o and R_i, take the signs of ω_o and ω_i respectively. For most of the experiments, the cylinders turned in opposite directions, and ω_o and R_o were negative.

2.2 Measurement of Cylinder Speed

The angular velocity of each cylinder was measured using a magnetic pickup whose field was cut once per revolution by a small iron rod attached to the driving gear of the cylinder. At moderate and high speeds, the period between successive pulses was measured with an electronic counter. At low speeds, the pulses were too weak to trigger the counter directly, and the pickup signal was used to trigger an oscilloscope which in turn triggered the counter.

Each cylinder was dynamically balanced by systematically adding weights at different points on the circumference until a

combination of added weight and position was found which minimized the variation in speed during each revolution. This variation was determined by measuring the time intervals between successive openings of a microswitch actuated by individual teeth of the driving gear. As new instrumentation was added to the cylinder, it was sometimes possible to avoid an additional balancing operation by weighing the added components and adding an equal weight at a point 180 degrees around the cylinder.

For the tape-recording sessions, the maximum variation in speed within one revolution amounted to less than 1 percent for the outer cylinder and 3 percent for the slower inner cylinder. For either cylinder, the overall period of revolution, as measured by the magnetic pickup, was constant to about one part in a thousand for hours at a time. In fact, it was this excellent speed regulation which made the experiment possible.

2.3 Hot-Wire Instrumentation

For all of the preliminary experiments described in part III, the hot-wire instrumentation consisted of single-wire probes operated at constant current by a Shapiro and Edwards Model 50 hot-wire system. The stem of each probe was a length of 0.042-inch O.D. stainless-steel tubing with a 90-degree bend. The tubing served as one electrical conductor. A second central conductor, of insulated 0.018-inch diameter drill rod, protruded from the end of the tube. The hot-wire was soldered to the pointed tips of the central conductor and another short length of drill rod soldered to the tube wall.

The probe used for measuring the three components of velocity consisted of four hot-wires in a double V-array, each wire being approximately 0.04 inches long. Eight copper-plated steel needles, tapering from 0.014 inches in diameter to 0.003 inches at the tips, formed the hot-wire supports. Soldering of the hot-wires to the needle tips was accomplished by viewing the operation through a stereoscopic microscope and using micromanipulators to position and tension the wires. The eight signal leads ran inside the 0.065-inch O.D. stainless-steel tube that served as the probe stem. Viewed in the direction of the airflow, the area of the probe (excluding stem) was 0.007 square inches. The dimensions of the L-shaped probe stem (Fig. 5) were influenced somewhat by the need to install and remove the probe through the 0.625-inch diameter holes in the 0.50-inch thick walls of the inner and outer cylinders. The delicacy of this operation, and the need for repeated calibrations of the same hot-wires throughout the course of the experiments, precluded any scheme for calibrating the wire array in an external flow.

For all the experiments, the hot-wire material was 0.1 mil (0.0001-inch) diameter, 90 percent platinum-10 percent rhodium Wollaston process wire[1] from which the silver coating was removed before soldering the wire in place. The temperature coefficient for the particular spool of wire used for the tape recorded data was measured as 0.00158 ohms/ohm/°C. With an overheat ratio (ratio of hot to cold wire resistance) of 1.15, the wire hot temperature was about 100°C above room temperature.

---

[1]Sigmund Cohn Corp., Mt. Vernon, N. Y.

The hot-wires used for quantitative velocity measurements were operated at constant temperature. This method avoided a conflict between a need for linear amplification at frequencies from DC to several hundred cycles per second and a need for compensation at the higher frequencies. Apart from initial adjustments for a particular set of hot-wires, the system was left untouched throughout the course of the main experiment. Each of the four wires on the velocity data probe, with its slip rings and leads, formed one arm of a bridge circuit in a Model M-5 Hot-Wire Amplifier Unit.[2] By using an overheat ratio of 1.15 or less, free convection effects could be made negligible at the lowest wire Reynolds numbers encountered in the experiment. The amplifier frequency response was flat up to about 7,000 cycles/sec whereas the velocity fluctuations contained very little energy at frequencies above 100 cycles/sec.

2.4 Probe Traverse Gear

The multiple hot-wire probe was permanently affixed to a traversing mechanism (Fig. 5) which allowed the radial position of the probe to be varied across the full extent of the annulus. The traversing mechanism was mounted on a slightly modified pad attached to the cylinder in the usual fashion. To allow calibration of the probe in pitch and yaw, the entire traversing mechanism could be pivoted about an axis parallel to the axis of the cylinders (pitch), and the probe could also be rotated about its own axis (yaw). The probe could be

[2]Transistorized version of equipment originally designed by L. S. G. Kovasznay. Constructed by L. T. Miller, Baltimore, Maryland.

pitched and yawed over ranges of ±10 degrees and ±15 degrees respectively, with an uncertainty in measuring the angles of, at most, 0.1 degree.

The radial position of the probe was determined optically by sighting on the central needle tips and on the cylinder walls with a cathetometer attached to the supporting frame of the cylinders.

2.5 Intermittency Meter

The intermittency meter used for direct measurements of the intermittency factor γ was designed and constructed by H. Oguro. The lowest frequencies in the hot-wire signal, corresponding to mean flow variations, were filtered out, and the amplitude of the resulting signal was adjusted until the oscilloscope trace was completely masked, during the flat laminar intervals, by a thin horizontal strip of opaque tape. The smoothed output of a photomultiplier tube, looking at the oscilloscope face through a lens system, was converted to a square wave and used to gate an oscillator signal into a counter during intervals of turbulent flow. To obtain the intermittency factor, the reading of the gated counter was divided by the reading of a second free-running counter driven by the same time base. A half-silvered mirror allowed the masked signal to be observed without disturbing the discrimination process.

The intermittency meter was calibrated by adjusting the trigger level until the rise and fall of the square wave gate signal coincided respectively with the apparent beginning and end of turbulence.

III. EXPLORATORY EXPERIMENTS

3.1 General Observations of Transition

The research began with a general survey of the transition region. The initial object was to determine experimentally the most regular mixed-flow configuration obtainable with the apparatus, using two criteria; (1) sharply delineated laminar and turbulent regions for all radial locations in the annulus, and (2) minimum dispersion for fluctuations of the interface geometry about its mean position in suitable rotating coordinates. Except where noted, the length of the working space for the preliminary experiments was kept fixed at its maximum value of 54.7 inches. The flow was normally observed at $r = 17$ inches in the axial mid-plane of the cylinders, $z = 0$, using hot-wire probes mounted on either cylinder.

The angular velocities of the two cylinders were first increased until transition to fully or partially turbulent flow occurred. As expected, intermittency was found to be the dominant feature of the transition region when the cylinders turned in opposite directions. For a wide range of Reynolds numbers, the hot-wire signals showed a regular alternation between laminar and turbulent flow (as in Fig. 2), or else showed turbulent flow in which the amplitude of the turbulence varied periodically with a comparable frequency. More irregular flows were also observed, in which the laminar and turbulent regions were not as uniformly compartmented. In some instances a tendency was noted for successive turbulent regions of the signal to bunch together, swallowing up the laminar region. In other cases brief

periods of turbulence appeared randomly in the normally laminar portion of the signal. The latter behavior is probably due to corrugations in an interface, causing it to cross a circle r = constant at more than one circumferential location, rather than to islands of turbulence separated from the main body of turbulent fluid.

3.2 Catastrophic Transition

To investigate more closely the manner in which these intermittently turbulent flows were established, the speeds of the cylinders were varied in a more systematic fashion. Starting with laminar flow and keeping the Reynolds number of the outer cylinder constant, the angular velocity of the inner cylinder was increased slowly from zero in the opposite direction. The flow remained entirely laminar up to a repeatable critical value, R_{ic}, where the flow became turbulent with catastrophic suddenness. In some cases, the subsequent signal showed a periodic alternation between laminar and turbulent flow; in other cases it was fully turbulent, with or without an observable low-frequency variation in amplitude. Several runs were made at each fixed R_o, increasing R_i as slowly as possible, to obtain a lower bound for R_{ic}. These limiting values are plotted in figure 6.

For R_o less than about 100,000, the catastrophic transition points lie above but close to the theoretical Taylor instability boundary (reference 2). In this range transition is probably caused by breakdown of the toroidal vortices that form upon crossing the Taylor boundary and increase in strength as R_i increases. The Taylor instability

itself produces no circumferential flow variation, and could not be detected during the present observations.

For R_o greater than 100,000, a different behavior was found; R_{ic} decreased to zero for increasing R_o. For infinitely long cylinders, it seems likely that the laminar flow is stable to infinitesimal disturbances of Tollmien-Schlichting type (reference 3) as well as Taylor type. For these higher Reynolds numbers, however, transition may be initiated by either of two finite disturbances that always exist in the flow. These are (a) the vorticity concentrations at the endplates and (b) the wake of the probes.

A similar transition boundary has been observed by Coles (reference 1), who employed a flow visualization technique in which there were no probes to disturb the flow. From his visual observations, he concluded that transition was initiated in the vorticity concentration at the endplates. In the present case, where the endplates rotate with the outer cylinder, the strength of this vorticity concentration is given by $(\omega_o - \omega_i)r_i$. The similarity between the present transition data and Coles' results strongly suggests that the vorticity concentration at the endplates is also the source of transition in the present case. As shown in figure 6, there was a small systematic change in the transition boundary when the length of the working space was decreased by 40 percent. It should be kept in mind that the laminar velocity profile at large Reynolds numbers may be profoundly influenced by the proximity of endplates (reference 4).

The effect of probe Reynolds number was not investigated in any detail. At three speeds, runs with different radial probe positions

showed no significant change in the transition Reynolds number, suggesting that the probe played no important role in initiating the turbulence. On the other hand, it was found in later probe calibrations, with the inner cylinder at rest, that the wake of a larger multiple hot-wire probe definitely triggered transition when the probe Reynolds number (based on stem diameter and relative velocity at the tip) exceeded a value of about 300.

Increasing R_i beyond R_{ic} caused the flow to become increasingly turbulent (γ increasing). In all cases, a value of R_i could be reached for which the intermittency factor at mid-gap was unity and the turbulence was of uniform intensity. When the Reynolds numbers were varied unsystematically for $R_i > R_{ic}$, the state of the flow at a given operating point, as characterized by the measured angular velocity of the interfaces (see section 3.4) and by a rough visual estimate of the intermittency factor, was independent of the means used to reach the point in question.

3.3 Hysteresis Effects

Upon decreasing R_i below R_{ic}, turbulence persisted, the alternations between laminar and turbulent flow usually becoming at first more regular and sharply defined. As R_i was further decreased, both the intervals between the bursts of turbulence and the lengths of the bursts became increasingly random, until the turbulence degenerated and disappeared permanently at a lower critical Reynolds number. This lower bound, denoted by the curve $\gamma = 0$ in figure 6, was established by varying the speed of the inner cylinder as slowly as possible.

For sufficiently large R_o, intermittency persisted even when both cylinders rotated in the same sense.

Except for the hysteresis just described, which means that two distinct states (one completely laminar, the other partially or fully turbulent) could be observed for identical values of R_o and R_i, the flow throughout the transition region appeared to be unique, independent of how the cylinder speeds approached their equilibrium values. If the angular velocity of the inner cylinder was fixed at some value above the Taylor boundary and the angular velocity of the outer cylinder was increased slowly from rest, transition occurred gradually through a progression of increasingly irregular motions,[3] but the final state of the flow was the same unique function of the two Reynolds numbers.

3.4 Interface Propagation Velocity

The average angular velocity of the interfaces relative to the laboratory, ω_t, and the number of turbulent regions propagating around the annulus, N, were calculated from the frequency of the pattern as observed from probes on both cylinders. Frequencies were obtained by timing thirty or more cycles of the flow pattern with a stopwatch. The relevant expressions, in which f_o and f_i are the frequencies of the pattern observed from the outer and inner cylinders respectively, are:

$$\omega_t = \frac{\omega_i f_o + \omega_o f_i}{f_o + f_i}$$

---

[3] Because the transition boundary has a negative slope in figure 6, catastrophic transition will not be observed when operating in this manner, except for ω_i near or equal to zero.

$$N = \frac{2\pi(f_o + f_i)}{f_o - f_i}$$

In all cases, the number of turbulent regions calculated was unity (to one part in a thousand). The quantity ω_t has the same sign as ω_o. Thus, the interfaces travel in the same direction as the outer cylinder, which is always rotating faster than the inner cylinder. The angular velocity ω_o is arbitrarily taken as negative, so that ω_t is negative and, for most of the measurements, ω_i is positive.

As shown in figure 7, the quantity $2\omega_t/(\omega_o + \omega_i)$, although a weak function of Reynolds number over most of the transition region, is nearly equal to unity for most of the observations. At least below the Taylor boundary, ω_t is approximately equal to the mean angular velocity of the two cylinders, and the turbulence propagates essentially as if it were being convected with the mean angular velocity of the fluid. Above the Taylor boundary there is a relatively rapid rate of increase in $2\omega_t/(\omega_o + \omega_i)$, as exhibited in figure 7, and Taylor instability may therefore play a role even after turbulence has been established.

For R_o less than 100,000, the data in figure 7 were obtained with hot-wires located at mid-gap, but for larger values of R_o the signals there lost their modulated character as the intensity of the turbulence became independent of Θ. Since the flow near the outer cylinder remained periodically intermittent for larger Reynolds numbers, most of the data for $R_o > 100,000$ were obtained at $r = 17.9$ inches.

3.5 Evidence for Helical Structure

3.5.1 Helix angle. To verify that the flow in the large machine had the same spiral pattern as in figure 1, the differences in arrival times of a given interface at three probes having different axial locations were roughly measured for a few cases with R_o between -18,000 and -60,000. The time intervals were measured from photographic records obtained with a dual-beam oscilloscope and (at the lower speeds) with a stopwatch. The probes were all mounted on the outer cylinder, at r = 17 inches. One probe was at z = 0, Θ = 0 degrees, while the other two probes were located at z = -24 inches, Θ = 0 degrees and z = -12 inches, Θ = +15 degrees. Assuming the mean interface pattern to be helical, the helix angle was computed from the average time interval between the beginning of successive turbulent bursts in the signals from each pair of probes.

Since the hand of the helix was not known a priori, the helix angle was computed twice for each pair of probes, assuming first a left-handed and then a right-handed helix. The angles calculated from different pairs either differed substantially (usually by about 20 degrees, or roughly a factor of two) or were very close together (within 1 or 2 degrees in several cases). For two cases in which the calculated angles differed by less than 1 degree, the calculated helix angles were 27.5 and 28.0 degrees. The latter case was for R_o = -18,300, R_i = 6,370, fairly close to the operating point of the smaller machine in figure 1 (R_o = -15,900, R_i = 5,300). One full turn of a helix with a pitch angle α of 28 degrees $\left[\tan \alpha = (dz/rd\Theta)_h\right]$ would have

an axial length of 57 inches, implying that the helix in the large machine was also wrapped nearly once around the annulus, whose actual length was 54.7 inches.

The calculations showed that both right- and left-handed helical patterns had been observed. In one case measurements taken several minutes apart showed that the helix had changed hands while both cylinder speeds remained constant. This transition from one hand to the other was observed as a brief period (about 15 seconds, or 5 normal cycles of the flow) of very irregular, fully turbulent flow.

Although these measurements were relatively crude, since only about 10 cycles of the flow were used to obtain the average time intervals, they confirmed both the helical structure of the flow and the existence of right- and left-handed configurations in the large apparatus.

3.5.2 Axial flow component. Further evidence for right- and left-handed helices was obtained while estimating the magnitude of the mean axial flow component for the "optimum" spiral turbulence configuration discussed in section 3.6. To detect the mean axial flow component, the difference signal from two hot-wires forming a V-array in the surface r = 16.5 inches was examined. The low-frequency component of the signal was definitely periodic, with extreme values in the laminar and turbulent portions of the cycle (cf. figure 2). The sensitivity of the wire array to changes in flow angle was measured by yawing the probe in a laminar flow with nearly the same mean tangential velocity as the spiral turbulence. From this calibration, the overall flow deflection per cycle was estimated to be about 10 degrees,

implying a maximum mean axial component of about 8 percent of the mean tangential component. The effect of the transition and antitransition interfaces was to turn the flow in opposite directions. When the intermittent flow was reestablished from rest a number of times, it was found that roughly half the time the low-frequency part of the difference signal was reflected in the horizontal axis, showing the random occurrence of two flows having opposite hands. The two hands deflected the mean flow in opposite directions as corresponding laminar and turbulent regions of the flow pattern were traversed.

3.6 The Search for an Optimal Flow

During the early experiments, a group of extremely stable mixed flows was noted in the region R_o = -40, 000 to -50, 000, R_i = 3, 500 to 10, 000. Further visual inspection of hot-wire signals in this region indicated that the most regular flow, having sharply defined interfaces at all radial locations, would be found in the neighborhood of R_o = -50, 000, with R_i between 5, 000 and 6, 000.

With R_o fixed at -48, 000, a quantitative measure of the regularity of the flow at various values of R_i was obtained by measuring the dispersion in the time interval, P, between successive observations of the same interface at r = 17 inches. The intermittency meter produced a square wave whose positive going edges marked the beginning of turbulence for each cycle. For various R_i, several hundred time intervals between successive pairs of these edges were measured with an electronic counter and recorded manually, producing in each case a nearly Gaussian distribution function for P, as shown in figure 8. On

such a plot, the distribution function for a true normal or Gaussian probability density is a straight line. Given the mean, $\overline{P}$, and the standard deviation σ (determined graphically), the ratio $\sigma/\overline{P}$ shown in figure 9 provides a measure of the relative dispersion in interface position at different speeds. The brackets in figure 9 represent the uncertainty in σ that arises in graphically fitting a straight line to the measured distribution functions. This plot of $\sigma/\overline{P}$ versus R_i exhibits a minimum near $R_i = 5,600$. On the basis of these measurements and the previous observational evidence, the operating point $R_o = -50,000$, $R_i = 5,600$ was chosen for the more elaborate experiments to follow. Hereafter, this particular combination of Reynolds numbers will be referred to as the "standard configuration" or the "final operating point".

The normalized angular velocity for the interfaces, computed from the average of each group of 300 periods, confirmed the previous data obtained by counting 30 to 50 periods of the signal, as shown in figure 10. The final operating point lies near the center of the region in which the normalized angular velocity is practically independent of R_i, approximately halfway between the Taylor boundary for infinite length and the boundary ($\gamma = 0$) below which turbulence cannot persist.

3.7 Intermittency Measurements; Further Properties of the Optimal Flow

3.7.1 Interpretation of intermittency data. For the present measurements, the intermittency factor γ is defined as the percentage

of time that the flow at the moving probe is turbulent at the radius of measurement. Thus γ may be interpreted as the average length of the turbulent region at that radius divided by the circumference at that radius. Measurements of the apparent length of the turbulent regions and correlations between successive intervals (see Fig. 26 and Appendix B) indicate that the volume of turbulent fluid is continually changing its shape and size with a time scale considerably less than the time required by the probe to traverse once through the flow pattern. Consequently, no information about the instantaneous shape or length of the turbulent region can be obtained from these measurements.

All measurements of γ reported here were obtained by averaging over at least 100 cycles of the pattern (approximately 5 minutes). The pass band of the γ-meter filter (Kronhite 330-M) was 4 cycles per second to 20,000 cycles per second.

3.7.2 Variation of γ with R_i. With increasing Reynolds number, γ increased more slowly near the walls than in the center of the gap, increasing most slowly near the outer cylinder. For R_o = -50,000, the variation of γ with R_i, measured at $z = 0$ for three different radii, is plotted in figure 11. The flow can be essentially fully turbulent near the inner cylinder and at mid-gap, e.g., at R_i = 14,000, while the intermittency factor near the outer cylinder is still only 0.7. With regard to the radial distribution of γ, the flow studied by Oguro (R_o = -250,000, R_i = 0) was of this type.

3.7.3 Radial variation of intermittency and dispersion. The radial distribution of γ at $z = 0$ for R_o = -50,000, R_i = 5,600 is

shown in figure 12. There is a broad maximum at mid-gap, around which the distribution is nearly symmetrical. The dispersion in the time interval, P, between successive observations of the same interface, and the dispersion in the length of the turbulent region, ℓ_t, were larger near the walls than in the center of the gap. For three radii, the dispersion in ℓ_t was found by measuring individual intervals during which the intermittency meter indicated turbulent flow. This was accomplished by manually resetting the gated counter to zero during each interval of laminar flow and recording the number displayed on the counter after each interval of turbulent flow. From the approximately Gaussian distribution functions shown in figure 13, the dispersion in ℓ_t at points 0.1 inch from each wall was estimated to be perhaps 20 percent larger than at mid-gap. The intervals between observations of the same interface showed an even larger increase in dispersion near the walls, being nearly 60 percent larger at r = 16.25 inches than in the center of the gap (Fig. 14).

3.7.4 Axial variation of γ. Derivatives of mean velocity with respect to z occur in the expression for energy transfer (part I). These derivatives cannot be measured directly, but can be inferred by assuming local two-dimensionality of the flow in a helical coordinate system attached to the helical pattern. To investigate whether or not such a procedure might be valid, the intermittency factor for R_o = -50,000, R_i = 5,600 was measured as a function of axial position for two different radii. Since probes could be installed only at positions one foot apart along the cylinders, measurements at intermediate stations were

made by moving both end plates in the same direction, keeping the length of the working space fixed. To allow this freedom, it was necessary to reduce the length of the working space to 46.7 inches.

The interfaces were found to be sharply defined and stable for all axial locations. The measurements of γ, plotted in figures 15 and 16, are not inconsistent with the idea of two-dimensionality in the central region. On the other hand, there are regions at each end, accounting for nearly 40 percent of the working space, in which significant axial variations may exist.

3.7.5 Influence of cylinder length on interface stability and velocity. The effect of the length of the working space on the stability and intermittency of the mixed flow for $R_o = -50,000$, $R_i = 5,600$ was briefly studied by moving both endplates inward to decrease L, keeping the probe fixed at z = 0, r = 17 inches. The intermittency factor varied slowly with L, increasing from 0.58 at the maximum length of 54.7 inches to 0.62 at the minimum length of 34.0 inches, but there was a striking change in the stability of the interface pattern as L decreased. The flow was very stable for L greater than 44 inches, but became progressively more irregular as L was decreased below this value. For the minimum length, the hot-wire signals typically showed the usual alternation between laminar and turbulent flow for periods of several minutes, and then showed complete turbulence for intervals of 15 or 20 seconds (5 to 7 periods of the normally intermittent signal). It was conjectured that decreasing the length of the apparatus increased the tendency for the flow to change hand spontaneously, and this

conjecture was later verified by observations during which the hand of the flow was continuously monitored (section 4.2.3).

For fixed ω_o and ω_i, the angular velocity of the turbulence increased slightly as the length of the cylinders was decreased, as shown in figure 17. This result is consistent with the previous observation that ω_t tends to follow the mean tangential velocity in the annulus, since the latter would increase with decreasing L due to the strong effect of the endplates on the velocity profile (reference 4).

3.8 Role of Preliminary Data in the Sampling Process

3.8.1 Ensemble averaging scheme. The central problem kept in mind during these preliminary experiments was that of defining and executing a meaningful averaging process. The fluctuating properties of the flow, including interface position and velocity, are assumed to be statistically stationary functions of time in a coordinate system rotating with the mean angular velocity of the turbulence. Measurements of the quantities appearing in the expression for energy transfer (part I) are required at fixed points in this rotating coordinate system. Given a continuous record of the velocity from a probe on either cylinder, together with an a posteriori value for $\bar{P}$ (the average period of the laminar-turbulent cycle), average properties of the flow at a fixed point in the rotating system may be determined from the continuous record by sampling the record every $\bar{P}$ seconds. Each sampling interval can be further subdivided to obtain data at more points in the rotating system.

This formal scheme has several disadvantages in practice, even though the stability of the flow and the excellent speed regulation of the apparatus make it attractive in principle. Without a prohibitively exact knowledge of $\bar{P}$, and an equally precise method of generating initial sample commands every $\bar{P}$ seconds, the data might drift considerably out of phase during the several thousand cycles of the flow required for meaningful averages. For example, $\bar{P}$ might be in error by about one part in sixteen from a single cycle, or one part in a thousand from several thousand cycles of the flow. Even for a train of initial sample pulses fitted to the (perhaps atypical) first and last cycles of a long data record, there are problems either with variation of recorder playback speed or with the finite resolution of any clock signal recorded on the analog tape to serve as a time base for later operations (see section 4.3.5). To provide adequate frequency response and sufficiently long periods of uninterrupted recording time, it was decided to record the velocity data at a tape speed of 7.5 inches per second. The maximum frequency that could be recorded on the tape at this speed was about 20 kc/sec. After 3,000 cycles of the flow pattern, the cumulative round-off error could be a significant fraction of a cycle even if $\bar{P}$ were known with infinite resolution.

3.8.2 Use of mean velocity in sampling process. The scheme finally adopted for generating initial sample pulses made use of a function highly correlated with the overall structure of the flow pattern, namely, the mean velocity. The circumferential variation of the mean velocity produced a strong low-frequency variation in the hot-wire

signal, having precisely the mean period desired. Since, by the criteria of section 3.7.3, the flow was thought to be most regular in the center of the gap, the location r = 17 inches was chosen for the phase-monitor probe described in section 4.1.4 below. This fixed probe, whose primary function was to furnish a standard reference signal for determining the phase of data recorded at various radii, also provided a convenient means for generating a series of approximately equally-spaced initial sample commands. When the signal from the phase-monitor probe was fed into a band-pass filter crossed at approximately the frequency $1/\overline{P}$, the output of the filter was quite close to a sine wave of frequency $1/\overline{P}$. The time intervals between positive-going zero crossings of this wave were measured and found to exhibit a dispersion of about 2.3 percent of $\overline{P}$, or about one-third of the dispersion in the interval P itself. Typical distribution functions and dispersion data for the two signals are compared in figures 8 and 9. Sample pulses generated by the zero crossings of the filtered monitor-probe signal were selected as being probably the closest approximation to uniformly-spaced sample pulses that could be generated "on-line", i.e., while the data were being recorded. This scheme furnished a repeatable, consistent method of generating sample commands with the correct average period, but introduced a dispersion of about 2.3 percent of $\overline{P}$ in addition to the inherent dispersion in interface position amounting to 4-8 percent of $\overline{P}$ (see section 5.3.4). Whatever method is used, each fixed sample point in the rotating system has an effective width measured by the total dispersion in $\overline{P}$, so that the ensemble average at each point is really a space average over a corresponding

circumferential interval at the radius of measurement. The additional dispersion due to the sampling method just described is given by a Gaussian distribution with the same dispersion as the initial sample pulses; about 70 percent of the samples for each point will be taken from an interval equal to 4.6 percent of the circumferential length. Of the two effects, the dominant one is the unavoidable inherent dispersion in interface position. Moreover, measurements of fluctuation levels and correlations at points near the average interface position will include samples taken from both turbulent and laminar flow. This will produce an apparent decrease in the sharpness of the transition regions and could mask some of the important properties of the fluctuating quantities.[4] It was actually found (section 5.3.4), for sample pulses generated in the manner outlined above, that dispersion in the interval between the sample pulse and the following interface was always significantly less (7 to 35 percent, depending on radius and direction of tape playback) than the dispersion in the interval between one interface and the next, so that (with respect to smearing out of the data) the sampling scheme employed was superior to sampling at equally spaced intervals.

[4]Because of the two sources of dispersion just described, it may eventually prove to be desirable to perform certain averages using samples selected entirely from turbulent (or laminar) regions.

IV. ACQUISITION OF PRIMARY VELOCITY DATA

While the preliminary experiments were still in progress, additional instrumentation and techniques were developed to obtain and record the data needed to determine the velocity by sampling techniques. These efforts will be described elsewhere. However, a brief outline will be given here of the tape-recording operation for the mixed flow at the final operating point with $R_o = -50,000$, $R_i = 5,600$. The length of the working space was fixed at its maximum value of 54.7 inches, and the main data probe was mounted in the axial mid-plane, equidistant from both endplates. Three sets of four hot-wires were used during the course of the measurements. The first set, on the outer cylinder, was accidentally destroyed during calibration and was used for tape recording at only one radius. With the probe still mounted on the outer cylinder, data were obtained with a second set of wires at ten radial locations. These wires were damaged during the conversion required to adapt the probe to the other cylinder, and a third set of wires was therefore used to obtain data at nine radii with the probe mounted on the inner cylinder. Each of the last two sets of wires was used for approximately 100 hours of calibration and recording.

4.1 Tape Recording of Signals

4.1.1 General procedure. When the hot-wire calibration was completed at a given radius, the probe was set at zero pitch and zero yaw, and a tape recording was made of the hot-wire signals for the

standard configuration of spiral turbulence. During each recording session, about 3,000 cycles of the flow pattern were recorded. Since the basic period of the signals was very nearly 3 seconds, this required about 2-1/2 hours. The remainder of the 3 hours and 12 minutes of recording time available (from 7,200 foot tape reels at 7.5 inches/sec). was spent calibrating the tape-recording system. Each tape consisted of three or four sections of data, each preceded and followed by a shorter calibration section. The recorder, an Ampex FR-100, ran continuously throughout. Since the tape transport was designed for 14-channel tape one inch wide, but the 7-track head recorded on only the odd numbered channels of the tape, each reel of tape was used twice by turning the reel over between recordings, without rewinding. A second complete run was then recorded in the opposite direction on the previously unused channels.

4.1.2 Recording of hot-wire signals. The output of each of the four M-5 hot-wire amplifiers consisted of a D.C. level of roughly -1.4 volts, a noise level of about 0.003 volts (much of this at frequencies above the recorder cutoff frequency of 1200 cycles /sec in the FM mode), and the intermittent turbulent signal, with a peak to peak value of perhaps 0.050 volts. To achieve the desired input recording level, each hot-wire signal was further amplified by an Epsco DA-102 differential D.C. amplifier whose second input was a constant D.C. bucking voltage, adjusted to nearly cancel the D.C. component of the hot-wire signal. An Evenvolt Model 200 zener-stabilized power supply provided a stable voltage source for the four bucking-circuit potentiometers.

Maximum tape-recording resolution was obtained by adjusting the gain so that the largest fluctuations in the turbulent signals covered about 90 percent of the ±1.4 volt linear input range of the F.M. recording electronics. The D.C. amplifier gain was fixed at 100, and the overall gain of roughly 20 to 30 was determined for each wire and each tape by a fixed attenuator resistor in series with the recorder input.

4.1.3 Calibration of F.M. recording system. Previous experience with the tape recorder had indicated the necessity of frequent calibrations in order to cope with drift in the center frequencies of the (vacuum tube) F.M. recording electronics. The hot-wire recording system, including the D.C. amplifiers, attenuators, and tape recorder electronics, was therefore calibrated several times during each recording session by interrupting the taping of turbulence signals to record known voltages with the same system. This operation was controlled by a switch box between the hot-wire amplifier and the Epsco inputs. When the main switch was moved from the "record" to the "calibrate" position, the hot-wire and bucking voltages were disconnected, a common calibration source was substituted for the hot-wires, and the remaining differential inputs were shorted. Seven positive or negative D.C. calibration voltages, in steps of about 0.014 volts, were available to cover the range of the D.C.-bucked hot-wire signals.

4.1.4 Phase monitor signal and sample command pulses. A fixed monitor probe, with a single hot-wire sensitive primarily to the tangential component of velocity, was mounted at $z = 0$, $r = 17$ inches on the same cylinder as the main data probe and displaced approximately

180 degrees from it. The signal from this probe, recorded in the F.M. mode, served as a reference for following the changing phase of the spiral pattern as the radial location of the main data probe varied from tape to tape. As previously noted, the same signal served as a convenient and suitable source for generating the sample commands needed for subsequent sampling of the recorded data. The monitor probe signal was passed through a Kronhite 330 M band-pass filter, crossed at the mean frequency of the overall flow pattern as observed by the probe. The output of the filter was an approximately sinusoidal wave with the same mean period as the hot-wire signals from the main data probe. A Tektronix Type 555 oscilloscope, triggering on the positive-going zero crossings of the sine wave, produced a pulse whose length, or dwell, was equal to the sweep time of the scope; the latter was set at about 2/3 of the basic period, so that the scope could reset itself before the next zero crossing. The resulting pulse train was recorded on a separate tape channel in the NRZ[5] mode. Hereafter, a member of this pulse train will be referred to as an "initial sample command", "initial sample pulse", or simply as an "NRZ". The NRZs were discontinued during the recorder calibration sections to avoid any possibility of mistaking D.C. calibration signals for turbulence data during the sampling operation.

4.1.5 Clock signal. The seventh and final signal recorded on the tape was a clock signal, a sine wave at 10 kc/sec, to serve as a

[5] NRZ = Non-return-to-zero, referring to a 2-state saturation technique used for recording and reproducing pulses.

time base for operations on the tape during playback. Use of such a clock signal minimized errors in time-interval measurements due to fluctuations in tape speed, differences in tape speed between the different machines used for recording and playback, and possible tape stretching. The clock source was an oven-stabilized 100 kc/sec crystal in a Hewlet Packard 522 B counter. The counter internally divided the crystal output frequency by 10, and the resulting waveform was passed through a low-pass filter and amplifier to produce a suitable sine wave for recording. In the recorder calibration sections, the clock signal was switched off and the clock channel served as a voice channel on which information about the current calibration voltages and other comments, some of them unprintable, were recorded.

4.1.6 Résumé of recorded data. Twenty full 192-minute runs were recorded, corresponding to 17 radial locations of the multiple hot-wire probe (see table I). Since each reel of tape was used for two separate runs, this required 10 reels or about 14 miles of magnetic tape. Eighteen tapes were made with the probe at 15 positions spaced 1/8 inch apart across the two-inch gap, and two tapes were obtained with the probe as close as possible to either cylinder. To keep the magnitude of the relative velocity large enough to avoid free convection effects, the hot-wire data for each half of the gap were recorded with the probe mounted on the far wall. To provide some redundancy in the experiment, data at $r = 17.000$ inches and 17.125 inches were obtained with the probe mounted on both cylinders, and at $r = 16.875$ inches

two tapes were made with different sets of wires with the probe on the outer cylinder.

Several shorter runs were also made with the probes on the outer cylinder to obtain information about the sweep angle of the interface pattern. The recorded data included the NRZ pulse train and the hot-wire signals from a sweep-monitor probe, the phase-monitor probe, and one wire on the velocity probe. These data were recorded for both right- and left-hand versions of the spiral turbulence, as well as for shortened lengths of the working space for the standard (left-hand) pattern.

4.2 On-Line Measurements and Observations

4.2.1 Mean-mean voltages. Within the two or three minutes immediately before and after each tape recording, with the spiral turbulence present in the working space, the average voltage of each hot-wire was measured over about 20 cycles of the flow pattern using an integrating digital voltmeter (voltage-to-frequency converter and counter). These mean-mean voltages, so called because they represent an average of the mean velocity over the whole flow, furnished useful information about mean voltage levels and drift of the hot-wires during the recording period, for comparison with data obtained later on from the tapes.

4.2.2 Air properties. The ambient air temperature was measured to the nearest 0.01°C using two mercury thermometers symmetrically located near the ends of the cylinders. A third thermometer

measured the air temperature near the hot-wire amplifiers to allow a correlation of temperature and drift.

Ambient air pressure was measured with a mercury barometer having a maximum resolution of 0.01 inch Hg.

4.2.3 Helix hand monitor. Since right- and left-hand versions of the spiral configuration were found to occur with equal probability, it was necessary to monitor the hand of the helix in order to maintain the same experimental conditions from run to run. This was done by generating audible signals during periods of turbulent flow at the phase-monitor probe and at another probe, called the sweep-monitor probe, mounted on the same cylinder as the phase-monitor probe but displaced axially by about 12 inches and circumferentially by about 13 degrees. The radial position of the sweep-monitor probe was adjusted until both monitor probes entered the turbulent flow region almost simultaneously when the flow had the standard hand (chosen arbitrarily, and later found to be the left-hand model). The intermittency meter operated on the phase-monitor signal in the usual fashion, and the output of the gated variable-frequency oscillator in the intermittency meter was connected to a loud-speaker, producing an audible tone which was on when the flow was turbulent at the phase-monitor probe and off when the flow was laminar. The occurrence of turbulence at the sweep-monitor probe was detected in a similar way by rectifying the signal, filtering out the low-frequency component, and using a Schmitt trigger turbulence discriminator to gate on and off a fixed-frequency oscillator driving a second loud-speaker. Thus, when the

desired flow was established, two distinct tones were heard, beginning almost simultaneously each time the probes traversed the flow pattern. When the opposite hand was present, the tones from the two loudspeakers were nearly 180 degrees out of phase, allowing an unmistakeable distinction to be made between the two hands. The hand of the helix was continuously monitored by this method throughout each recording session. At no time in any of the three-hour recording sessions did the flow change hand or become erratic enough to cause noticeable changes in the rhythm of the sound pattern.[6]

[6] When the length of the working section was reduced to 42 inches, for recording of the sweep-angle tapes mentioned earlier (section 4. 1. 6), this was no longer true; the spiral was heard to change hand spontaneously three times during a period of about two hours.

V. OPERATIONS ON ANALOG TAPE DATA

5.1 Data-Handling-Equipment

Analog-to-digital conversion and other operations on the analog tape data were performed with the aid of data-handling equipment furnished and maintained by the computing group (section 372) at the Jet Propulsion Laboratory.

The first playback operation employed a machine called the "Scanner", which is essentially a multiplexer followed by a digital magnetic tape deck to record the results of each scan of a maximum of 50 input channels. The scanning rate could be controlled manually or fixed at a single internally generated rate. Since the device had ten channels permanently equipped with counter inputs, it was ideally suited for the first part of the data analysis, which was to audit simultaneously the frequencies on five channels of the analog tape.

The final two operations on the analog tapes employed another machine, called the "Digilog", which can be programmed for a variety of digital operations and automatically controlled by externally generated commands. The main components of the Digilog are an input register, a buffer memory, a digital magnetic tape deck, and controlling circuity programmed by a separate patch board for each particular application.

5.2 Mean Voltage Measurements via Frequency

5.2.1 Object and procedure. The first playback operation on the analog tapes was a measurement of average (mean - mean, see

section 4.2.1) voltages on the four hot-wire channels, in order to identify the sources of voltage drift during recording. The same operation also afforded an opportunity to check the quality of the clock signal and to edit the tapes. This measurement of mean-mean voltages proved to be a valuable independent check on an equivalent measurement made later on by averaging over digital sampled data. Since each data section was preceded and followed by a calibration section, it was possible at an early stage to separate drift in the hot-wire signals from drift in the recording electronics.

To avoid the effects of additional drift in the F.M. playback electronics (which convert the frequency-modulated carrier signals to analog voltages), and to simplify the problem of obtaining reliable measurements of average voltage, the following scheme was adopted. The four hot-wire channels (F.M. recorded) and the clock channel (direct recorded) were played back through direct-reproduce electronics, which simply reproduced the actual frequencies recorded on the tape. These five frequencies were simultaneously averaged by five counters in the Scanner. Because the maximum counting rate acceptable to the counters was 30 kc/sec, the maximum allowable playback speed was limited to 15 inches/sec (twice the recording speed). At this tape speed the positive extreme values in the hot-wire signals corresponded to nearly 20 kc/sec.

The spiral-turbulence data sections were therefore played back at 15 inches/sec, and the counters were gated on for 50 seconds at 3-minute intervals, producing a 100-second (real time) average that could be read directly as average frequency. The counting interval

was timed internally, using a 6,000 cycles/sec clock signal in the Scanner, and was automatically measured and recorded for each frequency measurement. When the counting interval ended, the five counts remained displayed on the counters until the "Single Scan" button was pushed, at which time the counter readings were multiplexed and written on a digital tape, and the counters were cleared for the next counting interval. The scanner was controlled manually for this application, as the internally generated scanning rate available was much too fast (20 scans/sec).

The calibration sections were played back at 7-1/2 inches/sec to allow time for performing the manual operations necessary to sample the frequencies three times in 15 seconds for each input voltage calibration step.

The binary information on the resulting digital tapes was converted to decimal form and printed out by an IBM 1401 computer, which listed the frequencies read on each channel with corresponding counting-time intervals, as well as identification numbers for the data sections and calibration sections of each tape.

5.2.2 Analysis. The variation in measured frequency for three (or more) consecutive readings of the same calibration step was normally about one part in a thousand. Typical overall variation in three hours of recording is illustrated in figure 18, in which measured center frequencies are plotted versus time for one tape. Using linear interpolation in these values between adjacent calibration steps in each calibration section and between calibration sections (see Fig. 18), the

hot-wire channel frequencies read in the data sections were converted to mean-mean wire voltages and plotted versus time for each tape. The results for two typical tapes are plotted in figures 19a and 19b (with data from a later operation). The curves fair nicely into the mean-mean voltages (referred to bucking voltages; see section 4. 1. 2) measured directly with a digital voltmeter at the beginning and end of each tape. Most of the tape-recorder drift is removed by referring mean-mean frequencies to calibration frequencies, interpolated linearly between calibration sections. The remaining drift is strongly correlated with small changes in the ambient air temperature measured during recording. This residual drift is as large as 3 millivolts in 3 hours for some of the tapes; it is due (a) to thermometer effect, caused by relatively strong dependence of wire temperature loading (and hence voltage, for constant Nusselt number) on ambient temperature ($\partial N_u/\partial T \simeq 0.01/^\circ C$, for a wire overheat of 100° C), and (b) to drift with temperature and time of the transistorized hot-wire amplifiers. These two effects can be separated, since the thermometer drift should be closely correlated for the four wires.

The scatter in the mean-mean frequencies is consistently about 0. 3 percent and is frequently closely correlated for all four hot-wire channels for a given counting interval. This behavior can be explained by observing that the strong low-frequency component of the signal (Fig. 2) produces a significant difference in the contribution to mean voltage from the laminar and turbulent parts of a cycle. The counting interval does not in general cover an integral number of cycles of the flow pattern, since the 100-second interval is not an integer multiple

of the basic period. Only rarely would the normal dispersion in the pattern cause the averaging interval to begin and end at the same location in the cycle, e.g., on a given interface. For example, for the flow in figure 2 the estimated difference in average frequency between laminar and turbulent parts of a cycle is roughly 1/4 of full scale or 1,350 cycles/sec. If the counting interval happened to differ by half a cycle (1.5 seconds) from an integral number of cycles, the difference between the measured frequency and the true mean-mean frequency would be of the order of (1,350) (1.5) = 2025 counts or 20.25 cycles/sec. With a center or average frequency of about 6,750 cycles/sec, the scatter or difference from the true average would be $20/6,750 \simeq 1/300$, which is the size of the observed scatter. If the signals for all four wires looked roughly the same, scatter due to this cause would be closely correlated.

The variation in the measured average clock frequency during playback was generally less than one part in a thousand for an entire tape, as illustrated by the examples in figures 19a and 19b. This overall variation, which is an order of magnitude larger than the uncertainty in the frequency source, was due primarily to slow variations in average tape speed and to a much lesser degree to occasional "dropouts" or lost counts due to defects in the oxide coating of the tape. Prolonged visual inspection of the clock signal while averaging confirmed that the dropout problem was not serious and that the clock signal was suitable for use as a time base for further operations on the tapes.

5.3 Measurement of Characteristics of the Initial-Sample-Pulse Train and the Interface Structure

5.3.1 Object and procedure. The object of the second playback operation on the analog tapes was to measure the mean period of the NRZ signal and the time intervals between each initial sample pulse and the beginning of turbulence at (1) the phase-monitor probe and (2) hot-wire No. 2 on the main data probe (see sketch in Appendix A). The mean NRZ period was needed to select the sampling frequency for the digitizing operation, while the average time between the NRZ pulse and the beginning of turbulence at the phase-monitor probe was needed to remove an uncertainty in tangential coordinate, arising in the filtering operation used to generate the NRZ. By playing back the tapes in both the forward and reverse directions, the average time between the NRZ and the beginning of turbulence at hot-wire No. 2 determined the mean shape of the interfaces and furnished an independent measurement of the intermittency factor as a function of radius. The same operations on the sweep-angle tapes furnished information about the interface velocity and geometry as a function of the length of the cylinders.

All time measurements were made in terms of the clock signal on the tapes. The analog tapes were played back at 60 inches/sec (8 times the recording speed) and the resulting 80,000 cycles/sec clock signal was used to drive a free-running counter in the Digilog. It was necessary first to divide this playback clock frequency by a factor of four (using two flip-flops), as the Digilog counter was not designed to

transfer information reliably while counting at a rate greater than 40,000 cycles/sec. Pulses generated by the occurrence of an NRZ, or by the beginning of turbulence at either hot-wire, transferred the instantaneous reading of the counter to the Digilog memory, along with a flag identifying the source of the transfer pulse as NRZ, phase-monitor probe, or hot-wire No. 2. The Digilog then wrote the transfer times and the accompanying flags serially on a digital tape.

The NRZ transfer pulses were generated from the delayed NRZ signal[7] by a Hewlett Packard 212A pulse generator, using either the positive- or negative-going transition of the NRZ to produce an output pulse compatible with Digilog logic (0 to -6 volts, 10 microsec. duration).

The beginning of turbulence for the two hot-wire signals was detected by passing each of the signals first through a Kronhite band-pass filter (model 310-AB) adjusted for a lower cutoff frequency of 40 cycles/sec and an upper cutoff of 200 cycles/sec. This produced a flat laminar portion for each cycle (low cut-off) and eliminated the noise level (high cut-off) as a factor in detection of interface position. The signal was then passed through an amplifier and full-wave rectifier circuit to allow detection of the interface position for both positive- and

[7]A first pass through this operation showed that the distribution of NRZ pulses sometimes overlapped (in time) the distribution for the pulses associated with one of the interfaces being detected. Unremedied, this situation could have greatly complicated the computer program, and errors would have been introduced by the fact that the Digilog logic circuitry could not accept pulses separated by an interval less than 80 microsec. For this reason, in the definitive runs each NRZ pulse was delayed by a constant time interval so that the three distributions of pulses were well separated.

negative-going initial fluctuations using standard oscilloscope triggering. Each of the resulting signals was then displayed on an oscilloscope set to trigger on the beginning of turbulence, which was defined as a small fixed voltage level relative to the original hot-wire signals from the hot-wire amplifiers. Using information about the distributions for interface position and NRZ pulses obtained from the first (rough pass through the data) the sweep time of each oscilloscope was set so that the scope reset itself during each laminar interval to await the next burst of turbulence. At the start of its sweep, each scope produced a 0 to +20 volts pulse, which was converted to a compatible Digilog signal by a pulse generator in the same manner as the NRZ.

Measurements of the type just described were made in both forward and reverse directions for each tape. Identification numbers to identify the analog tape, the data section, and the direction of playback were recorded on the digital tape along with the primary data; i.e., the transfer times and identification flags.

The resulting digital tapes were processed by an IBM 7090 computer. The quantities calculated were the distribution function and the first two moments (mean value and dispersion) for the NRZ interval and for the two time intervals between the NRZ and the laminar-turbulent interfaces. In addition, serial correlations were computed for successive NRZ intervals (see appendix B). A second computer run was made with the program slightly modified to compute the distribution function, mean value, dispersion, and correlations for the hot-wire No. 2 intervals without reference to the NRZ pulses.

5.3.2 Sample pulse data; influence of main probe on interface velocity. The mean NRZ period, like the period of rotation of the two cylinders, varied at most by one or two parts in three thousand for different data sections of a given analog tape. The normalized dispersion, $\sigma/\overline{P}$, of the NRZ intervals for different tapes varied from a low of 0.022 to a high of 0.027, indicating that the initial sample commands were generated in a uniform and consistent fashion for all the tapes, and confirming the single preliminary observation (Fig. 9). The number of sample pulses in each data section was printed out for each tape pass and served as a check on the number of intervals to be expected in the digitizing operation.

These data also uncovered a weak dependence of the interface angular velocity on the location of the data and monitor probes (Fig. 20 and table I). When the two probes were mounted on the outer cylinder, the turbulent pattern rotated faster than when the probes were mounted on the inner cylinder. This result is consistent with the previous observation that the average angular velocity of the turbulent spiral behaves qualitatively like the mean velocity, as the drag and resulting wakes due to the probes would increase the mean velocity with the probes on the outer cylinder and decrease it with the probes on the inner cylinder. Since the variation in the angular velocity of the turbulence, ω_t, (and therefore the cumulative influence of the probes on the flow) is a fraction of one percent, the influence of the probes appears to be relatively unimportant for the present experiment.

This conclusion was further substantiated by the NRZ data from the sweep angle tapes. In figure 17, the increase in interface velocity

with decreasing length of the cylinders, as observed with the velocity data probe at r = 16.47 inches, is compared with preliminary data obtained with a considerably smaller probe (single hot-wire, 0.042 inch diameter stem) at r = 17 inches. Although the values of R_i are not exactly the same for the two sets of data, $\omega_t/(\omega_o + \omega_i)$ is practically independent of R_i in the range considered (Fig. 10) and the increased drag of the larger probe appears to have increased the angular velocity of the turbulence by at most a fraction of one percent over the values observed with the smaller probe.

5.3.3 Mean interface geometry. The data for the mean interface position are plotted in figure 21, which shows the mean cross-sectional shape of the interface pattern computed from the forward and reverse passes through the tapes. The mean cross section of the turbulent volume of fluid is roughly antisymmetrical around r = 17 inches, so that the interface pattern looks about the same when observed by probes mounted on either of the two cylinders. Viewed from the laboratory, a tail of turbulent fluid near r = 16.5 inches is stretched out in the direction of motion of the inner cylinder, while a nose near r = 17.5 inches is stretched out in the direction of motion of the outer cylinder. This fact can be made even more striking by plotting the same cross section in the physical coordinate system shown in figure 22. It should be kept in mind that the mean interface is sharply swept in two directions, so that if the dispersion in interface position and length of turbulence is due mainly to motion of the interfaces normal to themselves, a relatively small normal motion is required to produce

the observed circumferential dispersion. At r = 17 inches, for example, a normal displacement of the trailing interface (rear of the turbulent volume of fluid) of 0.25 inch would give rise to a fluctuation $P-\overline{P}$ equal to the observed dispersion, $\sigma/\overline{P} = 0.067$.

5.3.4 Interface dispersion and correlations. The dispersion in interface position as observed by the velocity probe (hot-wire No. 2) is plotted in figure 23 for both the forward and reverse passes through the analog tapes. The dispersion in the leading interface (the front of the rotating volume of turbulent fluid; upper half of Fig. 22) is considerably smaller at all radii than the dispersion in the trailing interface (lower half of figure 22). This is the first evidence of any significant difference in the structure or behavior of the various interfaces separating the laminar and turbulent regions of the fluid.

In figures 24 and 25, the dispersion in the position σ_p of the interfaces is compared with the dispersion in the time interval between each NRZ and the immediately following transition from laminar to turbulent flow. In all cases, the dispersion in the latter quantity is 15 to 25 percent less than the dispersion in interface position. These data also nicely illustrate the point that the dispersion in the time interval between pulses from two positively correlated, but individually random, pulse trains is less than would be obtained if the two generating events were independent. This is not at all surprising in the present case, as the generation of an NRZ depends on an integral property of the flow pattern, namely, the fundamental frequency, which is highly correlated with the interface positions.

The magnitude of the characteristic time scale of the random fluctuations in interface position can be inferred indirectly from the computed serial correlations between the time intervals, P_n, whose end points are determined by successive interface positions. The normalized correlations $\langle \delta_n \delta_{n+\nu} \rangle / \langle \delta_n^2 \rangle$, where $\delta_n = P_n - \overline{P}$ and $\langle \delta_n^2 \rangle = \sigma^2$, were computed for values of ν from 1 through 10. As shown in figure 26, the correlation between the lengths of the intervals becomes essentially zero for $\nu \geq 2$ and the general behavior of the correlations agrees favorably with preliminary results obtained by hand computation for a single case. The latter data were obtained from a preliminary tape recording (at nearly the same radial location and Reynolds number) using the intermittency meter as described in section 3.6. The correlation between adjacent intervals ($\nu = 1$) lies consistently between -0.45 and -0.52 for all radial locations (Fig. 27), indicating that an interval longer than $\overline{P}$ is likely to be immediately followed by an interval shorter than $\overline{P}$.

The observed correlations correspond fairly closely to what would be expected if the characteristic time scale (correlation time) for the random fluctuations in interface position is appreciably less than the time, P_n, required for the probe to traverse the flow pattern. This assumption implies (appendix B) that $\langle \delta_n \delta_{n+1} \rangle / \langle \delta_n^2 \rangle = -0.5$ for $\nu = 1$ and $\langle \delta_n \delta_{n+\nu} \rangle / \langle \delta_n^2 \rangle = 0$ for $\nu \geq 2$. These results, which are independent of the distribution function of P, explain how a strong first order ($\nu = 1$) correlation and negligible higher order correlations can obtain when a random variable is observed periodically and (compared with the correlation time for the fluctuations) relatively infrequently. The observed correlation of -0.45 to -0.52 for adjacent intervals, and the small values of the higher order correlations, indicate that the assumption that the interface memory or correlation time is less than P_n is probably nearly satisfied.

5.4 Sampling and Digitizing of Recorded Analog Signals

5.4.1 General considerations. The final and crucial playback operation on the analog tapes was to sample simultaneously the four hot-wire signals from the main data probe, or the corresponding four calibration voltages. The sampled analog voltages were multiplexed, converted to digital values by an analog-to-digital converter, and written on a digital tape by the Digilog. The analog tape ran continuously, and the whole sampling process was fully automatic except for one or two manual switching operations to change from a data-sampling mode to a calibration mode or vice versa.

An important element of the system was a sample-command generating loop, whose function was to generate a standard group of samples on receiving a command in the form of an NRZ pulse. The voltages were sampled, depending on the tape, at about 60 equally-spaced points in each cycle of the flow, giving a spatial resolution of about 6 degrees or 1.7 percent of the circumference at a fixed radius in the annulus. Since the dispersion in the interval between successive observations of the same interface was of the order of 5 percent, this resolution was felt to be more than adequate. The choice of 60 points per cycle was actually dictated by the fact that this sampling rate was near the upper limit of the Digilog performance in terms of conversion time, writing rate, and total capacity of the output tape. Since voltage samples could be discarded later by a simple specification in the computer program, no penalty was incurred by obtaining the maximum number of samples. Furthermore, the additional samples obtained

near the interfaces may be useful if it is ever desired to study these regions in more detail.

During the sampling of the spiral-turbulence data, the clock signal on the analog tape was used as the time base for generating the sample commands. For convenience in normalization and curve fitting of the final data, an integral number of samples per cycle was desired for each tape. The number of clock cycles in the mean NRZ period for each tape, divided by the number of samples desired per cycle, gave the number of clock cycles to be counted between samples. This number, which was also required to be an integer,[8] was selected on a recycling preset counter that generated a sample command each time it reached its preset count. During the recorder calibration sections, the clock signal was absent from the analog tape, and an external oscillator was used as a clock to generate uniformly spaced sample commands in a similar manner.

For the turbulence data, each group of 60 or so samples, corresponding to one cycle or one member of the ensemble, was initiated by the occurrence of an NRZ pulse (this and several of the following points are illustrated in figure 34). Not all of the NRZ pulses could be used as initiating commands in a single pass through the tape, because the NRZ's were not equally spaced, and groups of samples based on the

[8]For each tape, the number of samples per cycle was selected in the range 56-65 (see table I) to make the cumulative round-off error in the position of the last sample less than 0.1 percent of the mean period. For tape C (r = 16.248 inches), for example, the mean period was 2.927 seconds or 7,317 cycles of the reduced clock signal. For 59 samples taken 124 clock cycles apart, the round-off error was 1 clock cycle.

mean NRZ period would interfere with each other whenever a short NRZ interval occurred. It was therefore decided to use alternate (odd-numbered) NRZ pulses, and to minimize the resulting loss of information by increasing the number of samples in each group, leaving their spacing unchanged, to cover part of the next cycle of the flow. The two shortest NRZ intervals for each tape were known, from the previous playback operation (see section 5.3.1), and in all cases it was found that the number of samples in each group could safely be increased by 60 percent or more. This procedure also furnished an additional check on the data, since the ensemble averages should be periodic, with later values repeating those at the beginning of the cycle. In addition, the extra data could be useful if it is later desired to concentrate attention on samples taken near the interfaces, as the amount of such data was increased (in the most favorable case, doubled) by extending the number of samples in each group. For each tape, the total number of samples in each pair of adjacent cycles of turbulence (see table I) was selected on a second preset counter. The tape recorder and command loop ran continuously during each playback run. Since it was not convenient to clear the preset counters manually after a calibration section, the first group of samples in any data section always contained fewer than the standard number of samples. It was simpler to delete this small amount of data in the computer than to eliminate it during the sampling operation.

In addition to the four hot-wire channels from the tape recorder, a fifth input, consisting of a constant D.C. reference voltage, was sampled by the multiplexer and converter. This constant voltage

turned out to be extremely useful as a synchronous reference channel for later operations on the digital tapes.

Each of the voltage samples consisted of 10 binary bits plus sign. The maximum resolution (least significant bit) of the A-D converter was 2.5 millivolts. Since samples of the constant reference voltage tended to be constant or to fluctuate between two values 2.5 millivolts apart, the noise or uncertainty in the multiplexer-converter-digital-tape system was effectively equal to half of the least significant bit. The full-scale range of the converter (Packard Bell M-2 Multiverter) was ±2.56 volts, or about twice the range of the recorded hot-wire data after amplification by a factor of 20 to 30.

5.4.2 Operation of sampling system. The analog tapes were played back at the maximum available playback speed of 60 inches/sec. The operation of the sampling system during the data sections of the analog tapes is shown in the schematic diagrams in figures 28 and 29. The external calibration clock was switched off. Flip-flop A halved the frequency of the NRZ, whose remaining positive-going transitions gated on the 20 kc/sec clock (divided down from the playback frequency of 80 kc/sec to be safely within the limitation of 40 kc/sec for preset counter A) and also stepped the NRZ serial-number counter in the Digilog. Upon reaching its preset count, counter A recycled and triggered pulse generators A and B. The output of pulse generator A simultaneously closed the four transistor switches, thereby connecting the tape-recorder outputs to the sample capacitors and allowing them to charge to the output voltage of the tape recorder. The output of

pulse generator B (delayed 100 microseconds[9] from the output of pulse generator A) opened the transistor switches, leaving the capacitors charged to the sampled voltages; it also stepped preset counter B (counting samples), and triggered a burst of five 20 kc/sec "convert" pulses in the Digilog, causing the multiplexer to step and the A-D converter to read and convert sequentially the five inputs to the multiplexer. The speed of the multiplexing and conversion cycle was independent of the sample rate (prescribed by the clock frequency and by preset counter A). The time required for sampling and converting the five channels was about 4,000 microsec out of the 6,000 microsec available between sample commands. Upon reaching its preset count, counter B, which determined the number of samples taken in each group, reset both itself and flip-flop B, gating off the 20 kc/sec clock. The next positive-going NRZ edge then started the entire cycle over again. As each NRZ pulse stepped the serial-number counter in the Digilog, the current serial number was written on the digital tape ahead of the corresponding group of samples.

At the beginning of a calibration section, the calibration clock was switched on manually, and the flip-flops were also reset, so that the 20 kc/sec clock (now the voice channel) was gated off. The sampling and conversion sequence was the same as for the turbulence data, but the number of samples taken was controlled by the external clock frequency (set to produce 6 or 7 samples for each step in calibration

[9]The sampling aperture of 100 microsec, or 0.0008 seconds in real time, was chosen to be a small fraction of a cycle for the highest frequency of interest for the hot-wire signals, which was about 200 cycles/sec.

voltage). Preset counter A again determined the time between samples, but preset counter B and flip-flops A and B had no effect on the operation. Sampling in this mode continued until the low-frequency external clock was switched off manually at the end of the calibration section.

As the samples were obtained, the digital outputs of the A-D converter and NRZ-serial-number counter were continuously shifted from the Digilog input buffer register into the Digilog memory. Each time the memory was filled (about every 60 samples) the Digilog tape unit wrote the contents of the memory in serial order as a fixed-length record on a digital tape.

5.4.3 Digital Tapes. A separate digital tape was made for each of the 20 analog tapes. Three of the analog tapes were processed twice. Tape K_o (r = 17.122 inches; probe on outer cylinder) was run twice to check the repeatability of the sampling process; tape M (r = 17.374 inches; probe on inner cylinder) was run both forward and backward; and tape L' (r = 17.250 inches; probe on inner cylinder) was run at normal speed and at a reduced playback speed of 30 inches/sec. Each of the resulting 23 digital tapes consisted of about 1,500 groups of samples, or members of the ensemble, each group containing about 100 samples, each sample consisting of four hot-wire voltages and a reference voltage. Because of the effort required to generate these 23 digital tapes, they have been classified for practical purposes among the raw data of the experiment. In binary form, the digital information on these tapes amounts to about 180,000,000 bits.

voltage). Preset counter A again determined the time between samples, but preset counter B and flip-flops A and B had no effect on the operation. Sampling in this mode continued until the low-frequency external clock was switched off manually at the end of the calibration section.

As the samples were obtained, the digital outputs of the A-D converter and NRZ-serial-number counter were continuously shifted from the Digilog input buffer register into the Digilog memory. Each time the memory was filled (about every 60 samples) the Digilog tape unit wrote the contents of the memory in serial order as a fixed-length record on a digital tape.

5.4.3 Digital Tapes. A separate digital tape was made for each of the 20 analog tapes. Three of the analog tapes were processed twice. Tape K_o (r = 17.122 inches; probe on outer cylinder) was run twice to check the repeatability of the sampling process; tape M (r = 17.374 inches; probe on inner cylinder) was run both forward and backward; and tape L' (r = 17.250 inches; probe on inner cylinder) was run at normal speed and at a reduced playback speed of 30 inches/sec. Each of the resulting 23 digital tapes consisted of about 1,500 groups of samples, or members of the ensemble, each group containing about 100 samples, each sample consisting of four hot-wire voltages and a reference voltage. Because of the effort required to generate these 23 digital tapes, they have been classified for practical purposes among the raw data of the experiment. In binary form, the digital information on these tapes amounts to about 180,000,000 bits.

The Digilog wrote a standard half-inch, 7 track, low-density tape (200 bits/inch) suitable as input to an IBM 7090 computer. The tape format is illustrated in figure 30. The individual voltage samples, each consisting of 10 bits plus sign, occupied the first 4 tracks of the tape. The bit-packing scheme adopted required a minimum amount of tape while preserving a simple logical form that could be easily read in later operations. A separate track was reserved for the counter transfer flags marking the position of each NRZ serial number. This track was also used at the beginning of each tape file for identification numbers specifying the tape and the data section.

5.5 Corrections and Further Operations on Digital Data

5.5.1 Corrections. The digital voltage samples in the calibration sections of each digital tape were printed out in decimal form by an IBM 7090 computer. From a study of these values, two systematic extraneous effects on the values of the sampled voltages were discovered and eventually traced to deficiencies in the sampling system. Fortunately, it was possible to establish that corrections derived from the calibration data could also be applied to the turbulence data, as sampling tests run at various sample rates showed both effects to be independent of the sampling rate. The first, and smaller, systematic effect was a serial interaction between multiplexer channels, causing the voltage read on one channel to depend slightly on the voltage read on the preceding channel during the same sample. This interaction probably occurred during the multiplexer crossover time, during which the channel about to be sampled by the A-D converter and the one

just previously sampled were momentarily connected together. This defect appeared incorrectable with the hardware provided. Normally, the four tape recorder channels had been connected to a common D.C. calibration source during recorder calibration sections. Had it not been for certain variations on this procedure, during which each of the four inputs was varied separately, the interaction between channels might have escaped detection altogether. The effect was detected in calibration data for which the input voltage to one or more channels had been temporarily disconnected (essentially zero volts input) while the input level common to the remaining channels took various values. An example of the raw sampled voltage data, which clearly exhibits this interaction, is plotted in figure 31. For this case, the inputs to the hot-wire channels were disconnected one at a time in serial order (hot-wire 1 out for identification purposes; hot-wire 2 out, etc.) while the input voltage to the other channels remained constant at its maximum negative value. As is evident from figure 31, the interaction was confined to adjacent channels. The unperturbed channels show a nearly constant reading of the D.C. input level, with a noise level of one or two least significant bits of the A-D converter reading. The noise is usually well correlated between channels, indicating that the noise source is (analog) tape flutter.

Since the input voltages during sections of the calibration data like that in figure 31 varied from tape to tape, the printout information was sufficient to accurately determine the dependence of the sampled voltage for each channel on the reading of the preceding channel. No correction was necessary for the hot-wire No. 1 channel, as the input

to the preceding channel (constant reference voltage) did not vary. The correction for the voltage read on channel i during the n^{th} sample was successfully represented by a linear function of the reading on the previous channel according to the formula

$$\epsilon_i^n = e_i^n - \frac{\Delta e_i}{\Delta e_{i-1}} e_{i-1}^n$$

where e_i is the raw sampled voltage and ϵ_i is the voltage corrected for channel interaction. Each $\Delta e_i / \Delta e_{i-1}$ was a weak linear function of e_i with an average value of about 0.02 over the range of the data. For comparison with the raw data, the corrected values, ϵ_i, are also plotted in figure 31. As illustrated by these data, the corrections essentially eliminated the effects of channel interaction, as the residual coupling between channels was reduced to a level comparable to the noise level of the data.

A second, and larger, systematic error in the sampled voltages was produced by coupling the recorder, which had a relatively high output impedance, directly to the 0.01 microfarad sample capacitors (time constant ~36 microsec). Following a change in voltage, the capacitors did not charge to the full value of the recorder output voltage in the 100 microsec allotted, and the reading on each channel was therefore influenced by the preceding reading on the same channel. This effect could have been avoided by proper impedance matching, using a buffer amplifier in each channel between the tape recorder and the sample capacitors. The effect was discovered from the fact that the first one or two sampled voltages following a step change in input

voltage always fell short of the equilibrium values, as illustrated by the example in figure 32. Analysis of many such jumps in the calibration sections showed that the final corrected voltage (E_i^n) for the n^{th} sample could be related to the ϵ_i by the formula

$$E_i^n = \epsilon_i^n + C_i\left[\epsilon_i^n - \epsilon_i^{n-1}\right]$$

The C_i are weak functions of ϵ_i^n, taking values between 0.065 and 0.130. For comparison with the raw data, the corrected values, converted to input levels (I_i) as described in section 5.5.2 are shown in figure 32. The final corrected values faithfully reproduce the known input values, and the extraneous effects have been eliminated.

It should be noted that the formulas given above for the corrected voltages use only raw voltages from the Digilog tapes, so that each correction is independent of the previous one, and errors do not propagate.

The great amount of effort expended in deriving and applying corrections for both effects could probably have been avoided by using correctly buffered commercially available sample-and-hold circuits instead of the untested and poorly matched components provided.

5.5.2 Recovery of input voltages. Using a standard least-squares curve-fit program, a cubic curve was fitted to the corrected calibration data for each hot-wire channel for each calibration section of each tape (416 curves in all). These curves were of the form $I_i = A_i + B_iE_i + C_iE_i^2 + D_iE_i^3$, where I_i was the known input calibration on hot-wire channel i, E_i was the corrected sampled voltage on the

same channel, and A_i, B_i, C_i, D_i were constants. Several examples of these curves, which express the overall transfer functions of the recording, playback, and sampling operations, are shown in figure 33. The cubic provided an excellent fit in all cases. The calibration curves extended well beyond the range of the hot-wire data, which lay within the nearly linear region of each curve. In the range of the hot-wire data, the residual differences between the actual I_i and corresponding points on the fitted curves were normally less than 0.1 millivolt, and the standard deviation determined from all points in a given curve fit was typically 0.1-0.2 millivolts. These discrepancies are comparable to the resolution of 0.1 millivolt for the digital voltmeter used in the hot-wire calibrations. They are also comparable (allowing for D.C.-amplifier gain) to the resolution of 2.5 millivolts for the A-D converter used in the sampling operation.

The information on the digital tapes was next processed by an IBM 7090 program which applied corrections and curve fits to all the data in both the spiral turbulence and the calibration sections of each tape, in order to recover the hot-wire and calibration voltages in the original laboratory situation. To retain the desired accuracy in the data, it was necessary in each turbulence data section to interpolate linearly in the coefficients A_i and B_i of the curve fit, using the values in the preceding and following calibration sections. For C_i and D_i, average values were sufficient. The computed input voltages to the recorder and the corresponding NRZ serial numbers for the Digilog tapes were written on a second group of digital tapes which, together with the hot-wire calibration data, constitute the input to the program

for converting hot-wire voltages to velocity components. Since the 7090 computer wrote high density tapes (~500 bits/inch), it was possible to compress the data from two Digilog tapes onto a single tape, and this operation yielded 12 input voltage tapes[10] corresponding to the 23 Digilog tapes. The constant synchronous reference voltage, which was used to keep the computer operation in step with the data, was transferred without modification to the new tape to serve the same purpose in later operations.

The calibration sections of the tapes were again printed out to verify that only the known input voltages appeared there, and to see how well the corrections had been applied. Both corrections satisfactorily increased the accuracy of the data, restoring it to a level comparable with that obtained in the hot-wire calibrations. The residual uncorrectable errors in the turbulence data were estimated to be comparable to the noise level in the original recorded data.

The results of the sampling and computer operations up to this point are illustrated graphically in figure 34, in which the digitized input voltages for one hot-wire (hot-wire No.4 on the main data probe) in final corrected form have been plotted for the first few NRZs in the first data section of tape F' (r = 16.623 inches). For comparison, the same figure includes oscillograph records of (a) the corresponding continuous hot-wire signal from which the digital samples were obtained and (b) the NRZ signal which controlled the sample-pulse generating

---

[10] These 12 tapes are known as "Rodeo" tapes, inasmuch as the bucking voltages (see section 4.1.2) have not yet been taken into account.

loop. If all of the digital data were to be presented in this way, about 50,000 plots like figure 34 would be required.

5.6 Mean Voltage Measurements via Sampled Data

As a further check on the overall soundness of the sampled and corrected spiral-turbulence data, the voltages for each hot-wire were averaged by an IBM 7090 computer to produce a time average equivalent to the mean-mean voltages already measured directly and also inferred from the F.M. frequencies on the analog tapes (section 5.2). From each group of samples associated with an NRZ, just enough (the first 60 or so) were taken to span one average period of the flow. This was done for successive groups of 50 NRZs, and the computed input voltages in each group were averaged for each channel. These averaged sample voltages correspond to the previous time averages (via frequency) of the analog signals. In addition to the discrete nature of the digital averages, there was one other basic difference between the two kinds of averages. The digital averages covered a time interval equivalent to an integral number (50) of mean periods of the flow pattern, tending to decrease the dispersion below that encountered in the frequency measurements. There is good agreement between the two sets of data obtained from the playback operations, as shown in figure 19.

5.7 Program-Error Identification

In addition to the printouts of the data in the calibration sections and the averaged data for each channel in the spiral-turbulence

sections of each tape, several other checks were employed to ensure the correctness of the input voltages I_i computed from the Digilog data.

The computations were checked in detail for the spiral-turbulence data by printing out the results of various steps in the program and comparing with hand calculations done on a desk calculator. Voltages from the Digilog tapes, printed out using a standard program known as a tape dump, furnished the input for the hand calculations. The final results of the calculations (I_i) then served as a check on the data printed out from the Rodeo tapes. Larger blocks of data from both the Digilog and Rodeo tapes were printed out to verify the overall correctness of the tape formats (order of hot-wire channels and reference voltage, number of samples per NRZ, etc.). However, in spite of these and other precautions taken to check the programming, a good deal of time was lost when, in several instances, large quantities of input-voltage data (I_i) were computed before certain programming difficulties were uncovered. The detection and investigation of these errors were based on clues uncovered during initial runs of the data-averaging program, which included a printout of the number of times the computer failed to find a synchronous reference voltage at the proper location in a sample. Based on these findings, the Rodeo program was revised and all the Rodeo tapes were generated anew. The averaging program was also revised and extended to include a printout identifying the nature and location of all errors in tape format.

The sources of erroneous data generated by the computer program itself were (a) programming errors, which were corrected before making the final, definitive runs, and (b) infrequent tape-handling

errors, which were not entirely eliminated. Initial runs of the averaging program yielded occasional widely scattered values that were traced to faulty technique in discriminating on the synchronous reference voltage, allowing the computer to generate false information by operating out of step with the data. This problem was effectively eliminated by decreasing the size of the voltage window used to identify each reference voltage in both the Rodeo and averaging programs. The average values computed by the revised averaging program (see below) were free of the defects noted in the earlier runs. The computer tape-handling errors, which occurred at most once or twice in a given tape, were generated whenever (a) the IBM 7090 lost part of a Digilog record (probably because the Digilog had produced an inter-record gap whose length was not within the allowable limits for successful reading by the computer), or (b) the 7090 experienced difficulty in reading the Digilog tape and failed to recognize an NRZ flag. Although no cure was found for these difficulties, they occurred so infrequently that the small amount of unuseable information can be discarded without significant loss.

To identify occasional short sections of unuseable data generated by tape-handling errors, the averaging program was revised and extended to include a check of tape format for the entire tape. For each group of samples, the associated NRZ serial number was read from the Rodeo tape and printed out, followed by a series of binary symbols indicating success (0) or failure (1) in recognizing a synchronous reference voltage as the fifth voltage in each sample. Thus, an error-free group of samples was represented by a 3-digit number and

a row of 89 to 105 zeroes. The computer was instructed to print out the garbled sections of the Rodeo tape whenever one or more "1" entries occurred, and to omit the data in such sections from the computed averages. The results of this revised averaging program showed that the Rodeo tapes were relatively free of computer-generated errors. The printouts for 9 of the 23 tapes indicated no errors whatever in tape format, i.e., the correct number of NRZ records were present on the tape, each group of samples contained the correct number of samples, and the data remained in "synch" throughout the tape. Fourteen of the 23 tapes contained no computer-generated errors, but 6 of these tapes contained one or two groups of samples that were one sample short of the standard number (89-105). This type of error was traced to a Digilog malfunction in which the reference voltage was either misplaced or garbled for a given sample of five voltages. The 8 remaining tapes each contained at most one or two Digilog errors and one or two tape-handling errors. The tape-handling errors, which were confined to the data for one or two NRZs per tape, showed up in most cases as a long row of zeroes extending beyond the standard number of samples per NRZ, followed by a missing NRZ serial number. For a given tape, these errors did not always reoccur in the same places if the averaging program was rerun on the same Rodeo tape, indicating that they were probably due to occasional marginal compatibility between the Rodeo tape and the reading ability of the 7090, causing the computer to ignore an NRZ flag. Tape-handling errors produced unuseable data for about 20 of a total of roughly 35,000 NRZs. The relative frequency of occurrence of Digilog sample errors was about one in 10^5 (21 were found;

each tape contained roughly 150,000 samples). It will eventually be arranged for the computer to discard these defective data before or during the final operations used to generate digital velocity correlations and other quantities sought in the experiment.

VI. FUTURE OPERATIONS ON DIGITAL DATA

6.1 Check of Voltage-to-Velocity Conversion Scheme and Computation of Instantaneous Velocities

Before the input voltages I_i are converted to velocity components, the final values adopted for the constants in the conversion formulas (see Appendix A) will be checked by using the voltages measured during the hot-wire calibrations as input voltages (I_i) and comparing the computed magnitude and direction of the velocity with the known tangential calibration velocity and calibration probe-orientation. When satisfactory agreement between these data is achieved, the conversion program will be employed to compute instantaneous values of the velocity components from the data on the Rodeo tapes, each sample of four voltages yielding a single instantaneous measurement of the velocity components u, v (computed twice), and w. The computer program will write the velocity data on a third set of digital tapes that will serve as the input to the ensemble averaging program.

6.2 Ensemble Averages and Calculation of Energy Transfer

The velocity data derived from each original analog tape furnish about 1500 samples of the three velocity components at each of 56-65 circumferential points at the radius of measurement. The ensemble averages at each tangential point in the rotating coordinate system will be obtained by averaging the velocity data for corresponding samples in all the groups of samples (each group being identified with a particular NRZ serial number) on a given Digital tape. In order to calculate the energy transfer, the primary quantities to be computed

at each point are the mean velocities U, V, W and the six double products of fluctuating velocities (correlations) $\langle q_i' q_j' \rangle$, i = 1, 2, 3, j = 1, 2, 3. The mean velocity data will be curve fitted to obtain analytic expressions for the radial and circumferential variation of the three components of the mean velocity. Derivatives of the mean velocity components with respect to r and Θ will then be directly calculated, while derivatives with respect to z will be estimated using the results of the sweep-angle data (see section 4.1.6). The appropriate products of mean velocity derivatives and correlations of fluctuating quantities will then be computed and summed to determine the energy transfer at each point in the flow. Some other quantities of interest are the first few moments of the distribution functions for higher order correlations ($\overline{u'^3}$, $\overline{v'^3}$, $\overline{w'^3}$, etc.).

TABLE I

Tape	r (inches)	Date (1962)	R_o	R_i	$\overline{P}$ (sec)	$\frac{\omega_t - \omega_i}{\omega_o - \omega_i}$	No. of Samples Per Mean Cycle ($\overline{P}$)	Samples Per Group
FIRST WIRE ARRAY								
H_o	16.872	Sept. 24	50,000	5,630	2.820	0.4970	63	99
SECOND WIRE ARRAY								
A	16.081	Oct. 16	50,100	5,610	2.897	0.4969	63	102
B	16.136	Oct. 15	49,900	5,590	2.915	0.4969	65	105
C	16.248	Oct. 7	50,100	5,620	2.927	0.4966	59	96
D'	16.373	Oct. 6	50,100	5,600	2.919	0.4968	57	92
E'''	16.498	Oct. 8	50,200	5,620	2.941	0.4968	57	90
F'	16.623	Oct. 9	50,100	5,610	2.890	0.4968	56	90
G'	16.746	Oct. 11	49,900	5,600	2.907	0.4970	60	98
H_o'	16.873	Oct. 12	50,200	5,630	2.873	0.4967	63	103
J_o	16.999	Oct. 1	50,100	5,600	2.883	0.4969	60	97
K_o	17.122	Oct. 2	50,100	5,620	2.872	0.4969	63	98
THIRD WIRE ARRAY								
J_i	17.004	Nov. 15	50,100	5,620	2.959	0.4958	56	93
K_i	17.127	Nov. 14	50,000	5,590	2.951	0.4956	60	99
L'	17.250	Nov. 13	49,900	5,600	2.955	0.4956	61	101
M	17.374	Nov. 5	50,100	5,610	2.958	0.4954	56	89
N	17.500	Nov. 7	50,000	5,610	2.969	0.4952	58	95
P	17.626	Nov. 8	49,900	5,590	2.953	0.4951	60	99
Q	17.750	Nov. 9	49,900	5,590	2.953	0.4949	60	98
R	17.860	Nov. 10	49,900	5,600	2.957	0.4945	56	91
S	17.928	Nov. 11	50,100	5,610	2.975	0.4943	60	99

REFERENCES

1. Coles, D., "Transition in Circular Couette Flow", Harvard University, Contract Nonr-1866 (20), (1964).

2. Chandrasekhar, S., Hydrodynamic and Hydromagnetic Stability (Oxford at the Clarendon Press, 1961).

3. Schultz-Grunow, F., "Zur Stabilität der Couette-Strömung", ZAMM 39 (1959), pp. 101-110.

4. Coles, D., and Van Atta, C., "Distortion of a Laminar Couette Flow by End Effects" (to be published).

APPENDIX A

PROBE CALIBRATION

1. Velocity Probe

In principle, the three velocity components could have been measured in the present experiments with an array of only three hot-wires. Such a configuration would necessarily be unsymmetrical with respect to one or both of the natural planes of symmetry for calibration purposes (the orthogonal surfaces r = constant and z = constant), and each wire would be more or less sensitive to all three velocity components.

A double V-array of four hot-wires, on the other hand, has the advantage that each of the two (nearly) coplanar pairs of wires is most sensitive to the two components of velocity lying in the plane of the wires. The four-wire configuration also has the desirable property of redundancy, inasmuch as the circumferential component of velocity can be inferred twice from the four measured voltages. The assumption that each pair of hot-wires in a symmetrical configuration is primarily sensitive to only two velocity components is also very useful as a first approximation in analyzing both calibration and turbulence data.

2. Probe Calibration

Hot-wire calibrations were performed in laminar flow with the inner cylinder at rest, $\omega_i = 0$. The tangential profile in the calibration flow was accurately known from extensive measurements made with the same velocity probe (reference 4). The probe was calibrated

by varying the angular velocity of the outer cylinder, ω_o, with the probe at various fixed angles of pitch and yaw. Calibrations were made with pitch angles ϕ of 0, ±5, ±10 degrees and yaw angles ψ of 0, ±8, ±15 degrees. All of the 25 possible combinations of ϕ and ψ were employed during the calibrations, but the most extensive data are for variable ψ with $\phi = 0$, and for variable ϕ with $\psi = 0$. In particular, the probe was calibrated at zero pitch and zero yaw immediately before and after each of the twenty tapes.

3. Reduction and Correlation of Probe-Calibration Data

For fixed probe radius and orientation, the set of voltage measurements for all four hot-wires over a suitable range of speed is called a "point". The calibration data include 290 points in all (59 + 131 = 190 for the probe on the outer cylinder; 100 for the probe on the inner cylinder), each point representing about a half hour of running time. The data for three different velocities were first fitted to the formula $Nu_i = a_i + b_i R_{e_i}^{n_i}$ (usually called King's law), resulting in a set of values a_i, b_i, n_i ($i = 1, 2, 3, 4$) for each calibration point. From these results, standard values of the exponent n_i (usually in the range 0.5 to 0.6) were chosen for each wire, and a final set of a_i and b_i were determined using these values of n_i.

The original hot-wire Reynolds number, just referred to, $R_e = \rho V d/\mu$, is based on the magnitude of the tangential velocity V relative to the probe. The parameters a_i and n_i are presumably constant for each wire, while the b_i depend on probe orientation. This orientation is expressed by a set of values $\tilde{x}$, $\tilde{y}$, $\tilde{z}$, which give the

three velocity components, $\tilde{u}$, $\tilde{v}$, $\tilde{w}$, with respect to the probe in probe body coordinates: $\tilde{x} = \tilde{u}/V$, $\tilde{y} = \tilde{v}/V$, $\tilde{z} = \tilde{w}/V$. The quantities $\tilde{x}$, $\tilde{y}$, $\tilde{z}$ can also be expressed in terms of the angles of pitch and yaw, ϕ and ψ. The working hypothesis is that the hot-wire calibration should be universal in terms of the magnitude of the velocity component q normal to the wire, i. e.

$$Nu_i = A_i + B_i\left(R_{e_i}\right)^{n_i}$$

where $R_{e_i} = \rho q_i d/\mu$ is the hot-wire Reynolds number based on q_i, the component of velocity normal to the wire, and where $A_i = a_i$ and $B_i = b_i(V/q_i)^{n_i}$. The relationship between the velocities q_i and V depends on the orientation of the hot-wire with respect to the probe (defined by the angles β_i, γ_i shown in the sketch) and the orientation of the probe with respect to the flow defined by $\tilde{x}$, $\tilde{y}$, $\tilde{z}$. Specifically, the q_i are of the form:

$$q_i^2 = a_{i11}\tilde{u}^2 + a_{i22}\tilde{v}^2 + a_{i33}\tilde{w}^2 + 2a_{i12}\tilde{u}\tilde{v} + 2a_{i13}\tilde{u}\tilde{w} + 2a_{i23}\tilde{v}\tilde{w}$$

where the a_{ijk} are functions of β_i and γ_i. The angles β_i and γ_i were roughly determined by direct measurement, but for purposes of fitting the probe-calibration data the appropriate values are being inferred independently, using the observed response of each wire to changes in probe orientation. Constant values of β_i and γ_i are to be chosen and used with the known values of b_i, n_i, and $\tilde{x}$, $\tilde{y}$, $\tilde{z}$, to compute B_i from the expressions for the q_i. Appropriate values of B_i are then to be chosen, completing the correlation of the calibration data.

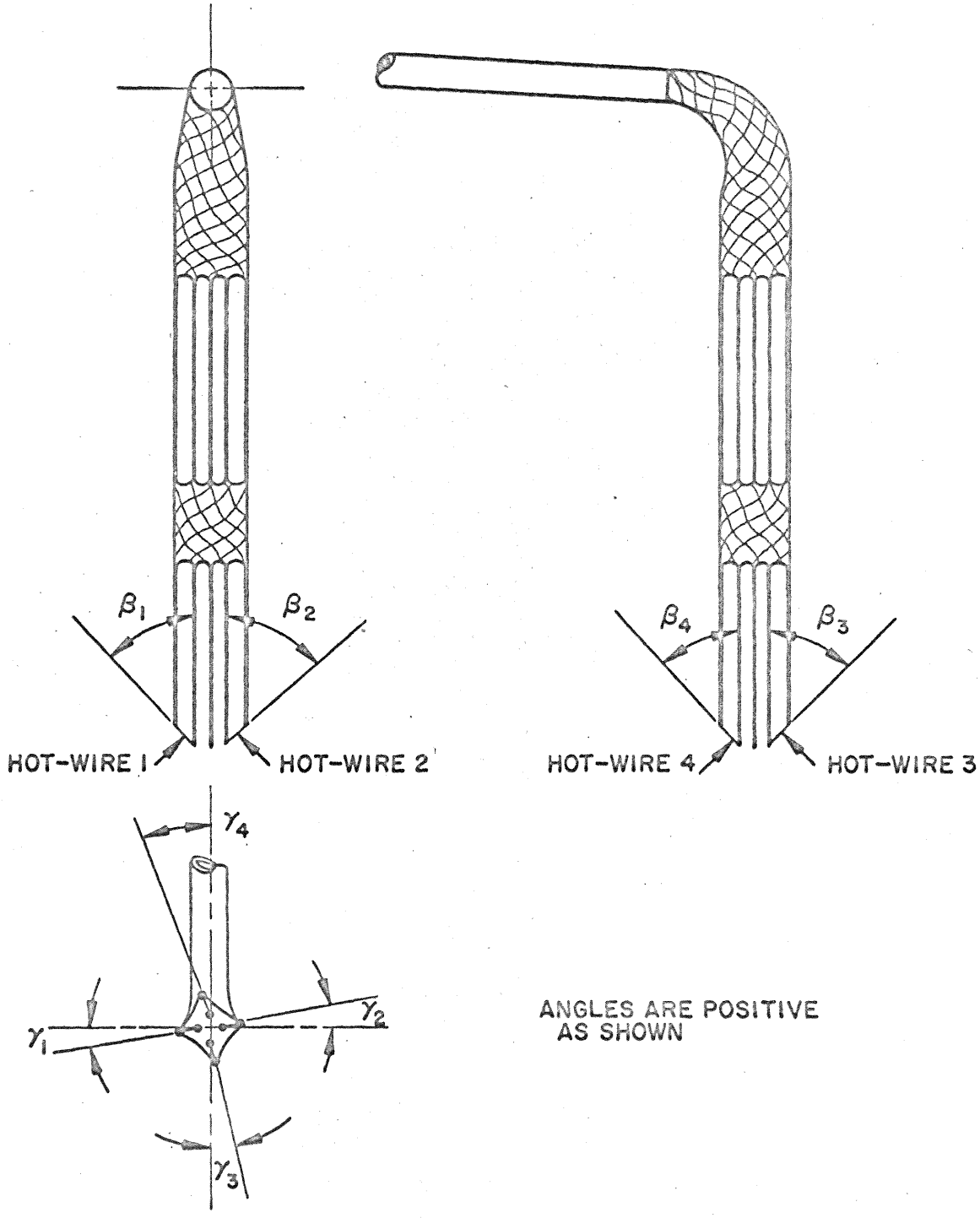
β_1
β_2
HOT-WIRE 1
HOT-WIRE 2
β_4
β_3
HOT-WIRE 4
HOT-WIRE 3
γ_4
γ_1
γ_2
γ_3
ANGLES ARE POSITIVE
AS SHOWN

4. Inversion of Correlated Calibration Data to Convert Sampled Spiral-Turbulence Voltages to Velocity Components

The expressions representing the hot-wire response may be rewritten as

$$\left(\frac{Nu_i - A_i}{B_i}\right)^{\frac{2}{n_i}} = \left(\frac{\rho d}{\mu}\right)^2 q_i^2$$

When the expressions for the q_i are substituted in these equations, a set of four algebraic equations for the three velocity components $\tilde{u}$, $\tilde{v}$, $\tilde{w}$ is obtained. The method of solution of these equations is based on the fact that the response of the yaw wires 1 and 2 is dominated by the tangential and axial velocities $\tilde{v}$ and $\tilde{w}$, while the response of the pitch wires 3 and 4 is dominated by the radial and tangential velocities $\tilde{u}$ and $\tilde{v}$. The four equations for $\tilde{u}$, $\tilde{v}$, $\tilde{w}$ can thus be treated as two loosely coupled pairs for $\tilde{w}$, $\tilde{v}$ and for $\tilde{u}$, $\tilde{v}$ respectively. In fact, these pairs of equations can be solved explicitly to obtain the formal solutions:

$$\left.\begin{aligned} \tilde{v} &= \frac{|Q_2|\cos\beta_1 + |Q_1|\cos\beta_2}{\sin(\beta_1 + \beta_2)} \\ \tilde{w} &= \frac{|Q_2|\sin\beta_1 - |Q_1|\sin\beta_2}{\sin(\beta_1 + \beta_2)} \end{aligned}\right\} \qquad (1)$$

and

$$\left.\begin{aligned} \tilde{u} &= \frac{\pm|Q_3|\sin\beta_4 \mp |Q_4|\sin\beta_3}{\sin(\beta_3+\beta_4)} \\ \tilde{v} &= \frac{|Q_3|\cos\beta_4 + |Q_4|\cos\beta_3}{\sin(\beta_3+\beta_4)} \end{aligned}\right\} \qquad (2)$$

where the signs depend on the location of the probe (i. e., on the inner or outer cylinder), and by definition

$$\left.\begin{aligned} Q_1^2 &= \left(\frac{\mu}{\rho d}\right)^2\left(\frac{Nu_1 - A_1}{B_1}\right)^{\frac{2}{n_1}} - \tilde{u}(a_{11}\tilde{u} + 2a_{12}\tilde{v} + 2a_{13}\tilde{w})_1 \\ Q_2^2 &= \left(\frac{\mu}{\rho d}\right)^2\left(\frac{Nu_2 - A_2}{B_2}\right)^{\frac{2}{n_2}} - \tilde{u}(a_{11}\tilde{u} + 2a_{12}\tilde{v} + 2a_{13}\tilde{w})_2 \end{aligned}\right\} \qquad (3)$$

and

$$\left.\begin{aligned} Q_3^2 &= \left(\frac{\mu}{\rho d}\right)^2\left(\frac{Nu_3 - A_3}{B_3}\right)^{\frac{2}{n_3}} - \tilde{w}(2a_{13}\tilde{u} + 2a_{23}\tilde{v} + a_{33}\tilde{w})_3 \\ Q_4^2 &= \left(\frac{\mu}{\rho d}\right)^2\left(\frac{Nu_4 - A_4}{B_4}\right)^{\frac{2}{n_4}} - \tilde{w}(2a_{13}\tilde{u} + 2a_{23}\tilde{v} + a_{33}\tilde{w})_4 \end{aligned}\right\} \qquad (4)$$

These equations may be solved for $\tilde{u}$, $\tilde{v}$; $\tilde{v}$, $\tilde{w}$ by iteration. The basis of the first step in the iteration scheme is the fact that Q_1 and Q_2 are known constants if the effect of the radial velocity, $\tilde{u}$, on the yaw wires

is neglected, and similarly the fact that Q_3 and Q_4 are known if the effect of the axial velocity, $\tilde{w}$, on the pitch wires is neglected.

The iteration is carried out as follows:

1. Compute $\tilde{v}$, $\tilde{w}$, from equations (1) assume $\tilde{u} = 0$ in computing Q_1, Q_2 from equations (3).
2. Compute $\tilde{u}$, $\tilde{v}$ from equations (2); assume $\tilde{u} = \tilde{v} = 0$ in computing Q_3, Q_4 from equations (4), but use $\tilde{w}$ from step 1.
3. Recompute $\tilde{v}$, $\tilde{w}$ from equations (1); use $\tilde{v}$, $\tilde{w}$ from step 1 and $\tilde{u}$ from step 2 in computing Q_1, Q_2 from equations (3).
4. Recompute $\tilde{u}$, $\tilde{v}$ from equations (2); use $\tilde{u}$, $\tilde{v}$ from step 2 and $\tilde{w}$ from step 3 in computing Q_3, Q_4 from equations (4).

5, 6, ··· Repeat steps 3 and 4, *mutatis mutandis*, until $\tilde{v}$, $\tilde{w}$ and $\tilde{u}$, $\tilde{v}$ are constant; e. g., until there is no change in the 4th significant figure. This criterion will almost certainly be satisfied by step 8, as even the first approximation, e. g., for $\tilde{v}$, $\tilde{w}$ from step 1, should not be in error by more than a few percent. The accuracy of the entire experiment can be assessed at this point in terms of the discrepancy between the two almost independent values obtained for the tangential velocity component $\tilde{v}$.

APPENDIX B

Serial Correlations for Time Interval Between Successive Observations of a Given Interface

At a fixed radius, the angular position in laboratory coordinates of a given interface, θ_I, may be decomposed into mean and fluctuating parts. The mean part, $\omega_t t$, is a linear function of time while the fluctuating part, $\theta(t)$, is a stationary stochastic function of time with zero mean. Assume that the measuring probe is mounted on the outer cylinder (the argument is nearly identical for a probe on the inner cylinder). In the time interval, $P_n = t_{n,2} - t_{n,1}$, between probe crossings of a given interface, the angular distance travelled by the probe is $\omega_o P_n$, while the angular distance travelled by the interface is $\omega_t P_n + \theta\left(t_{n,2}\right) - \theta\left(t_{n,1}\right)$. Allowing for the fact that the probe traverses the interface at each end of the interval P_n, then (see sketch)

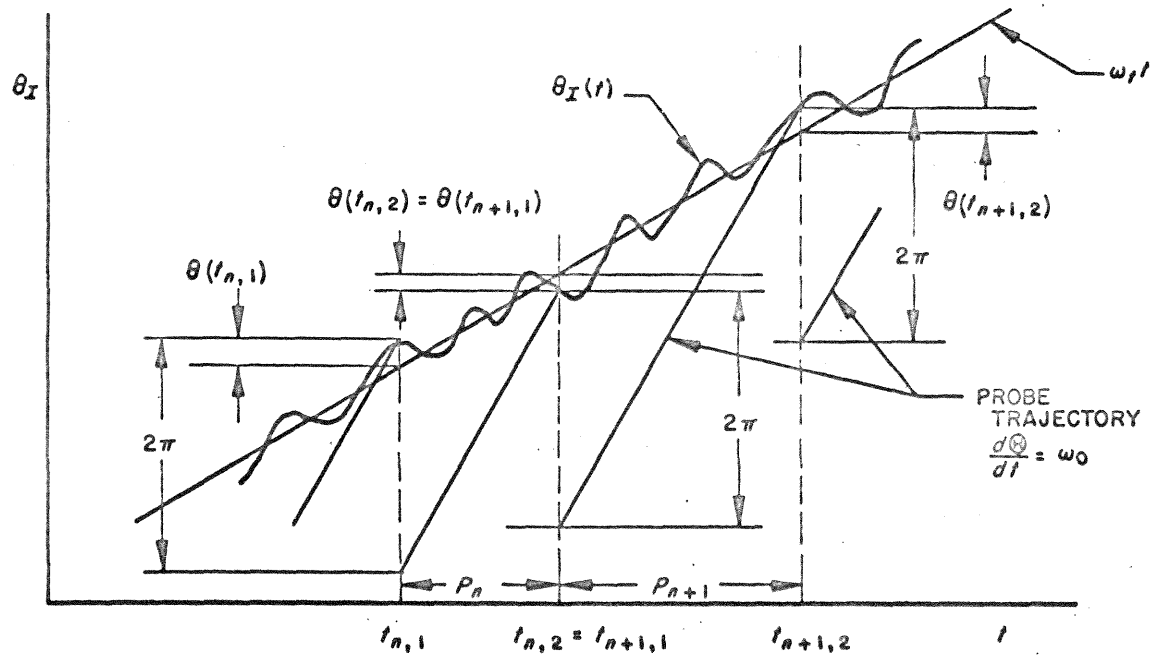

$$\omega_o P_n = 2\pi + \omega_t P_n' + \theta(t_{n,2}) - \theta(t_{n,1})$$

and

$$P_n = \frac{\theta(t_{n,2}) - \theta(t_{n,1}) + 2\pi}{\omega_o - \omega_t}$$

Similarly,

$$\omega_o P_{n+\nu} = 2\pi + \omega_t P_{n+\nu} + \theta(t_{n+\nu,2}) - \theta(t_{n+\nu,1})$$

and

$$P_{n+\nu} = \frac{\theta(t_{n+\nu,2}) - \theta(t_{n+\nu,1}) + 2\pi}{\omega_o - \omega_t}$$

but

$$\theta(t_{n+\nu,1}) = \theta(t_{n+\nu-1,2})$$

and

$$\overline{P} = \frac{2\pi}{\omega_o - \omega_t}$$

Then

$$\delta_n = P_n - \overline{P} = \frac{\theta(t_{n,2}) - \theta(t_{n,1})}{\omega_o - \omega_t}$$

and

$$\delta_{n+\nu} = P_{n+\nu} - \overline{P} = \frac{\theta(t_{n+\nu,2}) - \theta(t_{n+\nu-1,2})}{\omega_o - \omega_t}$$

The normalized correlation between the fluctuation for one interval and for the ν^{th} following interval is

$$\psi(\nu) = \psi_\nu = \frac{\langle \delta_n \delta_{n+\nu} \rangle}{\langle \delta_n^2 \rangle} = \frac{\left\langle \left[\theta\, t_{n,2}) - \theta(t_{n,1})\right] \left[\theta(t_{n+\nu,2}) - \theta(t_{n+\nu-1,2})\right] \right\rangle}{\left\langle \left[\theta(t_{n,2}) - \theta(t_{n,1})\right]^2 \right\rangle}$$

$$= \frac{1}{\left\langle \theta^2(t_{n,2}) + \theta^2(t_{n,1}) - 2\theta(t_{n,2})\,\theta(t_{n,1}) \right\rangle}$$

$$\left[\left\langle \theta(t_{n,2})\,\theta(t_{n+\nu,2}) \right\rangle - \left\langle \theta(t_{n,1})\,\theta(t_{n+\nu,2}) \right\rangle \right.$$

$$\left. - \left\langle \theta(t_{n,2})\,\theta(t_{n+\nu-1,2}) \right\rangle + \left\langle \theta(t_{n,1})\,\theta(t_{n+\nu-1,2}) \right\rangle \right]$$

If the correlation time of the random fluctuations in interface position is small compared with P_n, then values of $\theta(t)$ separated by intervals of P_n or greater will be uncorrelated in the mean; i.e., $\langle \theta(t)\theta(t+T) \rangle = 0$; $T \geq P_n$. Assuming that this is the case, then obviously (since $\left\langle \theta(t_{n,2})^2 \right\rangle = \left\langle \theta(t_{n,1})^2 \right\rangle$),

$$\psi_\nu = \frac{\langle \delta_n \delta_{n+\nu} \rangle}{\langle \delta_n^2 \rangle} = \begin{cases} +1 & \nu = 0 \\ -0.5 & \nu = 1 \\ 0 & \nu \geq 2 \end{cases}$$

These results are independent of the distribution function for P.

It has been implicitly assumed, in view of experimental evidence like that in figure 2, that the fluctuations in interface position, although rapid, are slow enough so that the probe may cross each interface only once (always in the same direction) during each encounter

with the turbulent volume of fluid. For less regular cases (for which the results here do not apply), the interfaces may possibly fluctuate so rapidly that they would appear to be poorly defined even though the interface itself remains sharp. In fact, relatively rapid crossing and re-crossing of the interface in opposite directions by the probe may account in part for the random occurrence of brief intervals of turbulence in normally laminar portions of the signal as noted in section 3.1.

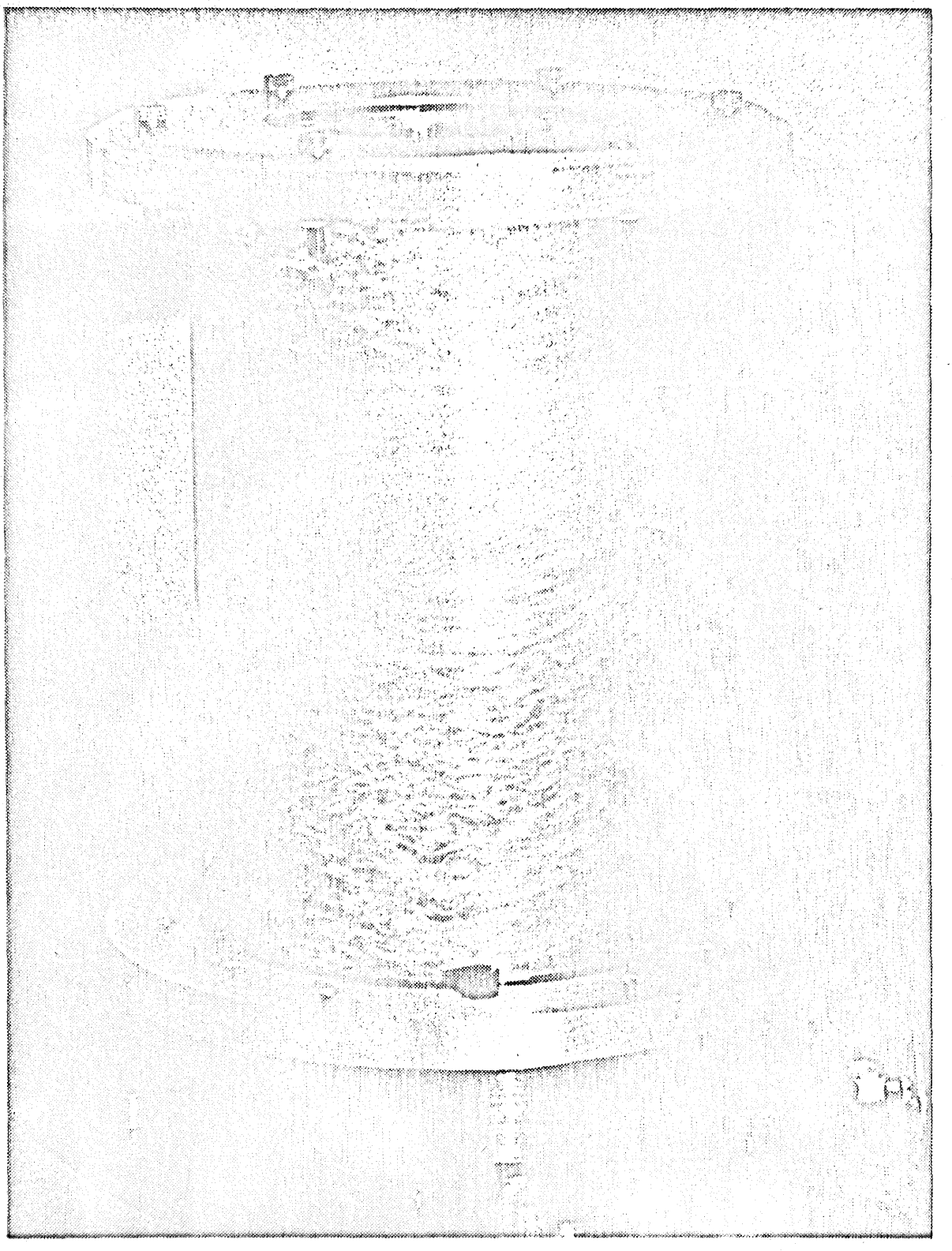

Fig. 1. Spiral Turbulence; Flow Visualization by Coles using Suspension of Aluminum Powder in Silicone Oil. $R_o = -15,900$, $R_i = 5,300$.

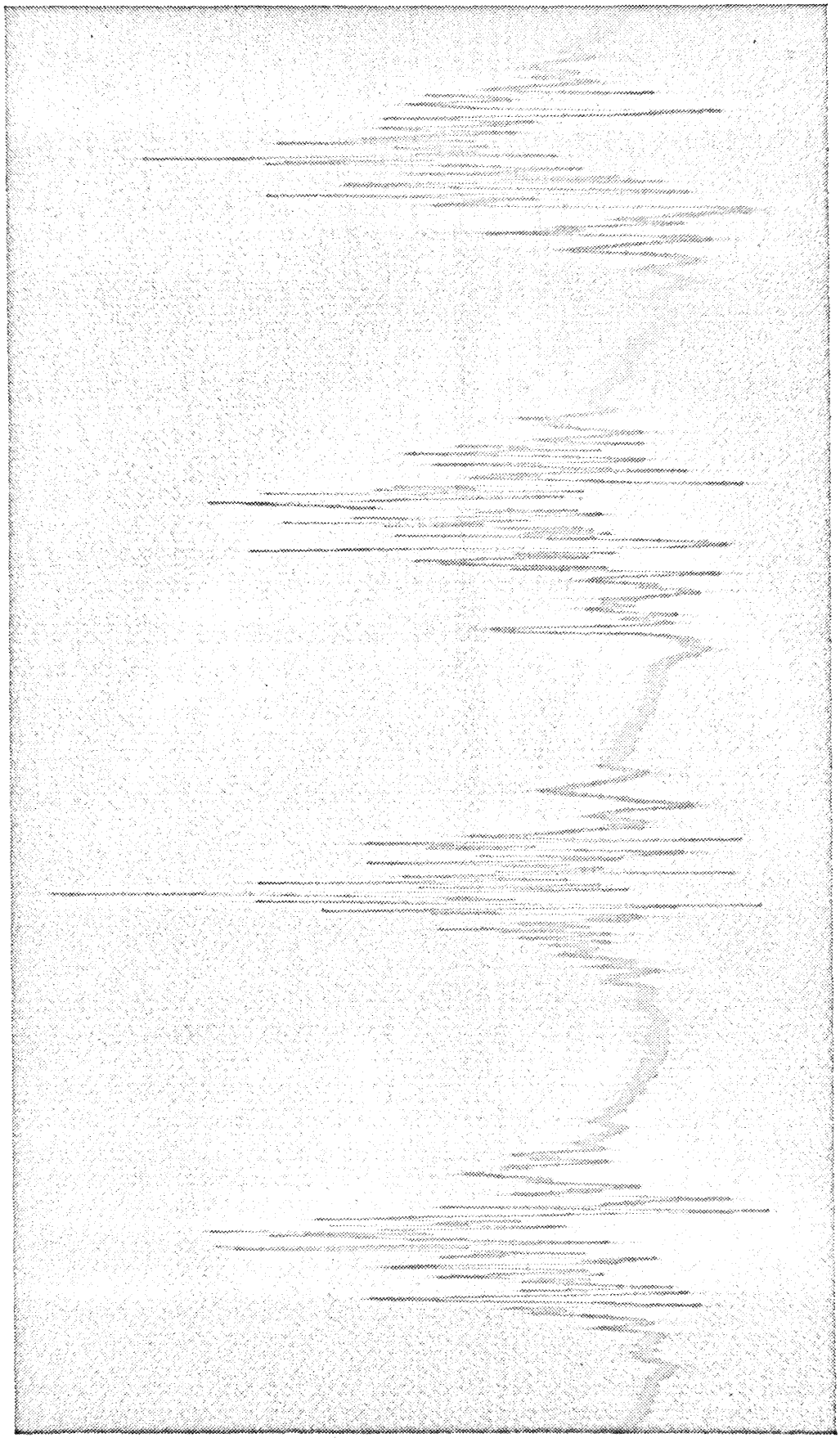

Fig. 2. Typical Hot-Wire Signal in Spiral Turbulence. R_o = -50,000, R_i = 5,600. Probe mounted on outer cylinder at r = 17.125 inches. Signal from wire 1, tape K_o (recorded Oct. 2, 1962).

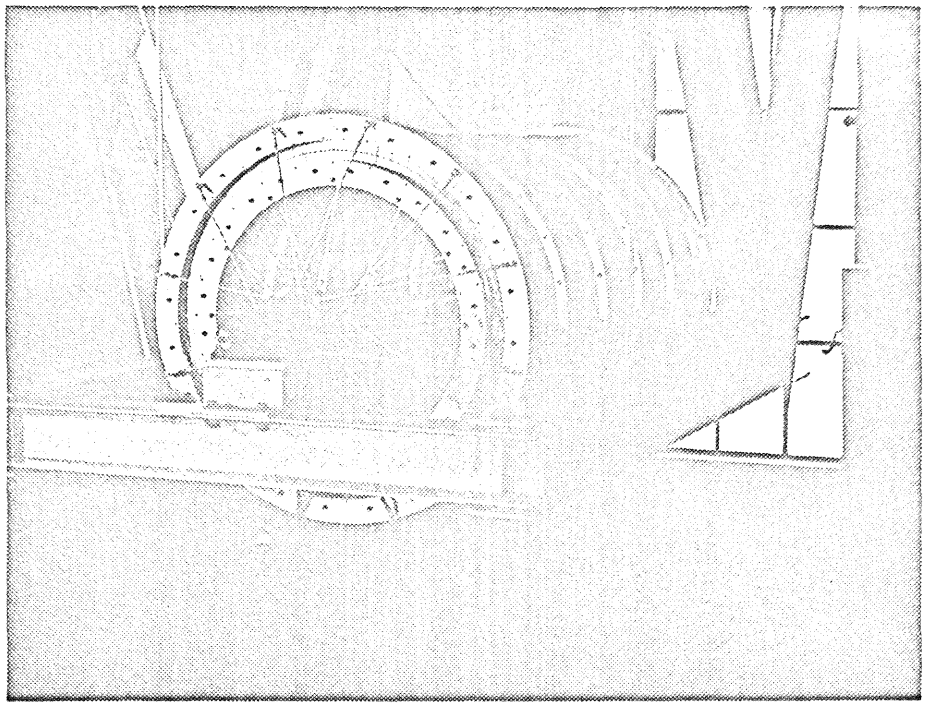

Fig. 3. The Large Rotating-Cylinder Apparatus

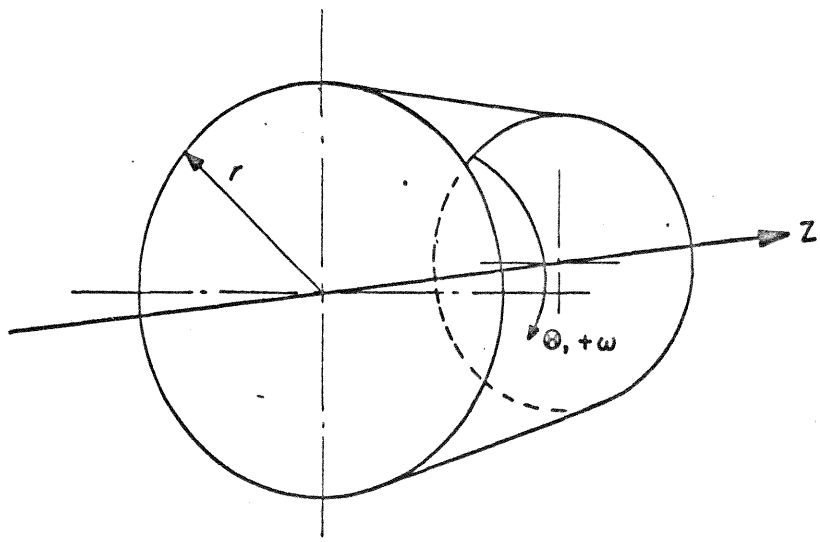

Fig. 4. Coordinate System for Circular Couette Flow

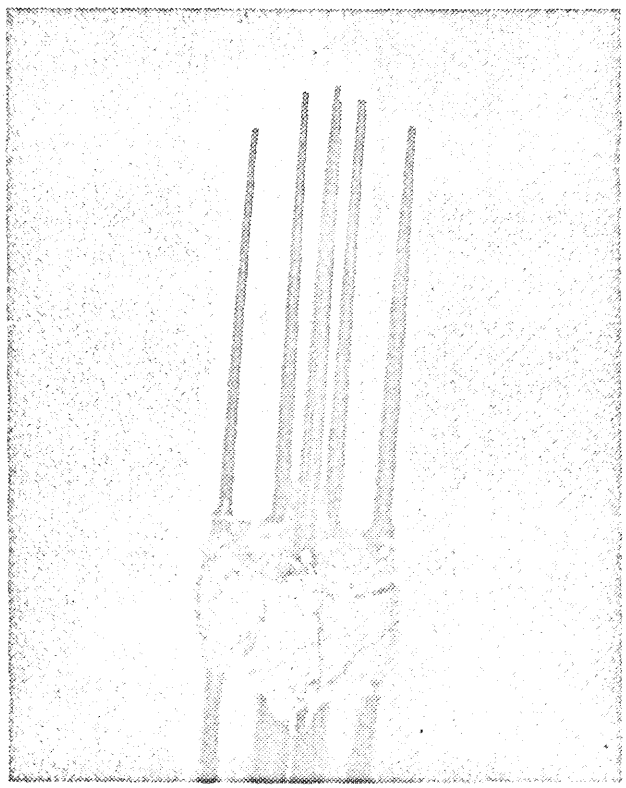

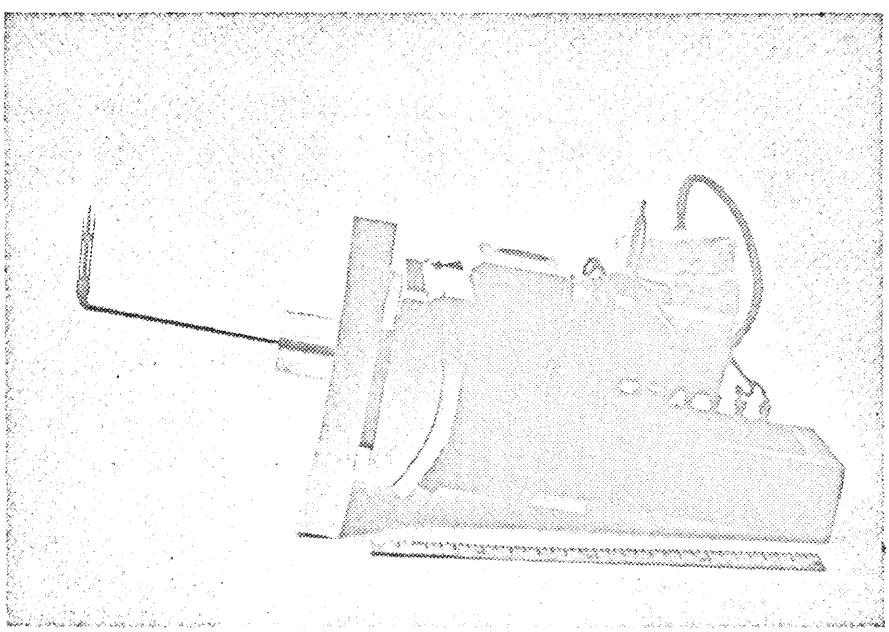

Fig. 5. Velocity Probe and Probe-Traverse Mechanism

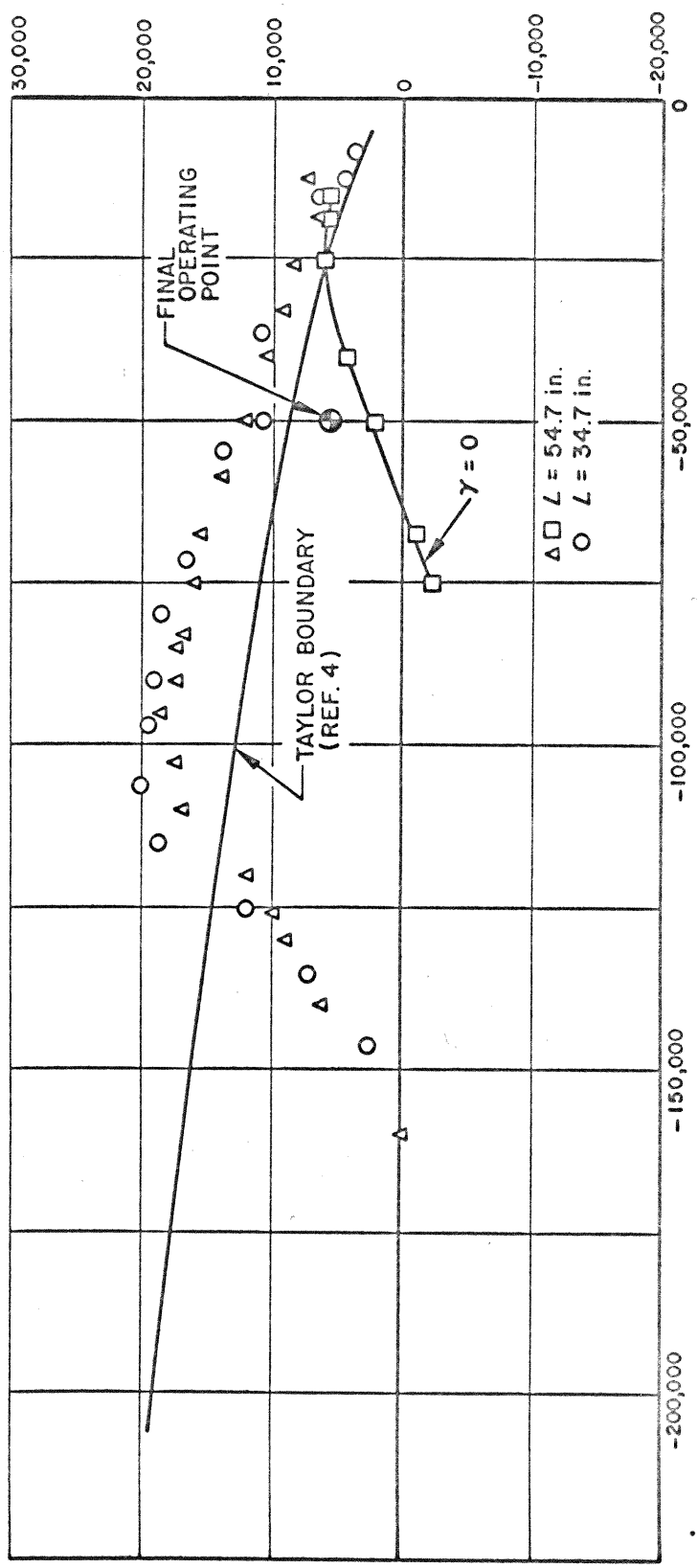

Fig. 6. Boundary for Catastrophic Transition. Circles and triangles show position of transition boundary (approached from below). Squares show boundary for permanent disappearance of turbulence (approached from above). Exploratory data of April-May 1961.

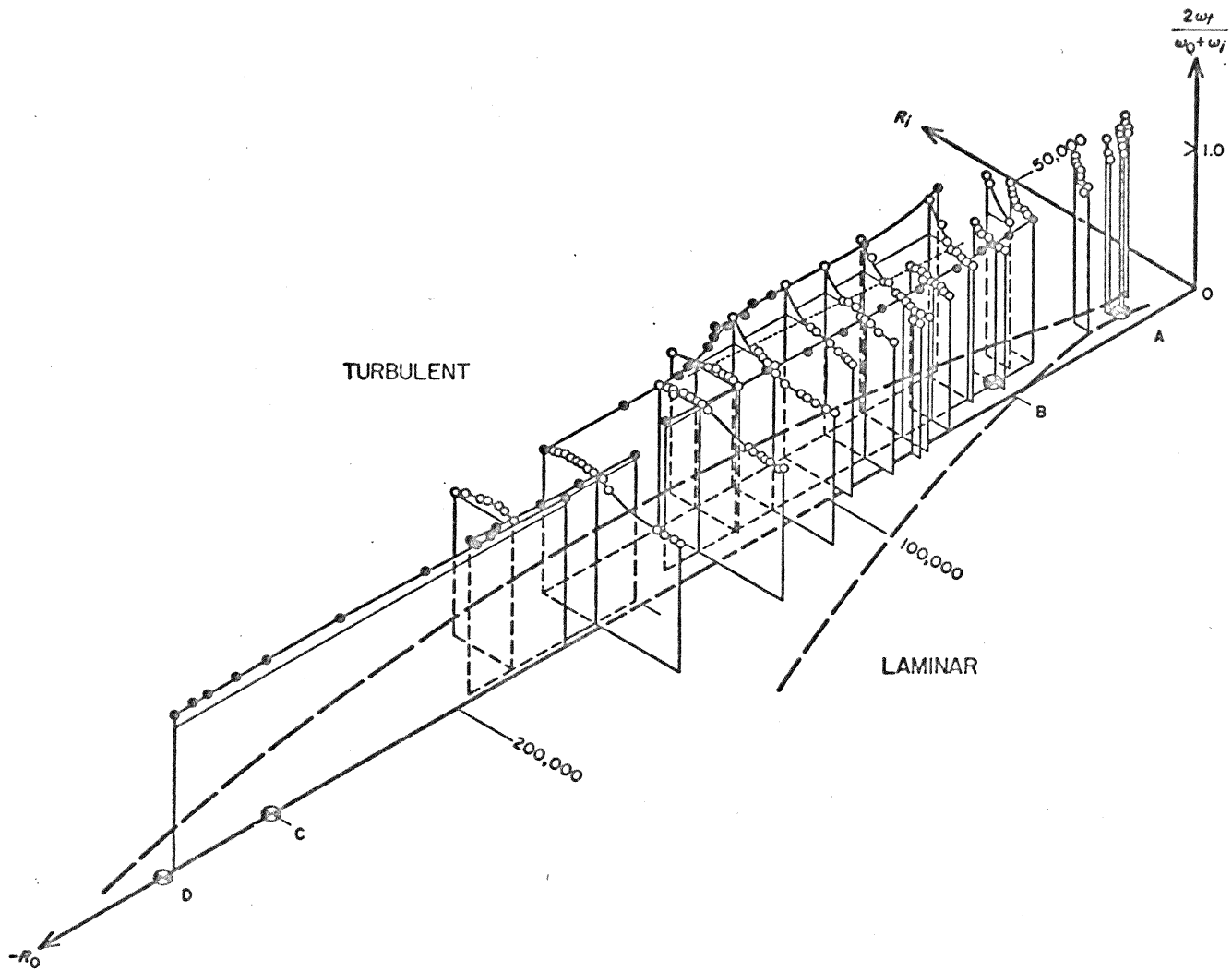

Fig. 7. Angular Velocity ω_t of Spiral Turbulence Pattern. Open circles are data for constant R_o; solid circles are data for constant R_i. Exploratory data of 1960-61. Dotted line is Taylor boundary. Point A corresponds to photograph in Fig. 1; point B to final operating point for the present experiments; points C and D to flows studied by Oguro (unpublished).

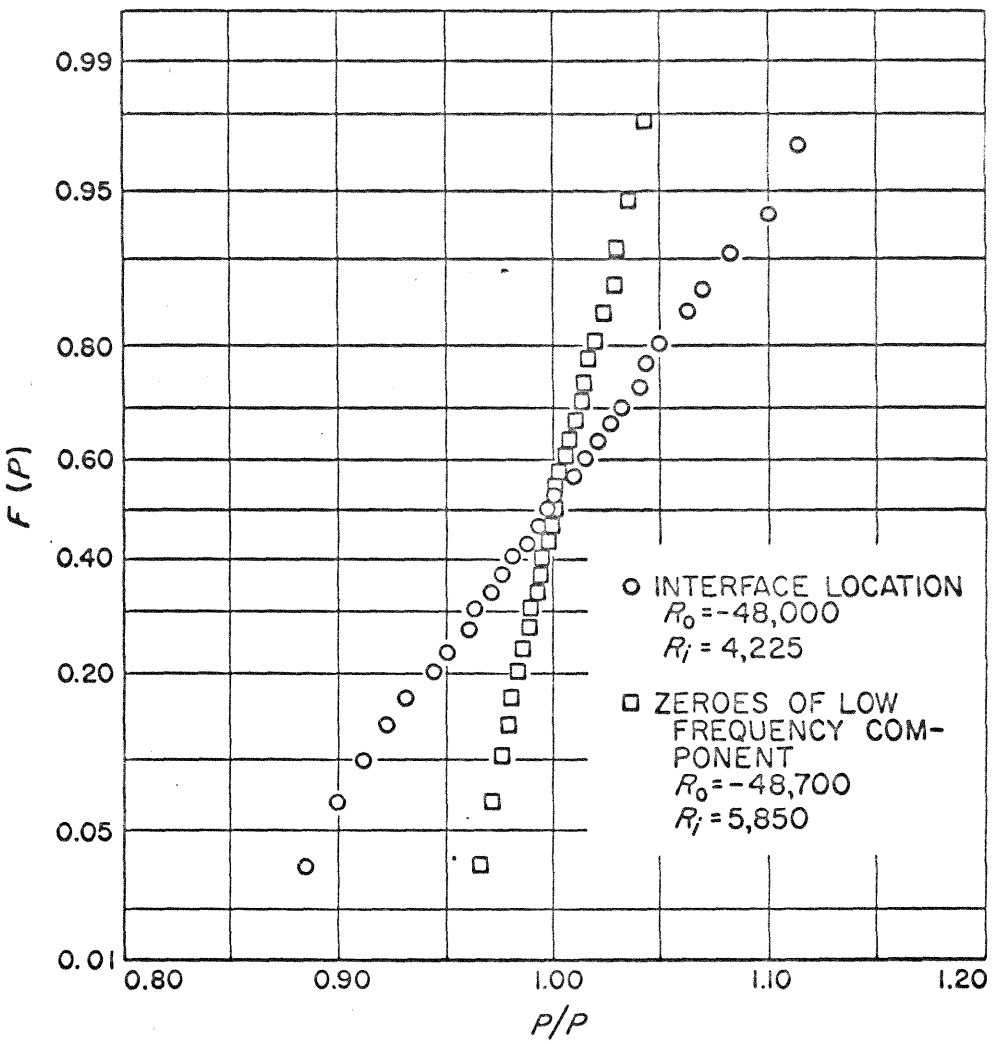

Fig. 8. Typical Distribution Functions for Interface Location and Low Frequency Component. Exploratory data of April-June 1962 (manual recording and analysis).

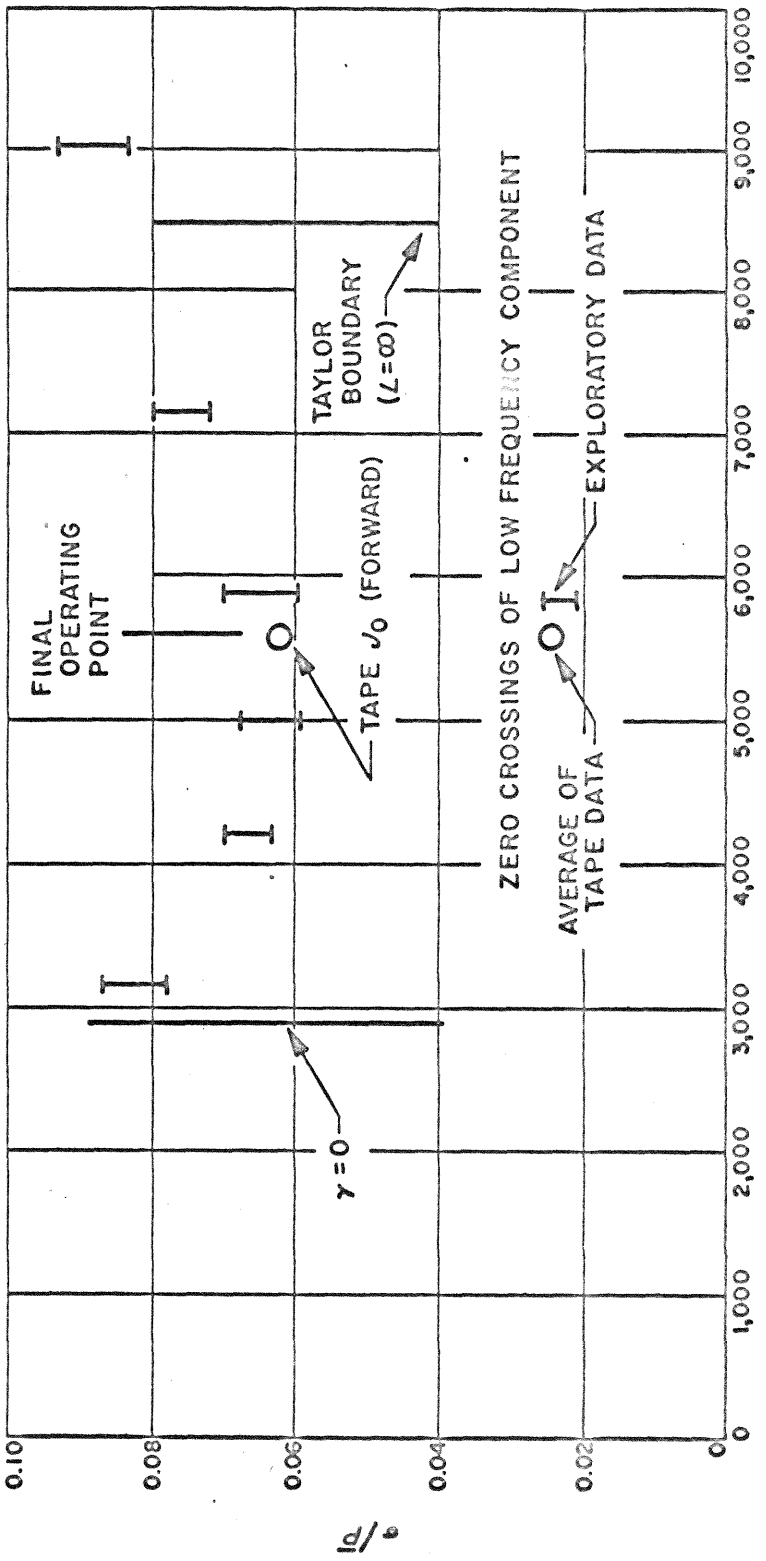

Fig. 9. Standard Deviation of Turbulent Front Position at r = 17 Inches as Function of R_i for Fixed R_o = -48,000. Exploratory data of April 1962 (manual recording and analysis), except for circles, which are from tape-recorded data of Sept.-Nov. 1962.

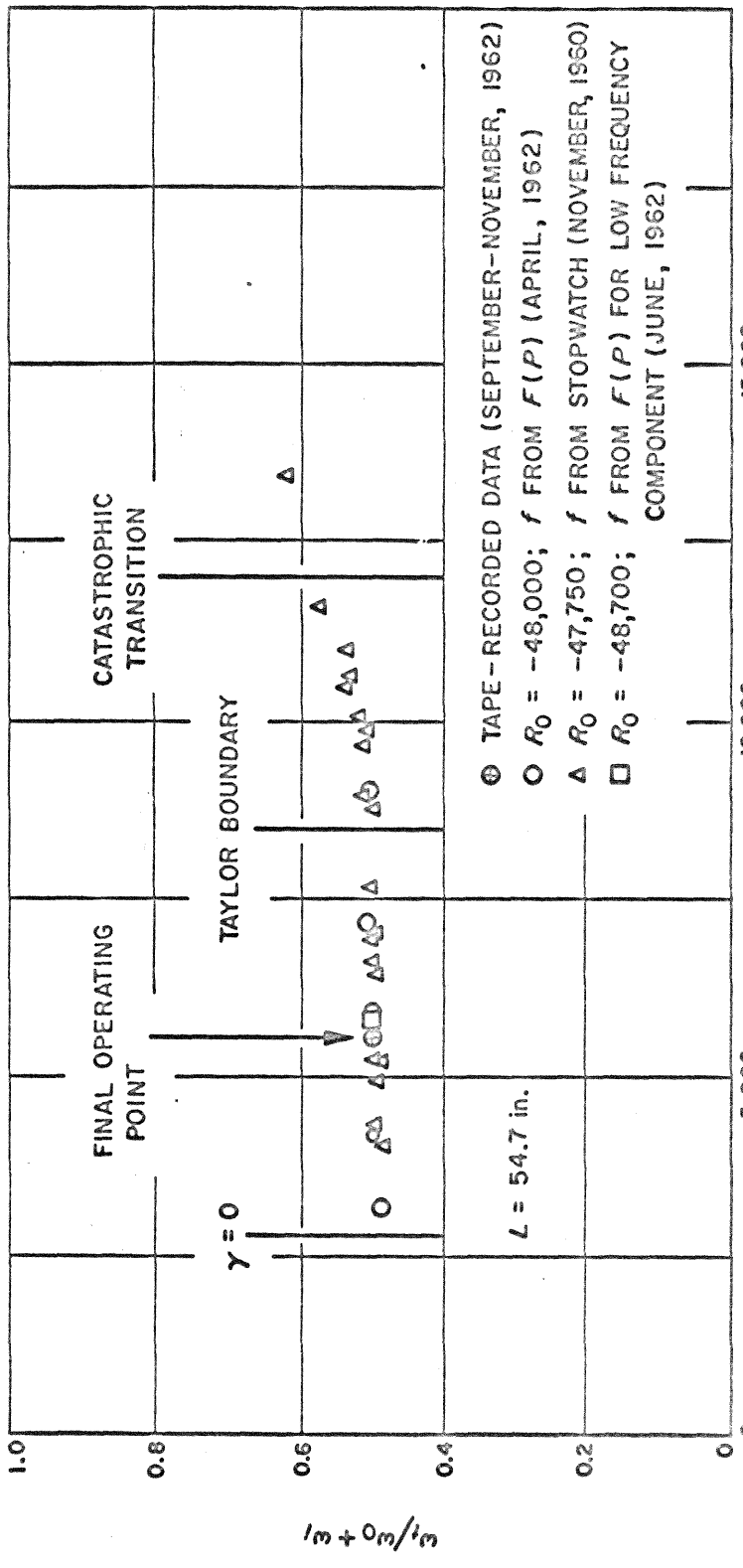

Fig. 10. Normalized Interface Angular Velocity as Function of R_i for Fixed R_o = -48,000

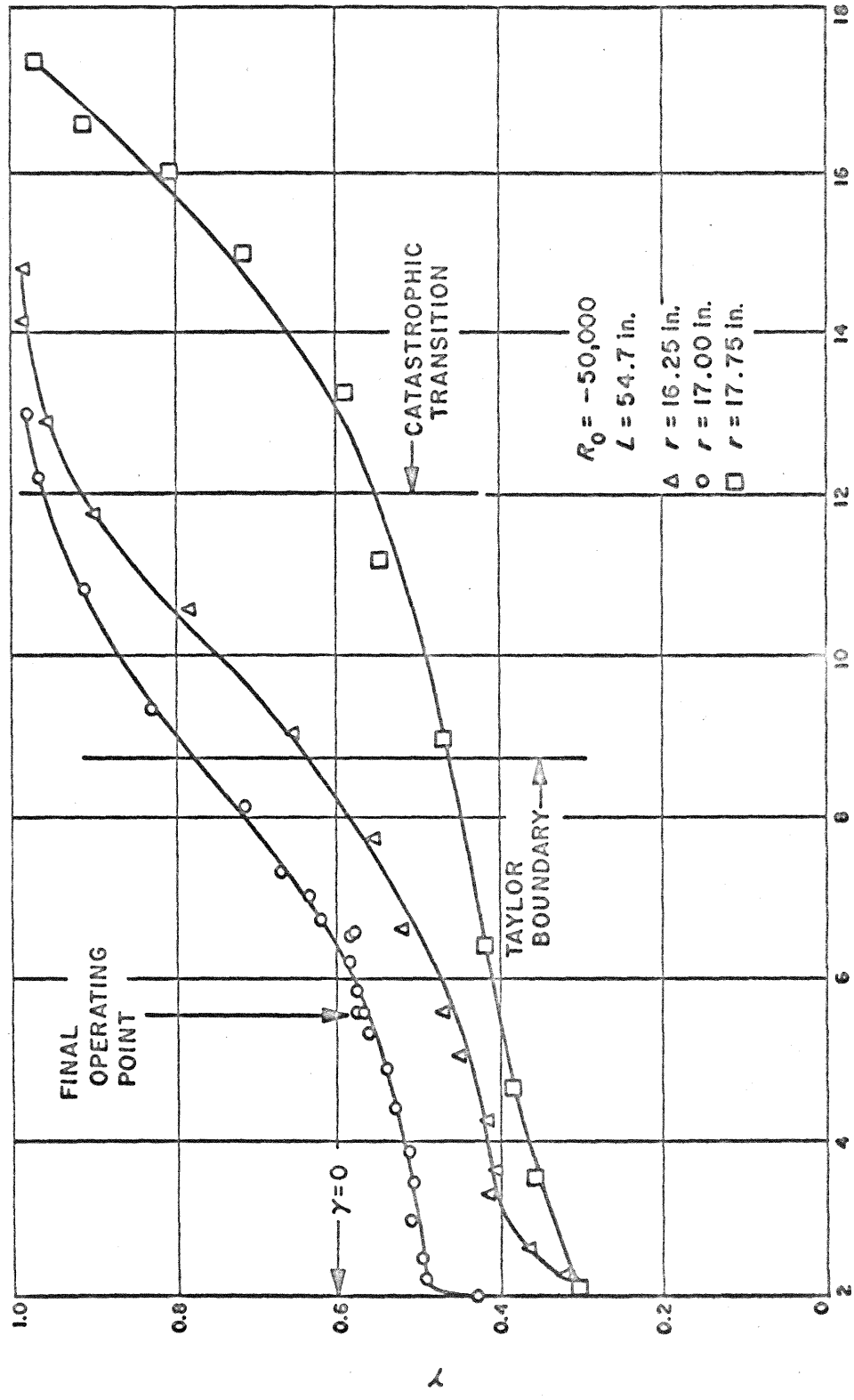

Fig. 11. Variation of γ with R_i for Fixed R_o. Exploratory data of April 1962, using intermittency meter. See figure 12 for variation with radius for fixed R_i = 5,600.

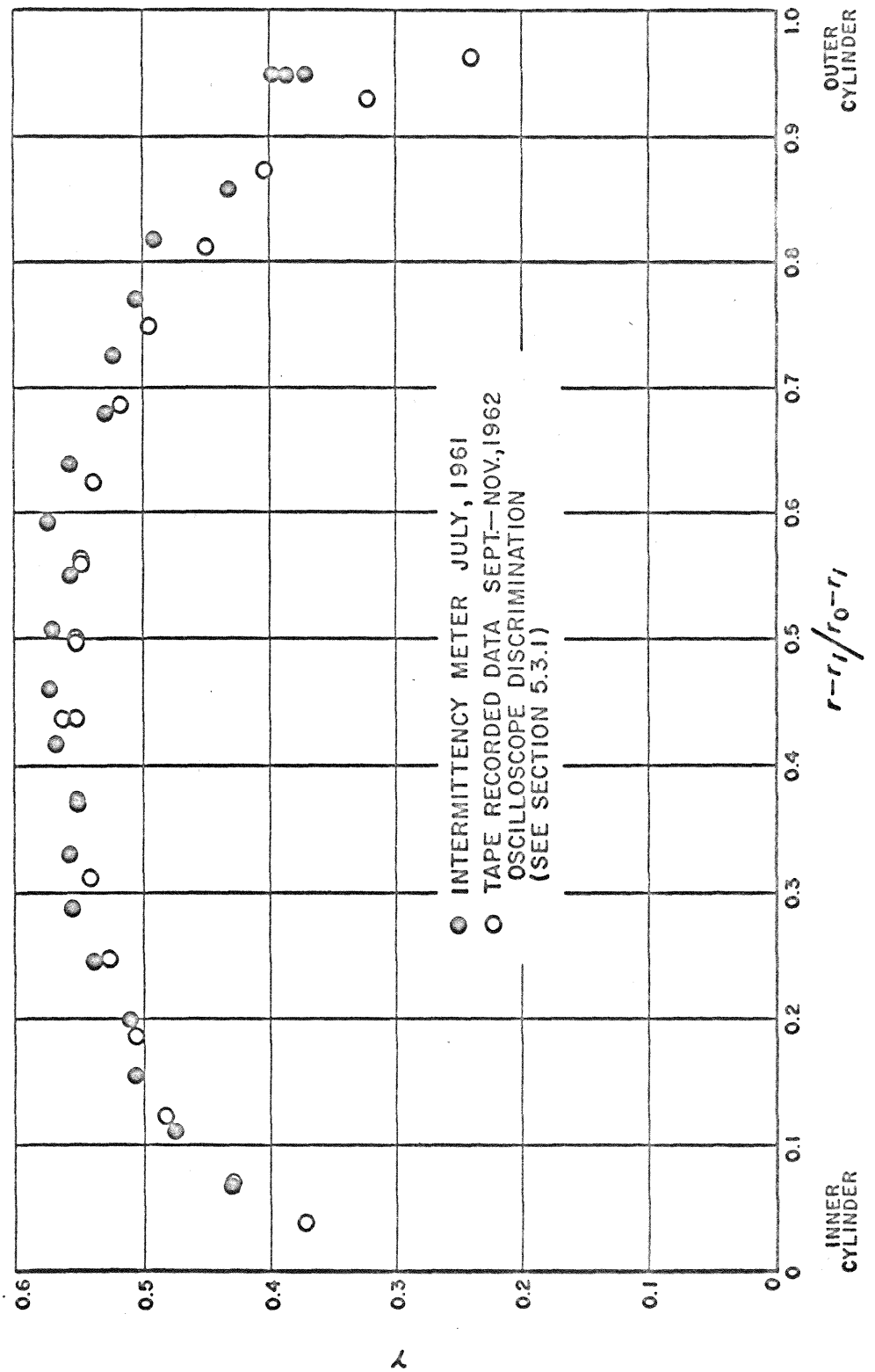

Fig. 12. Radial Distribution of γ for R_o = -50,000, R_i = 5,600.

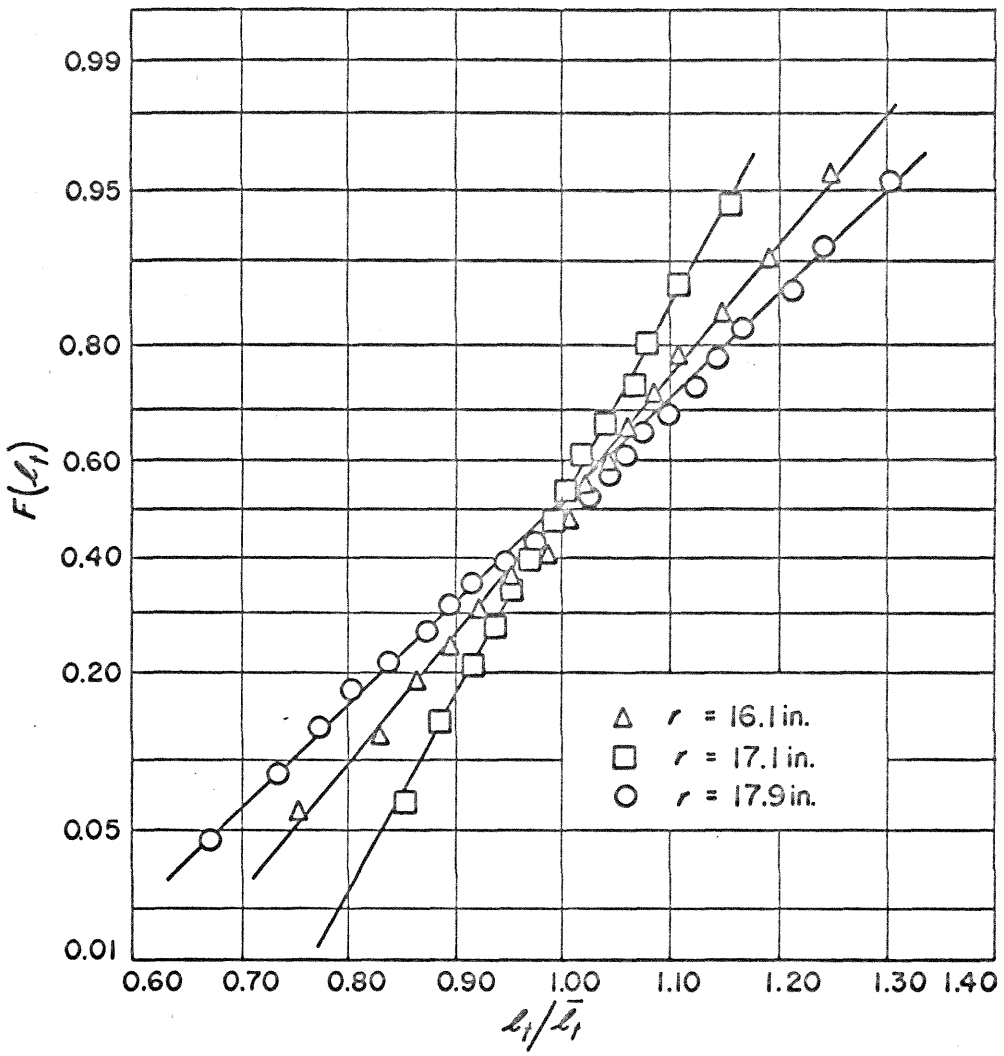

Fig. 13. Distribution of Observed Length of Turbulent Region. Exploratory data of Oct. 1961 (manual recording and analysis).

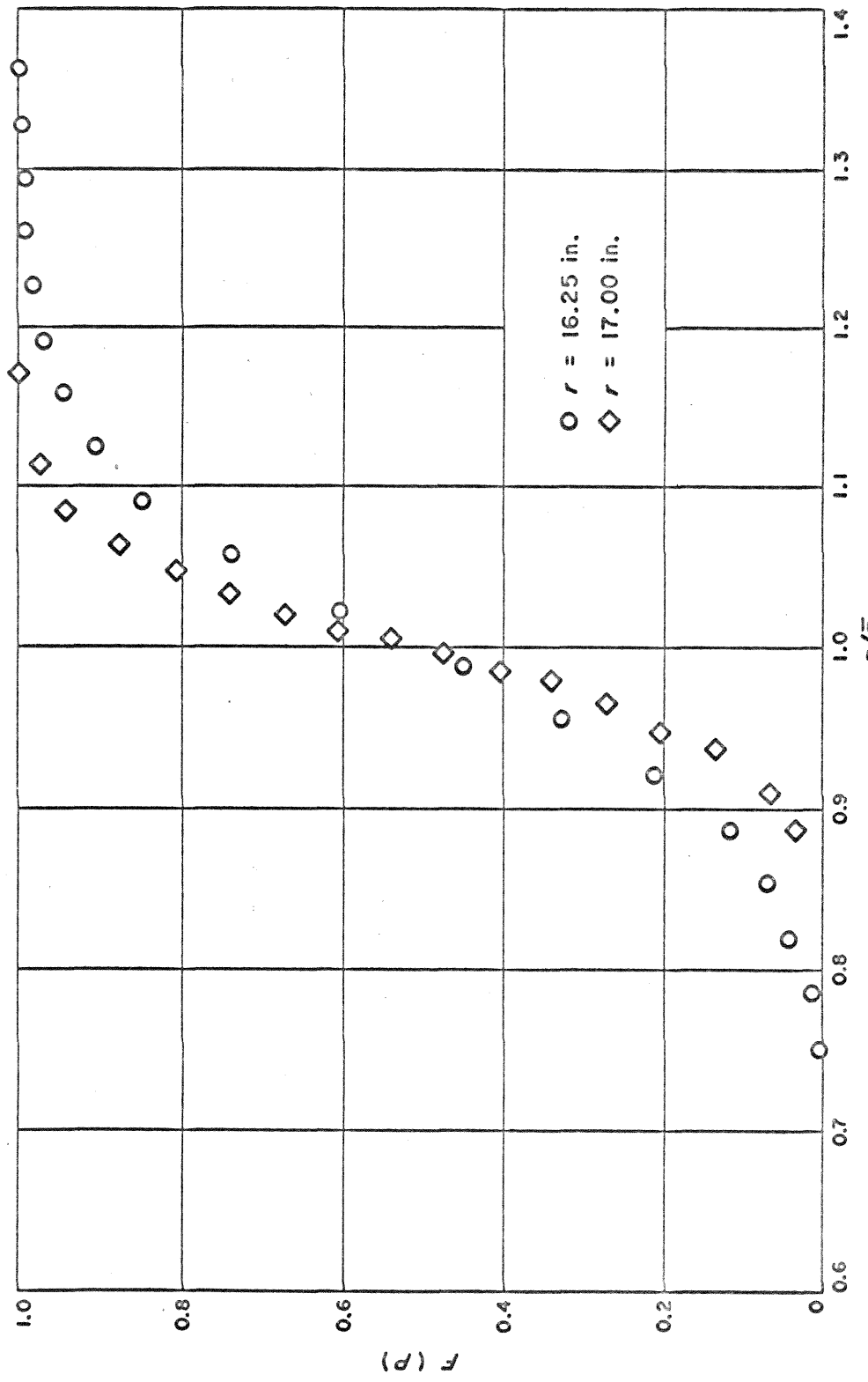

Fig. 14. Distributions of Front Location at r = 17.00 Inches and r = 16.25 Inches. Exploratory data of April 1962.

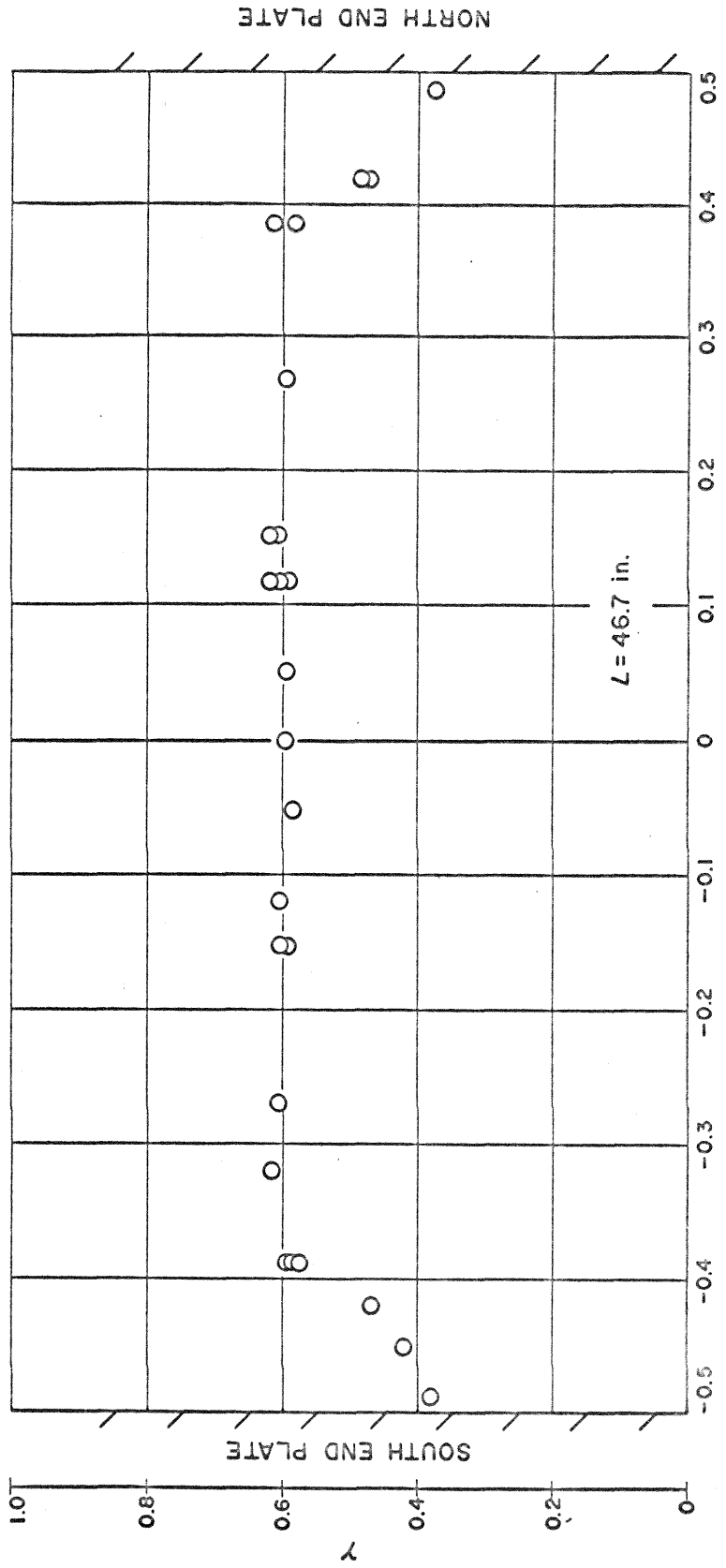

Fig. 15. Axial Distribution of γ at r = 17.00 Inches for R_o = -50,000, R_i = 5,600. Exploratory data of May 1962, using intermittency meter.

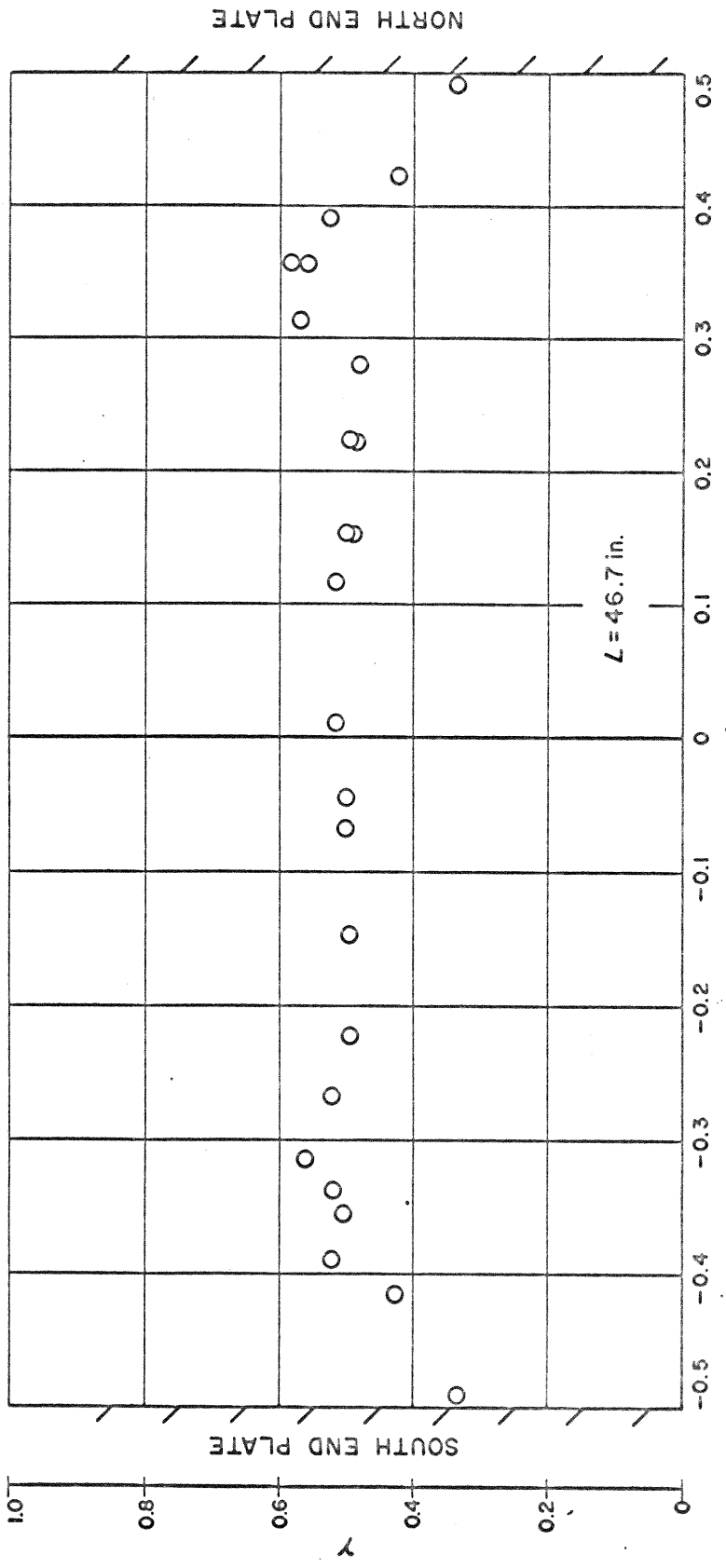

Fig. 16. Axial Distribution of γ at r = 16.25 Inches for R_o = -50,000, R_i = 5,600. Exploratory data of May 1962, using intermittency meter.

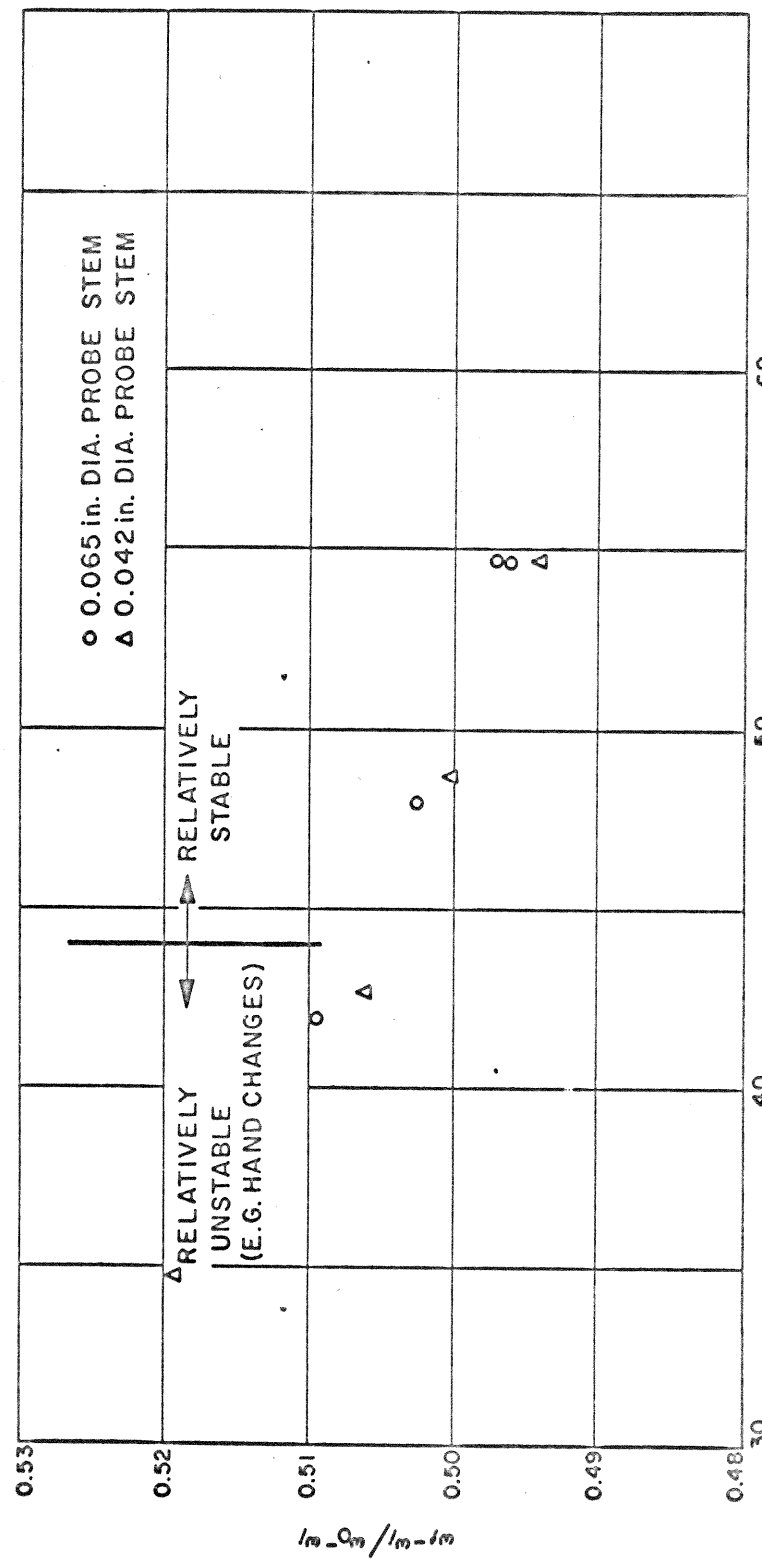

Fig. 17. Effect of Cylinder Length on Period of Turbulence. Triangles show exploratory data of May 1961 (probe stem diameter 0.042 inches, exposed length 1.50 inches). Circles show final tape-recorded data of Sept.-Nov. 1962 (probe stem diameter 0.065 inches, exposed length 1.53 inches).

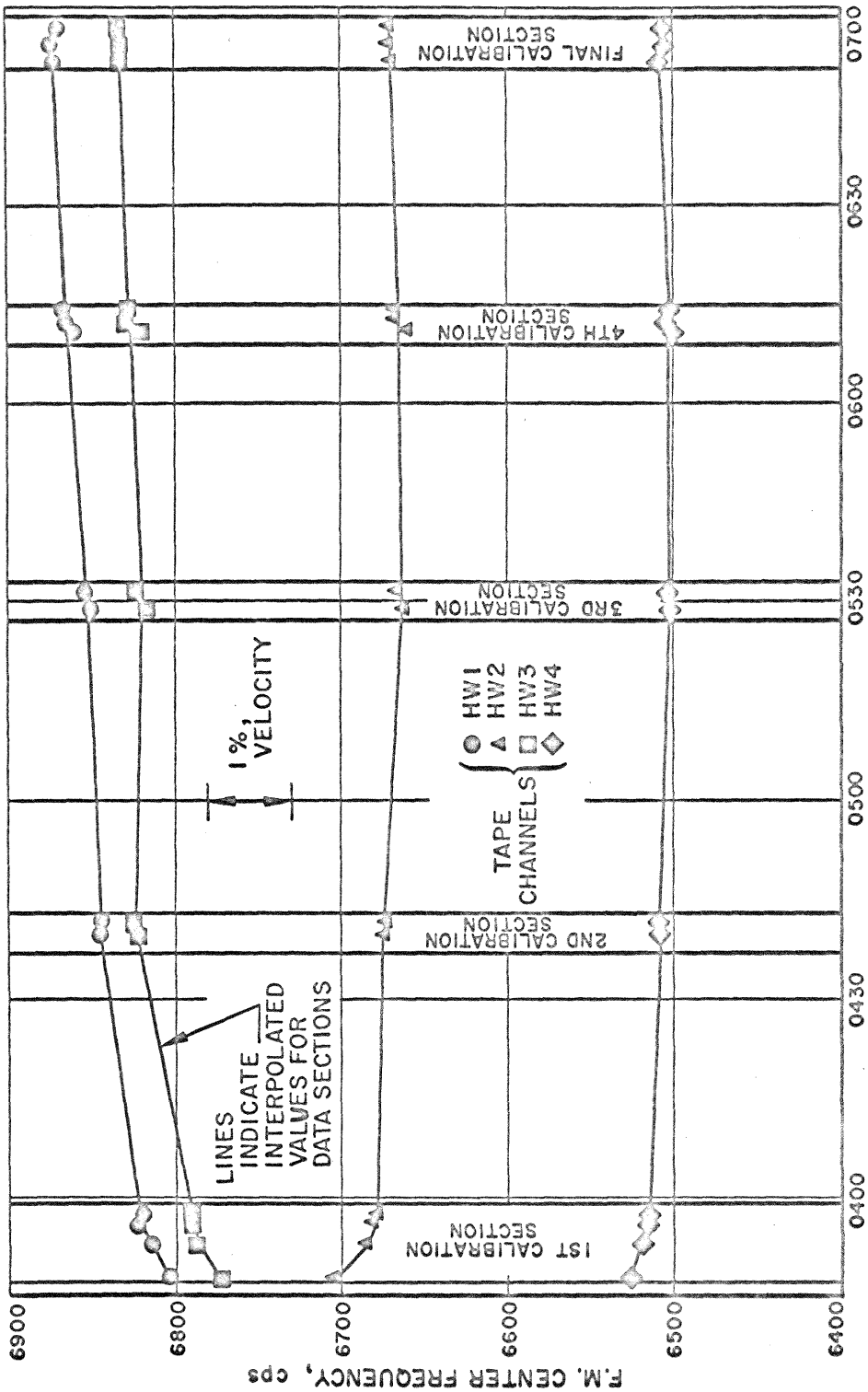

Fig. 18. Typical Variation in Recorder Calibration for Fixed Input Voltage Tape A, Oct. 16, 1962, Zero Volts Input Level.

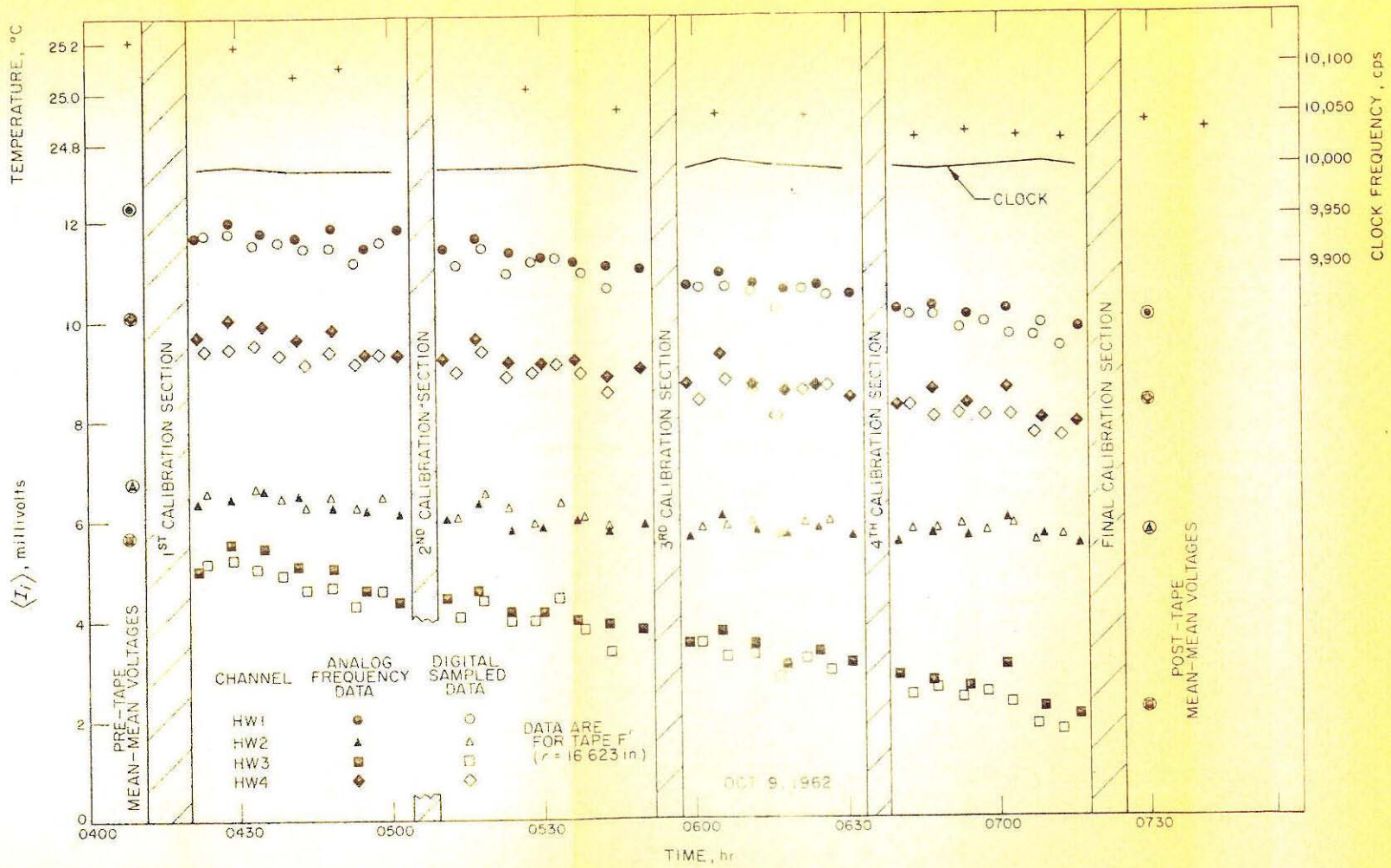

Fig. 19a. Examples of Mean Voltage Data Measured from Analog Frequencies and Digital Sampled Data

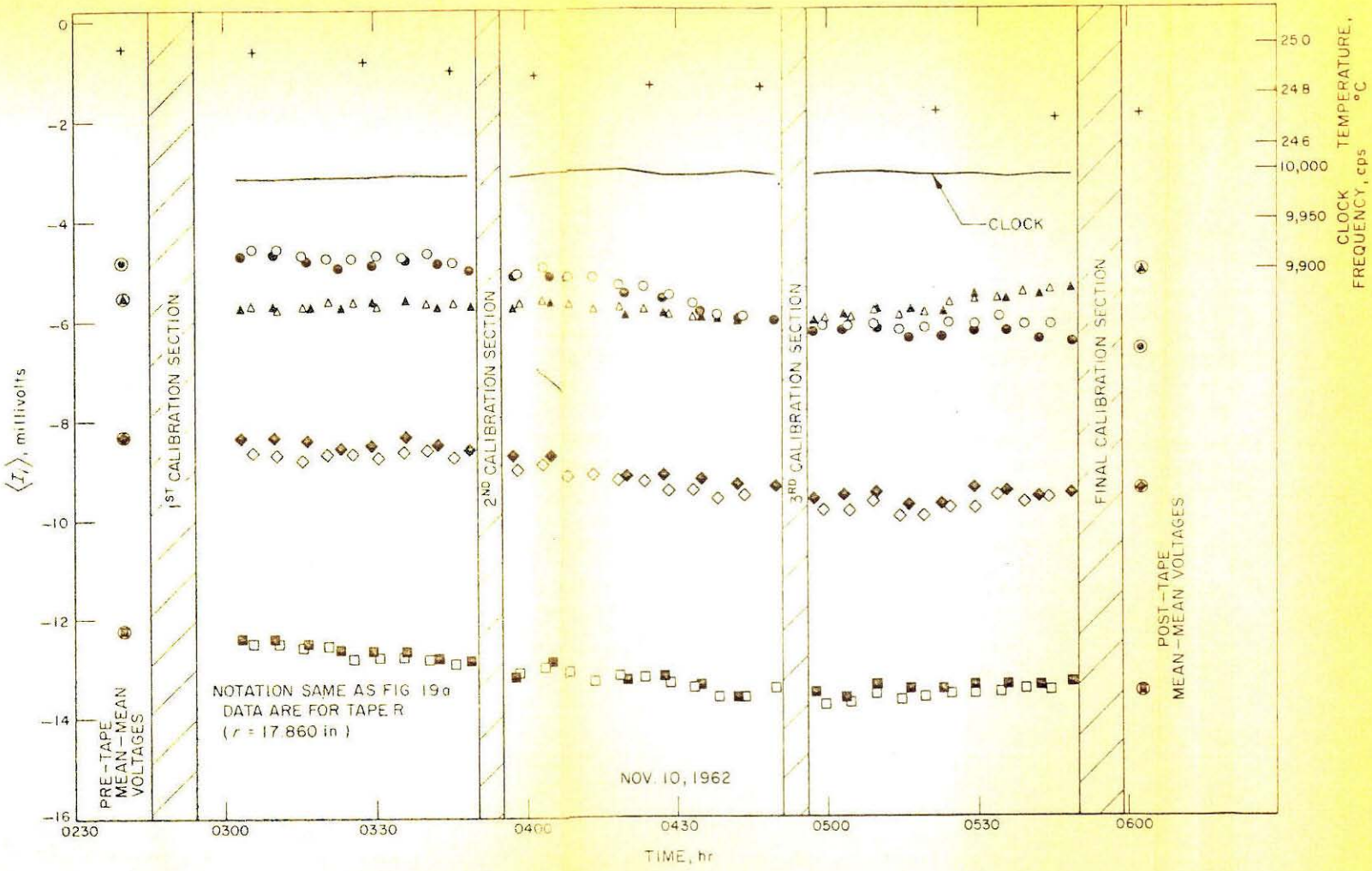

Fig. 19b. Examples of Mean Voltage Data Measured from Analog Frequencies and Digital Sampled Data

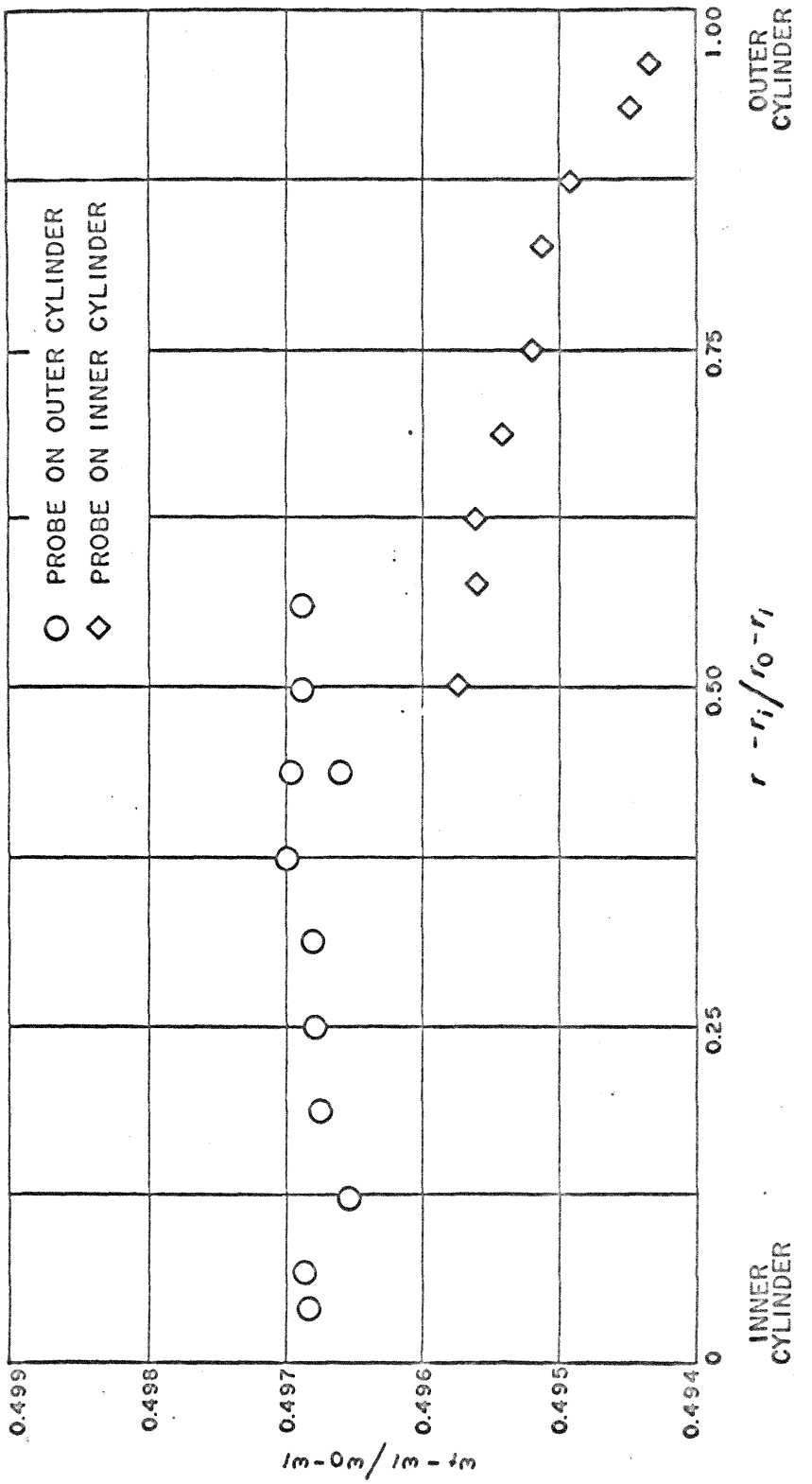

Fig. 20. Effect of Probe Wake on Period of Turbulence

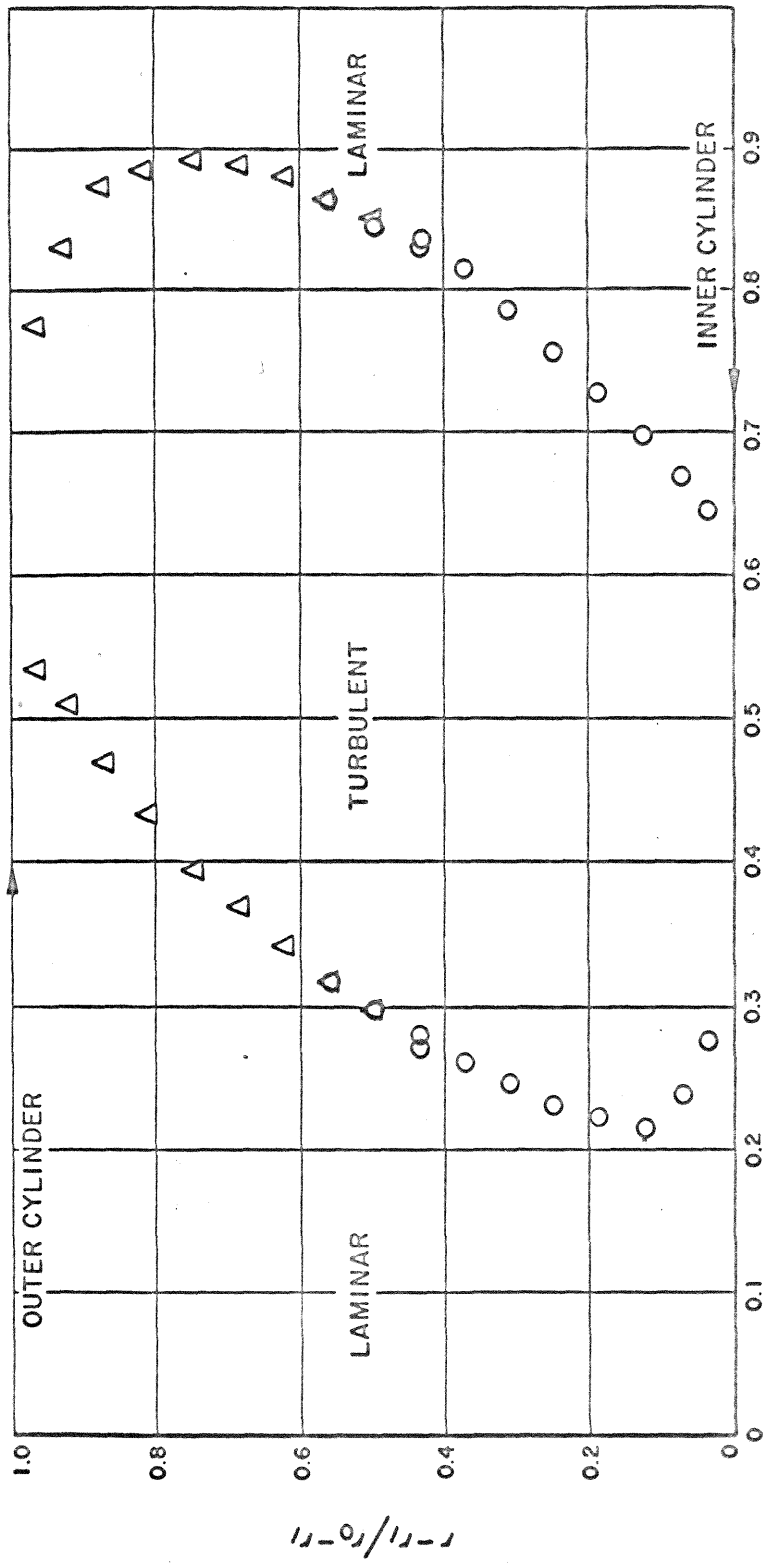

Fig. 21. Mean Interface Geometry

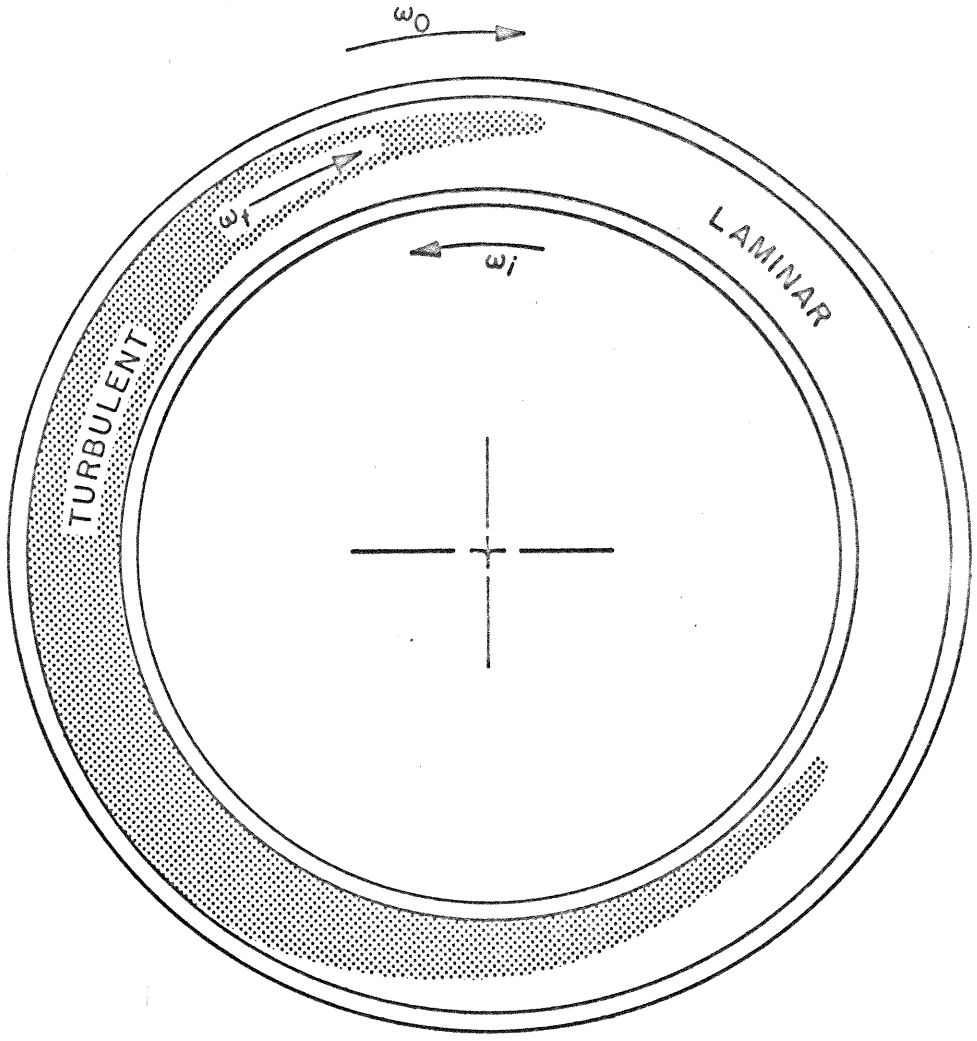

Fig. 22. Mean Interface Geometry in Cylindrical Polar Coordinates

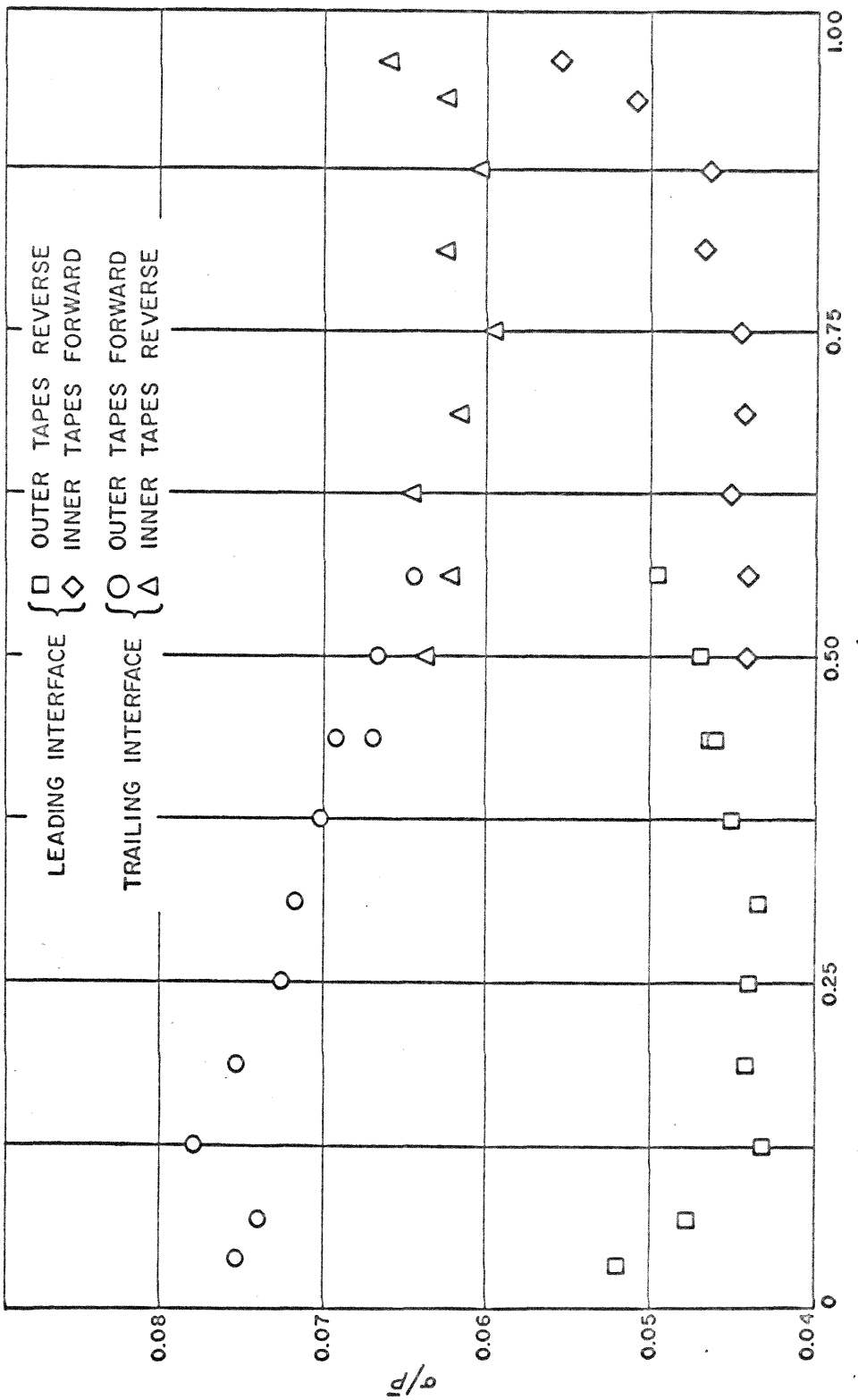

Fig. 23. Standard Deviation of Interface Location for Leading and Trailing Interfaces

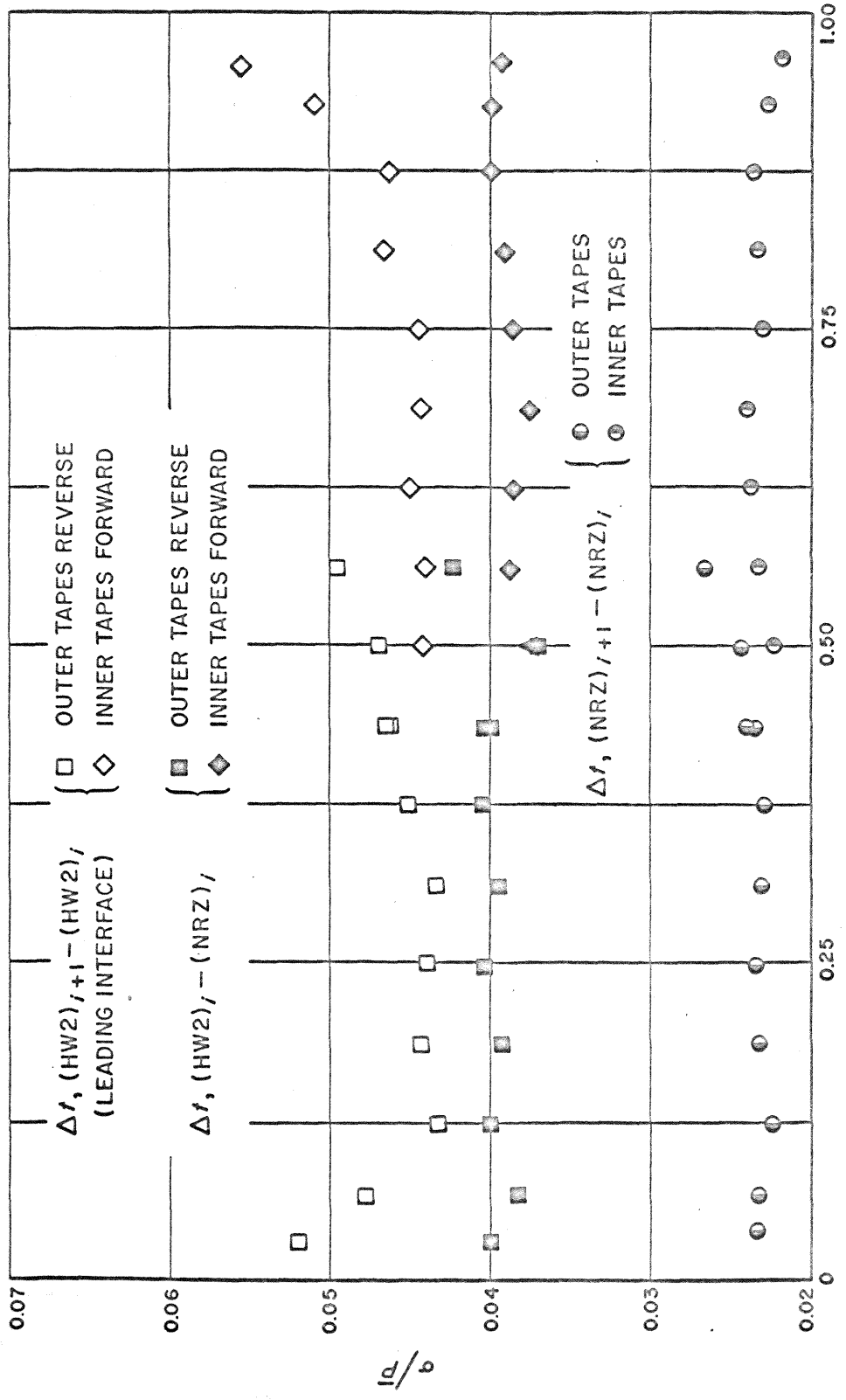

Fig. 24. Comparison of Dispersion for Leading Interface, Time Interval Between NRZ and Following Turbulent Front, and NRZ

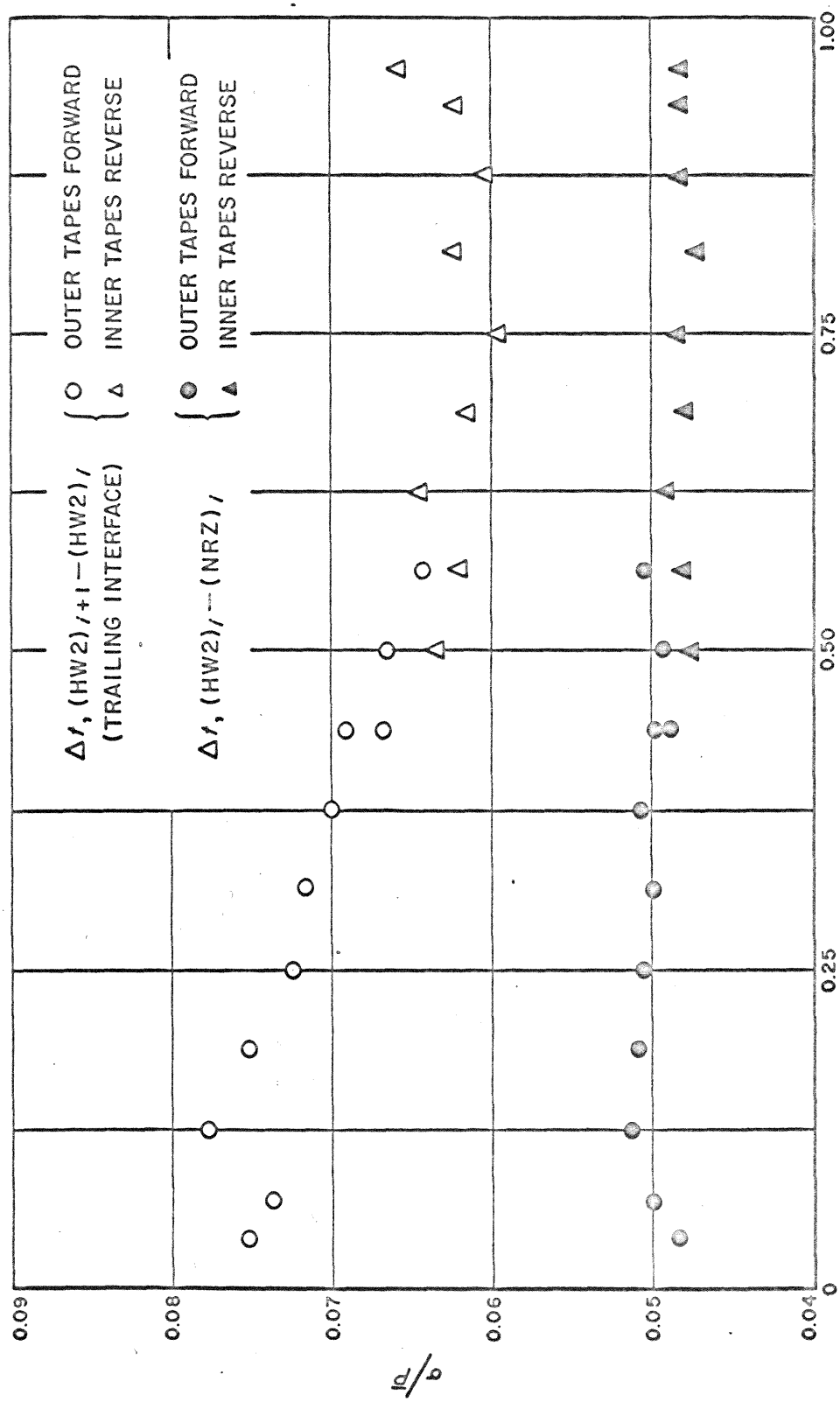

Fig. 25. Comparison of Dispersion for Trailing Interface and Time Interval Between NRZ and Following Turbulent Front

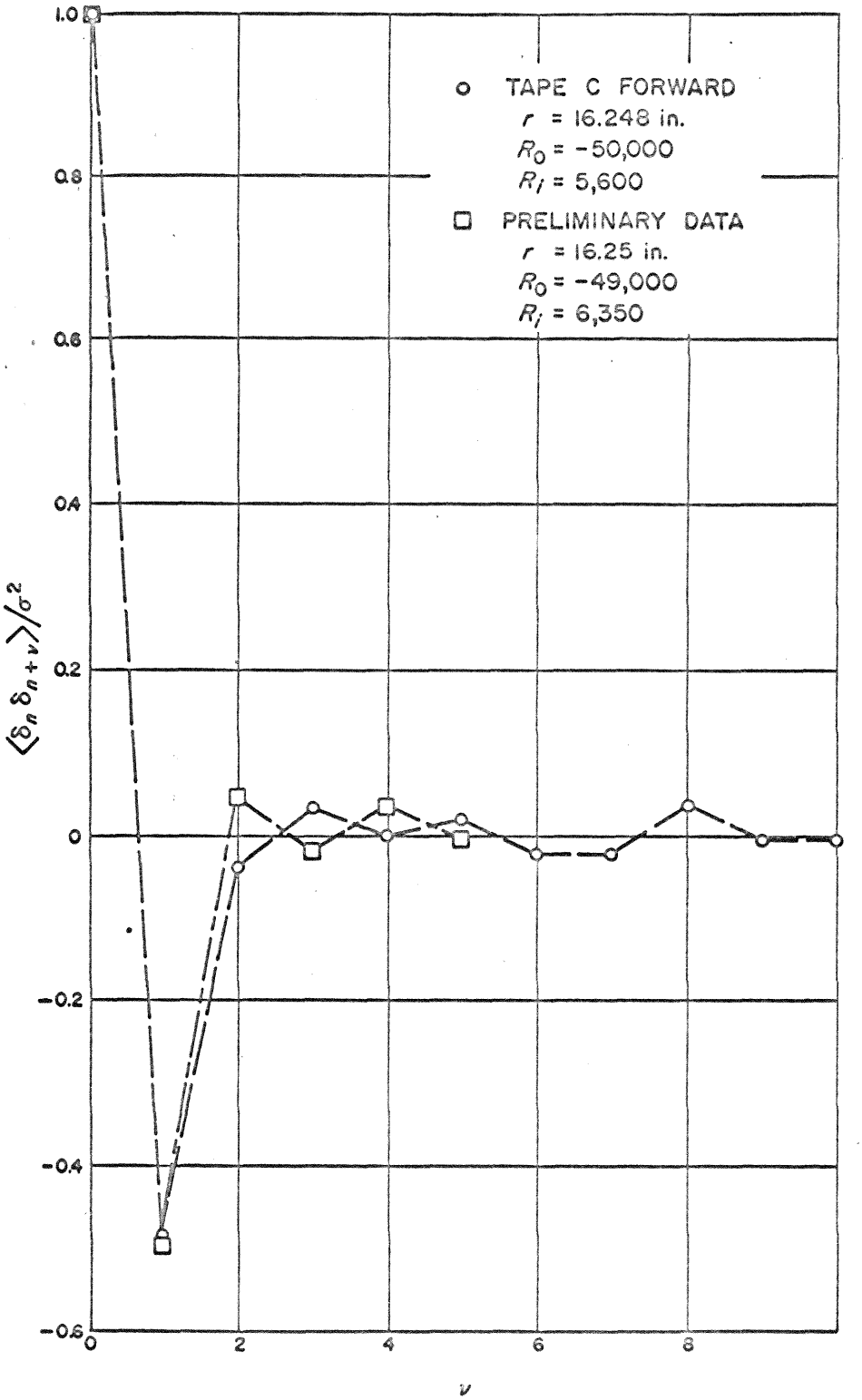

Fig. 26. Example of Serial Correlations for Interval Between Successive Observations of Interface

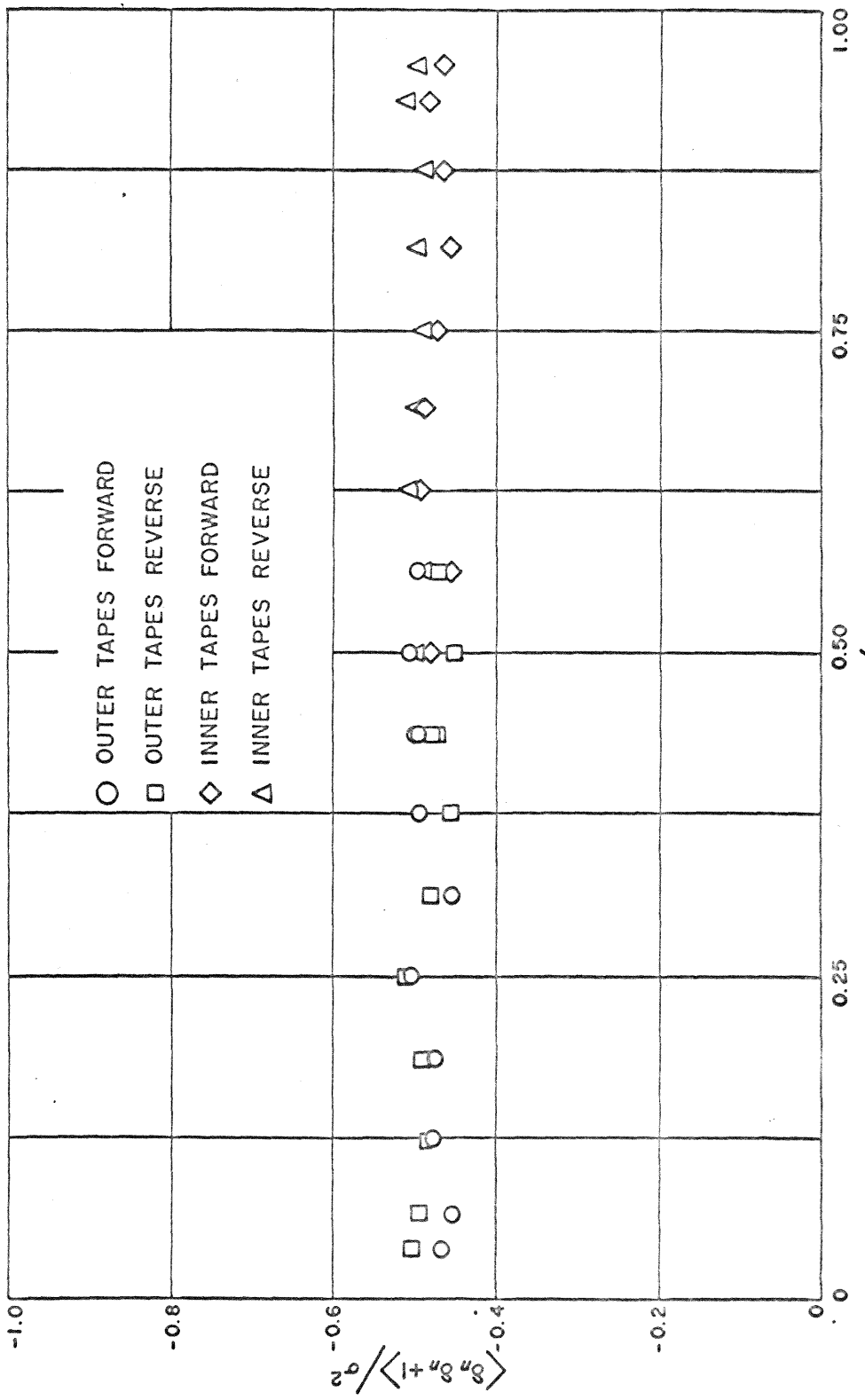

Fig. 27. Correlation for Adjacent Intervals Between Successive Observations of Interface

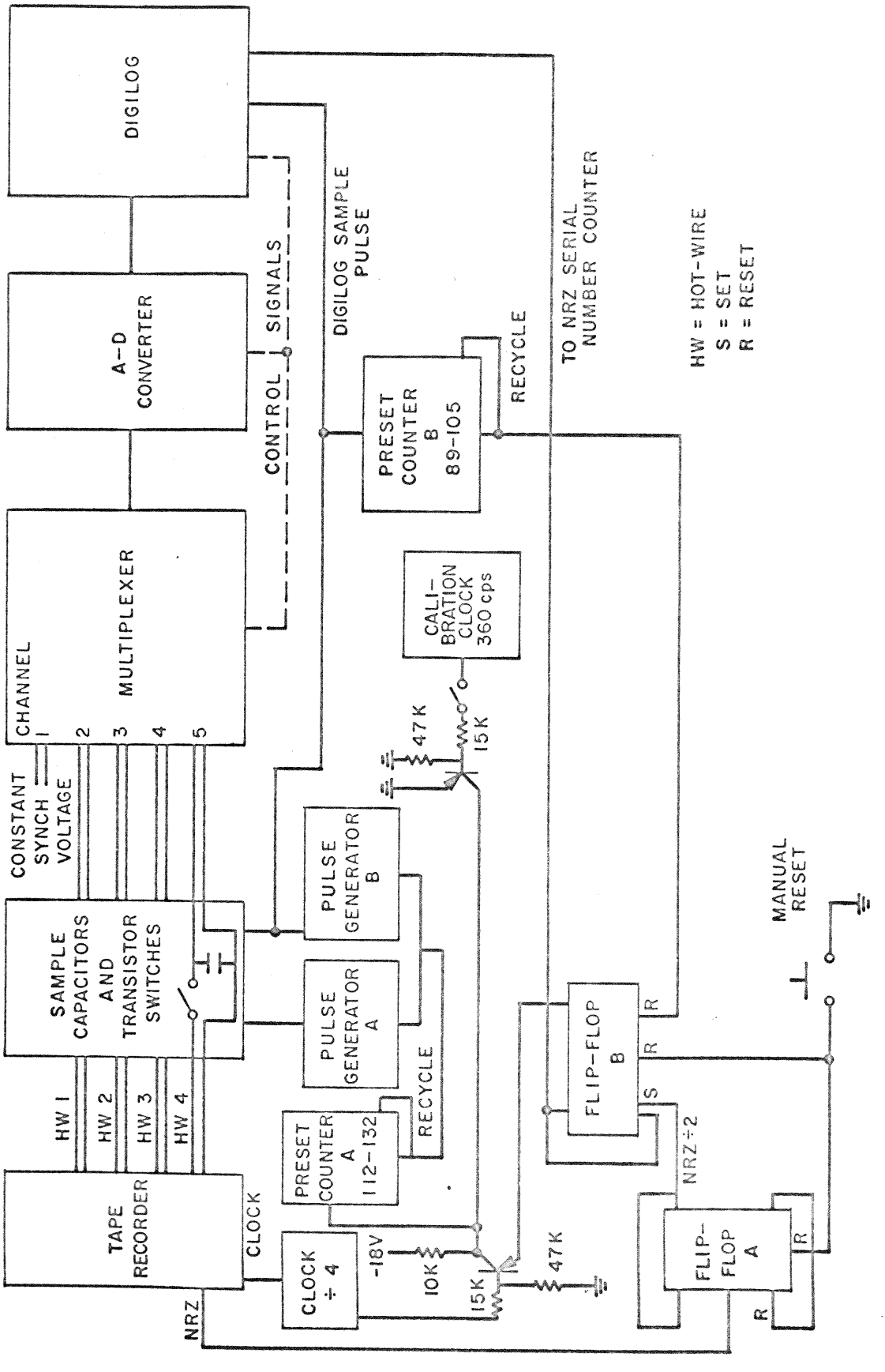

Fig. 28. Sampling System

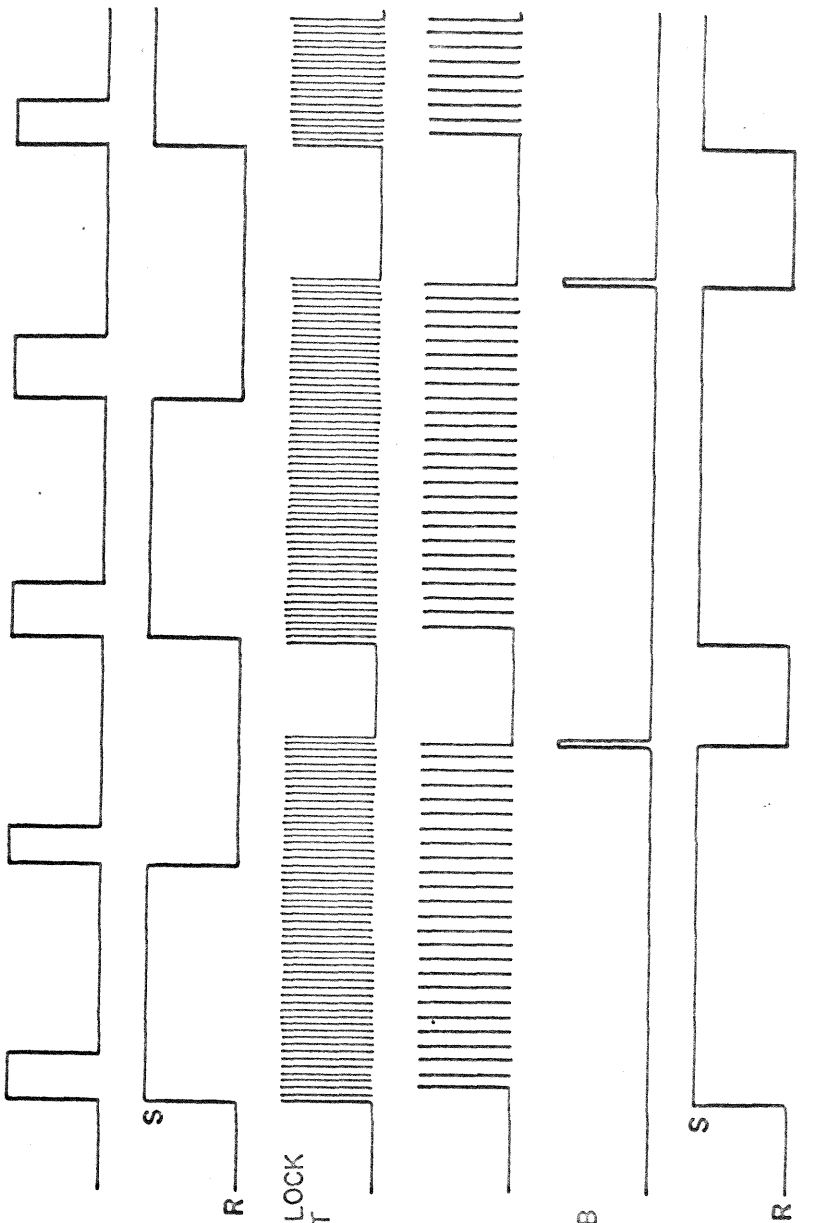

Fig. 29. Sample Pulse Generating-Loop Signals

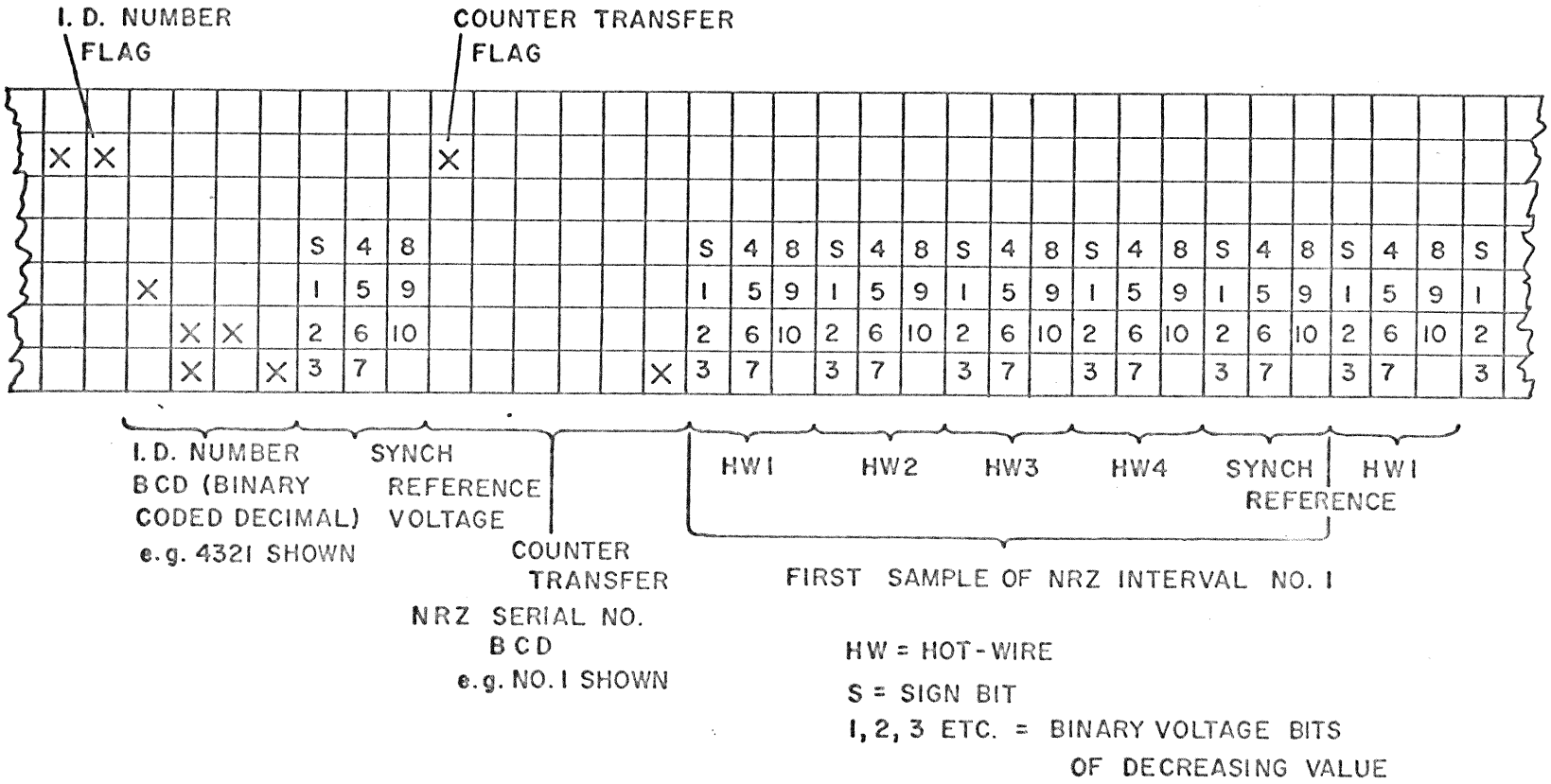

Fig. 30. Digital Tape Format for Sampling Operation

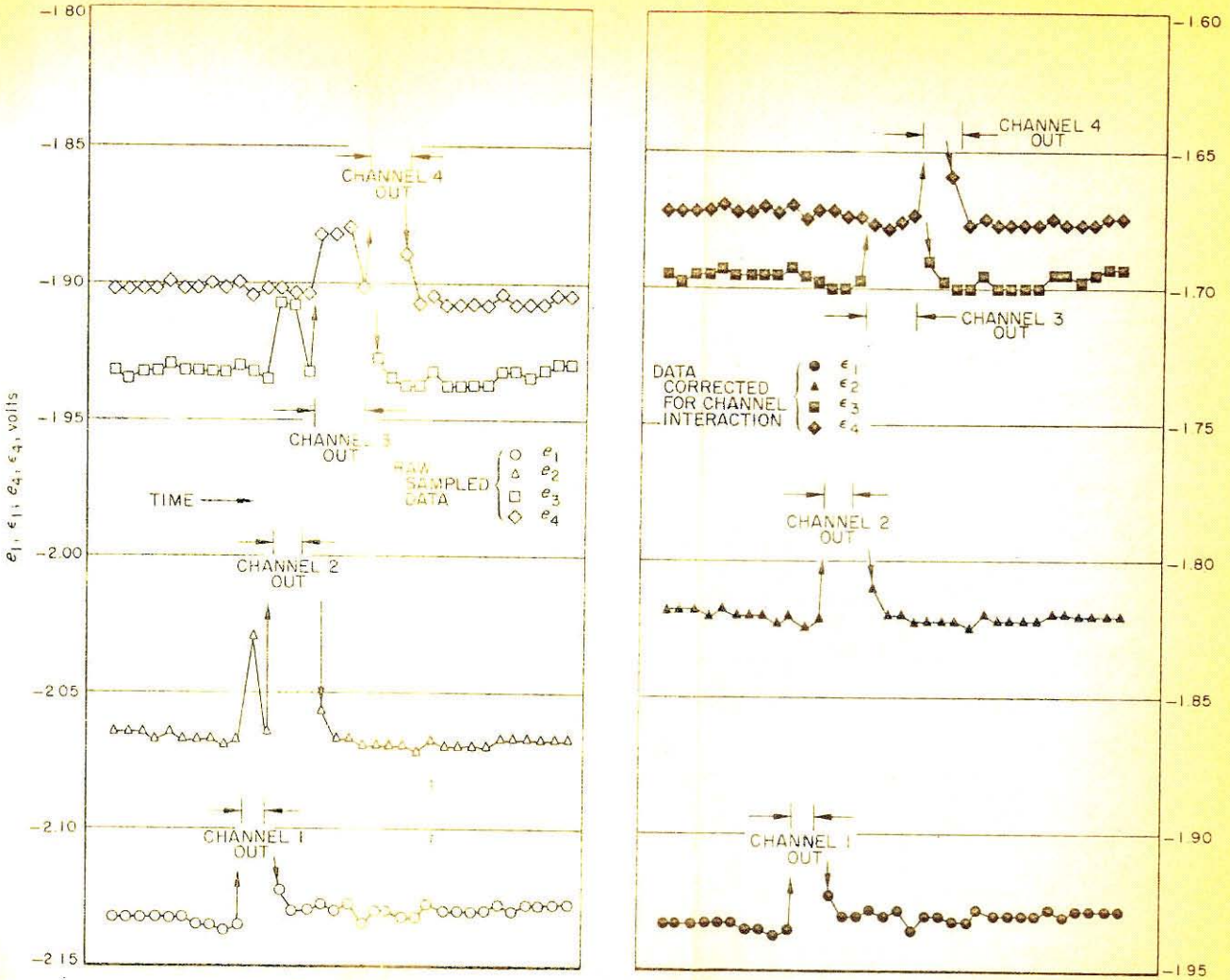

Fig. 34. Example of Multiplexer Channel Interaction Errors: Raw and Corrected Data. Data are from first calibration section of tape H_0^1.

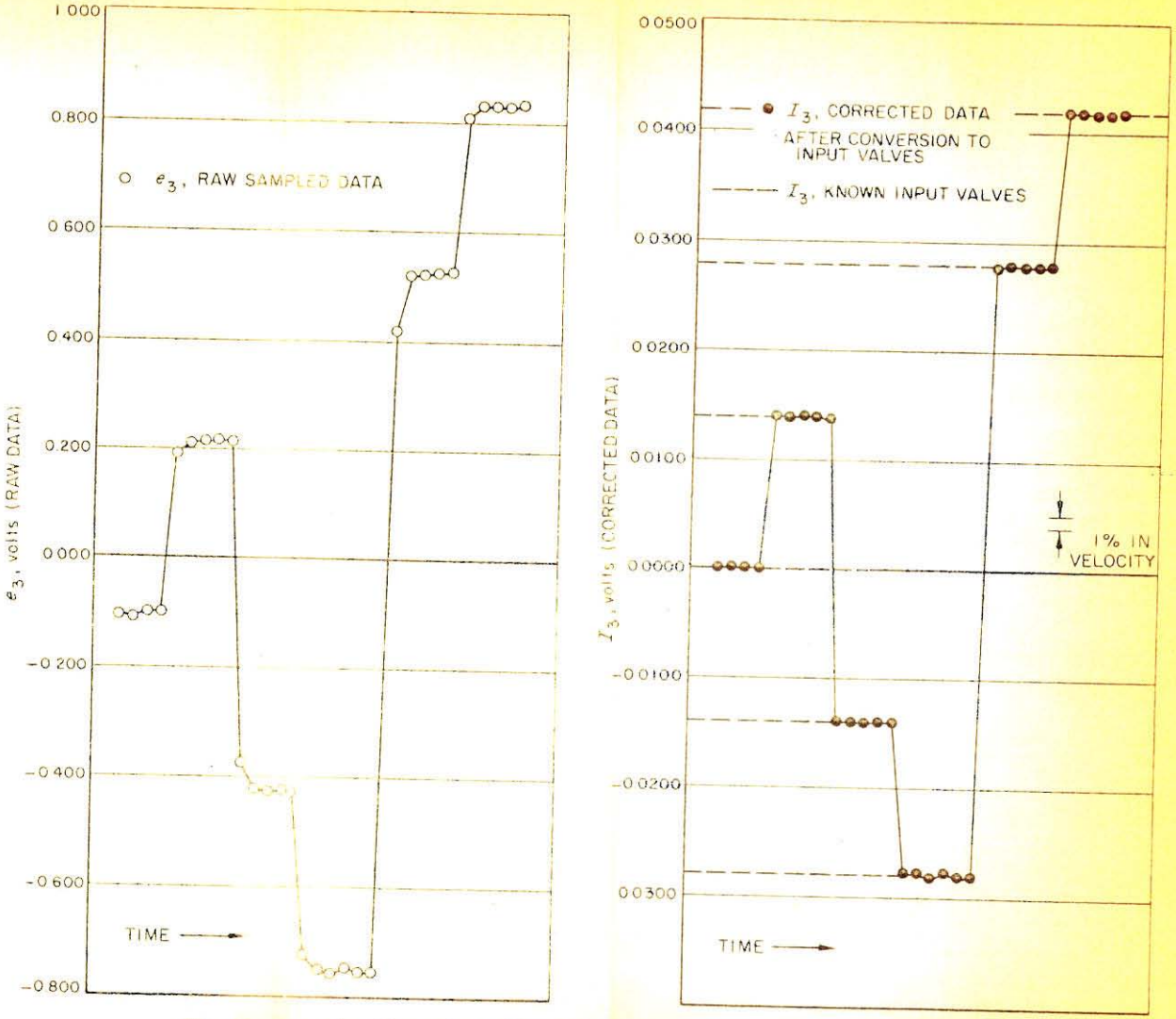

Fig. 32 Example of Impedance Mismatch Errors: Raw and Corrected Data. Data are from fourth calibration section of tape N.

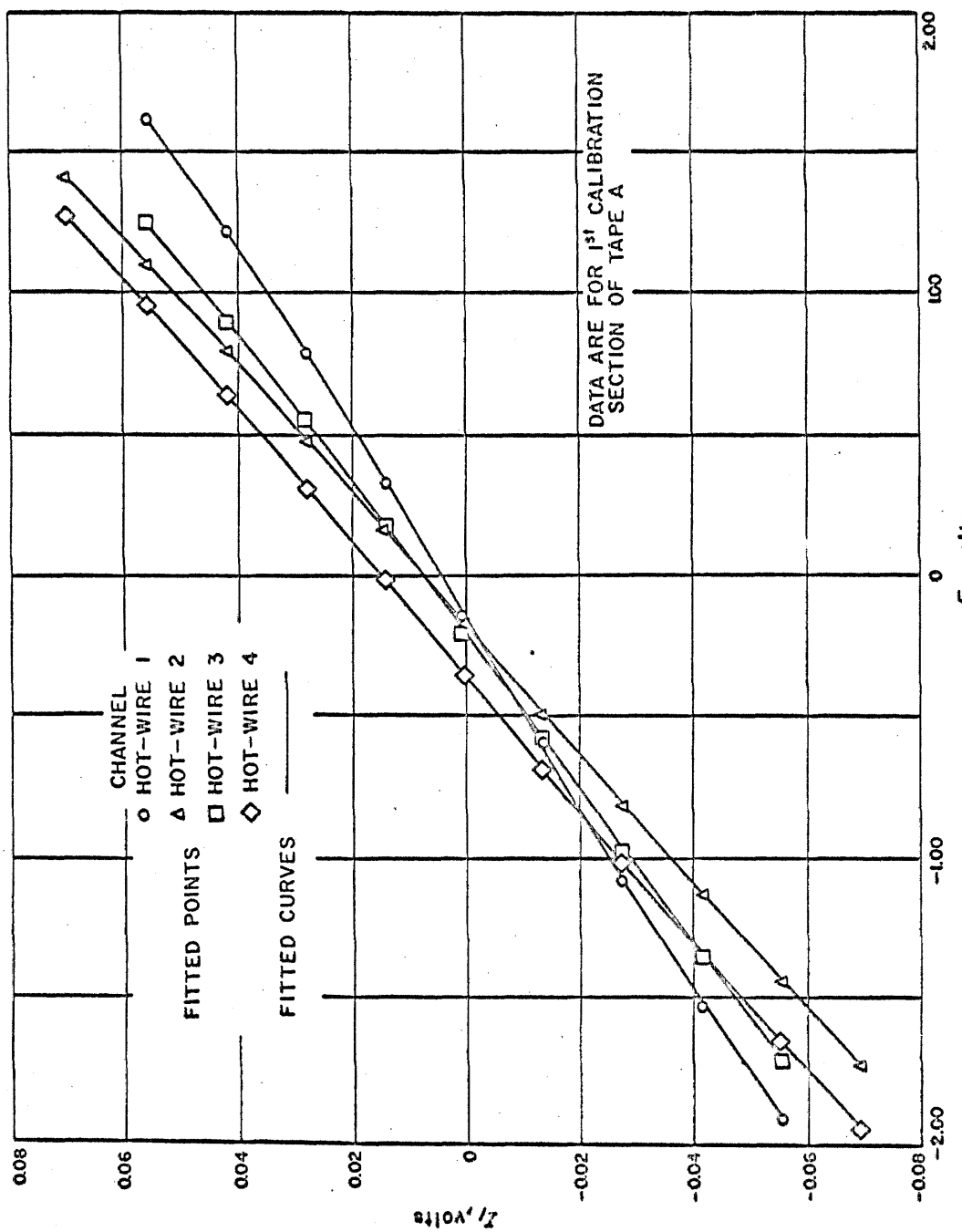

Fig. 33. Typical Overall Recording-Playback-Sampling Calibration Curves

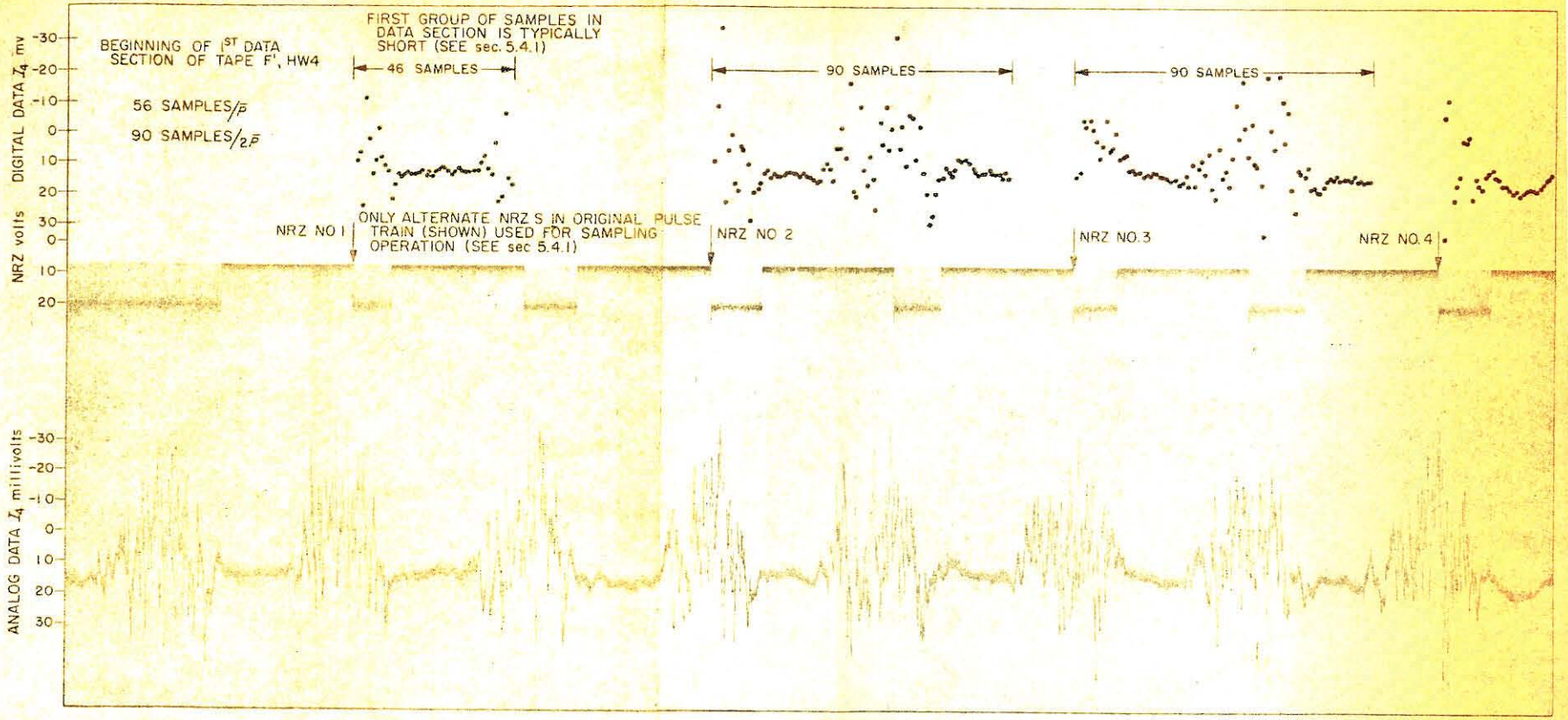

Fig. 34. Comparison of Raw Analog Voltages and Input Voltages Computed from Sampled Data